Glycosidic Bond Oxidation: The Structure, Function, and Mechanism of Polysaccharide Monooxygenases

John A Hangasky^a, California Institute for Quantitative Biosciences (QB3), University of California, Berkeley, Berkeley, CA, United States **Tyler C Detomasi**^a D, Department of Chemistry, University of California, Berkeley, Berkeley, CA, United States

Christopher M Lemon^a , Department of Molecular and Cell Biology, University of California, Berkeley, Berkeley, CA, United States; Miller Institute for Basic Research in Science, University of California, Berkeley, Berkeley, CA, United States; California Institute for Quantitative Biosciences (QB3), University of California, Berkeley, CA, United States

Michael A Marletta, California Institute for Quantitative Biosciences (QB3), University of California, Berkeley, Berkeley, CA, United States; Department of Chemistry, University of California, Berkeley, Berkeley, CA, United States; Department of Molecular and Cell Biology, University of California, Berkeley, CA, United States

© 2020 Elsevier Inc. All rights reserved.

1	Introduction	3
2	Chemistry of Copper	3
2.1	Properties of Copper Complexes	4
2.1.1	Cu(l): d ¹⁰	4
2.1.2	Cu(II): d ⁹	4
2.1.3	Cu(III): d ⁸	5
2.1.4	Cu(IV): d ⁷	5
2.2	Caveats in the Electronic Structure of Copper Complexes	6
2.2.1	Copper corroles	6
2.2.2	The tetrakis(trifluoromethyl)cuprate anion: [Cu(CF ₃) ₄] ⁻	8
2.3	Prototypical Mononuclear Copper Proteins	g
2.3.1	Type 1: Blue copper sites	g
2.3.2	Type 2: "Normal" copper sites	g
2.3.3	Peptidylglycine α -hydroxylating monooxygenase (PHM)	g
3	Introduction to Polysaccharide Monooxygenases	10
3.1	PMO Classification	11
3.2	Diversity of Polysaccharide Substrates	11
3.2.1	Cellulose	13
3.2.2	Hemicellulose	13
3.2.3	Chitin	15
3.2.4	Starch	15
3.3	Methods to Characterize PMO Activity	15
4	Structure of PMOs	16
4.1	Domain Architecture of PMOs	16
4.2	Active Site Contributions to Reactivity	17
4.3	Substrate Binding and Regioselective Oxidation	18
5	Catalytic Mechanism of PMOs	20
5.1	Details of O ₂ Reactivity	21
5.2	Uncoupled O ₂ Reduction: Oxidase Activity	22
5.3	Details of H ₂ O ₂ Reactivity	22
5.4	Potential Intermediates in Catalysis	23
5.4.1	Copper-superoxo: $Cu(II) - O_2^{\bullet}$	24
5.4.2	Copper-peroxo: Cu(II)-0 ₂ ²⁻	24
5.4.3	Copper-hydroperoxo: Cu(II)-OOH	24
5.4.4	Copper-oxyl: $Cu(II)-O \bullet \text{ or } [Cu(III)-O]^{\bullet+}$	24
5.4.5	Hydroxyl radical: ●OH	25
5.5	Electron Transfer Mechanisms	25
5.6	Biological Co-Substrate Availability: H ₂ O ₂ vs. O ₂	26
6	Conclusions and Outlook	26
Acknowled	dgments	27
References	S	27

^aThese authors contributed equally to this work.

Abbreviations

AA Auxiliary activity
AFM Atomic force microscopy

Asp Aspartate

B3LYP Becke 3-parameter, Lee-Yang-Parr functional

BDE Bond dissociation energy

CASSCF Complete active space self-consistent field
CAZy Carbohydrate active enzyme database
CBM Carbohydrate-binding module
CBP21 Chitin-binding protein 21
CDH Cellobiose dehydrogenase

CFEM Common in fungal extracellular membrane

Cu Copper

Cv Collariella virescens

DβM Dopamine β-monooxygenase DFT Density functional theory

DOMONDopamine β-monooxygenase N-terminalENDORElectron-nuclear double resonanceEPRElectron paramagnetic resonanceESEEMElectron spin echo envelope modulationESI-MSElectrospray ionization mass spectrometry

ET Electron transfer

EXAFS Extended X-ray absorption fine structure

Fc Ferrocene Fe Iron

FNIII Fibronectin III

FRET Förster resonance energy transfer

G Glucose

GbpA Glucan-binding protein A GH Glycoside hydrolase

Glu Glutamine Glu Glutamate Gly Glycine

GMC Glucose-methanol-choline GPI Glycosylphosphatidylinositol HAA Hydrogen atom abstraction

His Histidine

HOMO Highest occupied molecular orbital

HPAEC-PAD High-performance anion exchange chromatography, pulsed amperometric detection

LPMO Lytic polysaccharide monooxygenase

Ls Lentinus similis

LUMO Lowest unoccupied molecular orbital

MALDI-TOF MS Matrix-assisted laser desorption/ionization time-of-flight mass spectrometry

MCD Magnetic circular dichroism MD Molecular dynamics

MLCT Metal-to-ligand charge transfer

MO Molecular orbital

MP2 Møller-Plesset second-order perturbation theory

Mt Myceliophthora thermophila

Nc Neurospora crassa

NHE Neutral hydrogen electrode
 NMR Nuclear magnetic resonance
 PASC Phosphoric acid swollen cellulose
 PCET Proton-coupled electron transfer

PDB Protein data bank Phe Phenylalanine

PHM Peptidylglycine α-hydroxylating monooxygenase

PKD Polycystic kidney disease

pMMO Particulate methane monooxygenase PMO Polysaccharide monooxygenase PQQ Pyrroloquinoline quinone PTM Post-translational modification

QM/MM Quantum mechanics/molecular mechanics

RIXS Resonant inelastic X-ray scattering

ROS Reactive oxygen species
SCE Saturated calomel electrode
SEM Scanning electron microscopy
SHE Standard hydrogen electrode

Sm Serratia marcescens

SQUID Superconducting quantum interference device

SSN Sequence similarity network

Tyr Tyrosine

UV-vis Ultraviolet-visible VT Variable temperature

WSC Cell wall integrity and stress response component

X Xylose

XANES X-ray absorption near-edge spectroscopy

XAS X-ray absorption spectroscopy XPS X-ray photoelectron spectroscopy

1 Introduction

Nature has evolved a wide array of copper-containing proteins that mediate a myriad of biological processes including electron transfer, copper (Cu) and oxygen transport, and chemical transformations. The majority of Cu-catalyzed enzymatic reactions involve substrate oxidations that necessitate the coordinated transfer of electrons and protons in order to minimize deleterious off-pathway reactions and avoid high-energy intermediates. The kinetic challenge of multi-electron catalysis can be overcome by employing two or more metal centers or proximal redox-active cofactors to deliver multiple oxidizing (or reducing) equivalents to the substrate in either a stepwise or concerted process. For copper proteins, this is accomplished using dinuclear (e.g., type 3 and Cu_A sites), trinuclear (e.g., blue oxidases), or tetranuclear (e.g., Cu_Z cluster) sites, or a mononuclear copper site coupled to an iron porphyrin (e.g., Cu_B -heme a_3 pair). c_2

Enzymes with mononuclear copper centers are of particular interest because they lack other redox partners to delocalize charge and facilitate chemical reactions. Historically, inorganic model complexes of these enzymes have not been able to suitably recapitulate biological reactivity. In this way, mononuclear copper enzymes have provided new paradigms in catalysis that have informed the design of new model systems and molecular catalysts. A large superfamily of mononuclear copper enzymes, known as polysaccharide monooxygenases (PMOs) or lytic polysaccharide monooxygenases (LPMOs), has drawn a significant amount of attention to mononuclear copper enzymes. Originally annotated as hydrolytic enzymes, the discovery of their oxidative function has generated great interest in PMOs because they are exemplar enzymes for biomass degradation that could serve as catalysts for bio-derived fuels and chemicals. The mononuclear, type 2 copper active site is essential for substrate oxidation. PMOs reduce either molecular oxygen or hydrogen peroxide, its two electron reduced form, to generate a powerful active-site oxidant that hydroxylates the polysaccharide backbone. Cleavage of the glycosidic bond creates new chain ends for subsequent hydrolysis, enabling synergistic activity between oxidative and hydrolytic enzymes.

The purpose of this article is to provide a broad overview of copper chemistry, describe the overall architecture and fold of PMOs, and to discuss the unique active-site chemistry of PMOs. The activity and regioselectivity of these enzymes on their various polysaccharide substrates will also be discussed. Finally, the hydroxylation mechanism of strong C–H bonds by PMOs will be explored in depth, focusing on the potential oxidants and active site intermediates, as well as co-substrate and electron donor preferences. This article will contextualize key insights from computational studies, structure-function analysis, small molecule mimics, and electron transfer systems to summarize the emerging mechanisms of PMO reactivity.

2 Chemistry of Copper

Copper is broadly distributed in Nature and represents the 26th most abundant element in the Earth's crust, with an average concentration of 50 ppm. It is found in its elemental form and exists in minerals as chlorides, carbonates, sulfides, arsenides, etc. Copper is a rather soft, ductile metal with high thermal and electrical conductivities, second only to silver. The surface of elemental copper is slowly oxidized in air, developing a superficial green hydroxo/carbonate or hydroxo/sulfate coating, as seen on copper roofs and statues. This low reactivity has resulted in the element sometimes categorized as a noble metal; this term has also been used to reflect the fact that the element has a closed d shell (i.e., 4s¹ 3d¹⁰ electron configuration). Specifically, copper and its congeners, silver and gold, make up the triad known as coinage metals because of their stability in the elemental state, malleable nature, and ease of refining.

Additionally, copper is an element that is essential for life. It is the 20th most abundant element in the human body (by mass) and the average adult contains \sim 70 mg of copper. This metal is found in proteins with a diverse series of functions, ranging from electron transfer to oxidation chemistry. In mollusks and arthropods, copper centers are used for oxygen binding and transport, giving rise to the characteristic blue blood of these animals. Copper transport and homeostasis is tightly regulated. As a result, free copper is undetectable in cells with an estimated concentration <10 $^{-18}$ M. Free copper in the cytosol catalyzes Fenton-like reactions that generate reactive oxygen species, which leads to cell damage. Abnormalities in copper metabolism are observed in several human diseases, including Wilson's disease and Menke's disease, other neurodegenerative disorders, as well as many cancers.

Copper can exist in a variety of oxidation states, each with a distinct preference for the number and arrangement of the ligands, resulting in rich coordination chemistry for this element. Cu(I) and Cu(II) oxidation states are the most common; however, copper can access higher oxidation states. While there are many Cu(III) complexes, examples of Cu(IV) are exceptionally rare. This is evident from the ionization potentials for copper: 745 kJ mol⁻¹ for the first ionization (i.e., removal of an electron from Cu(0)), 1958 kJ mol⁻¹ for the second (i.e., removal of an electron from Cu(I)), 3545 kJ mol⁻¹ for the third, and 5682 kJ mol⁻¹ for the fourth. These higher oxidation states are often invoked as transient intermediates in copper-mediated oxidation reactions. As evidenced by the Latimer diagram in Fig. 1, Cu(III) is a powerful oxidant. It is also important to note that Cu(I) can disproportionate to give Cu(II) and Cu(0).

This ability to transition between oxidation states, in either one- or two-electron steps, enables copper to mediate multi-electron reactions that range from electrochemical carbon dioxide reduction¹⁷ to enzymatic methane oxidation.¹⁸ Molecular copper complexes can catalyze carbon–carbon bond formation in Ullman-type cross-coupling reactions via a putative Cu(I)/Cu(III) catalytic cycle.¹⁹ These examples illustrate that copper is well poised to mediate challenging transformations on unreactive substrates.

2.1 Properties of Copper Complexes

Copper complexes exhibit preferential geometries with characteristic properties that vary with oxidation state, although examples of ligand non-innocence have been demonstrated (Section 2.2). This section describes the most common coordination numbers and geometries for copper, ranging from d^{10} Cu(I) to d^{7} Cu(IV). Additionally, spectroscopic and magnetic properties will be presented to contextualize the known chemistry of copper-containing small molecules.

2.1.1 Cu(I): d10

While examples of coordination numbers of 2–6 have been documented, four-coordinate Cu(I) complexes with tetrahedral geometry are the most common, but distorted planar geometry (D_{2d} symmetry) is also prevalent.¹⁰ The low charge and relatively large size of the Cu(I) ion make it somewhat polarizable, rendering it a soft acid in the hard-soft acid-base (HSAB) classification.²⁰ Consequently, preferred ligands for Cu(I) are soft bases, such as thiol and alkyl. As a result, Cu(I) exhibits rich organometallic chemistry, ranging from lithium alkyl cuprates to modern cross-coupling catalysts.²¹

Although color may arise due to the presence of an anion or charge-transfer bands, Cu(I) complexes are generally colorless. Due to the d^{10} configuration, Cu(I) complexes are diamagnetic. Consequently, most spectroscopic techniques are not amenable to study such molecules, unless methods are used that cause electron ionization or excite transitions to unoccupied valence orbitals. This can be achieved with X-ray techniques including photoelectron spectroscopy (XPS) and X-ray absorption (XAS) and emission. Of these, K- β emission is the most useful, as it can provide detailed information about the ligand character and coordination number, as well as the oxidation and spin states of the compound. Additionally, K-edge XAS (1s \rightarrow 4p) is sensitive to the coordination environment of Cu(I) centers.⁴

2.1.2 Cu(II): d⁹

With an increase in charge, Cu(II) is a harder acid than Cu(I) and prefers nitrogen- and oxygen-based donor ligands to more polarizable sulfur donors. Given the d^9 configuration, Cu(II) complexes are subject to Jahn-Teller distortions, thereby precluding idealized tetrahedral and octahedral geometries. Cu(II) complexes adopt lower symmetry configurations, thereby removing the degeneracy of the d orbitals. The majority of Cu(II) complexes are four-coordinate and adopt distorted tetrahedral (D_{2d}) or square planar (D_{4h}) geometry; common examples include [CuBr₄]²⁻ and chelating ligands (e.g., porphyrin), respectively. Six-coordinate complexes with distorted octahedral geometry, exhibiting elongation along the *z*-axis (D_{4h}), are also common. Examples of five-coordinate species with trigonal bipyramidal geometry are known (e.g., [Cu(bpy)₂I]⁺), but are less prevalent.¹⁰

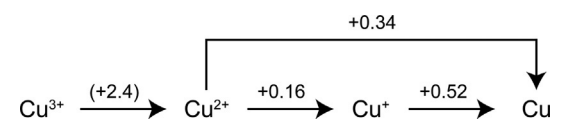


Fig. 1 Latimer diagram for copper. Potentials (in V vs. NHE) reflect standard reduction potentials and were obtained from Ref. 16. Values in parentheses are estimated.

With an unfilled d shell, optical d–d transitions occur in the 600–900 nm region of the spectrum, giving rise to blue or green colors for Cu(II) compounds. If charge-transfer bands are present in the UV region that tail into the blue end of the visible region, then complexes will appear red or brown. The magnetic moments for simple mononuclear Cu(II) complexes generally fall in the 1.75–2.20 μ_B range. The unpaired electron gives rise to a doublet ground state (S=1/2) that is readily characterized by electron paramagnetic resonance (EPR) spectroscopy. For Cu(II), g values are generally anisotropic, leading to distinct features that are dependent on the orientation of the magnetic moment relative to the applied field: $g \perp$ and $g \parallel$. Copper has two isotopes, 63 and 65, that account for nearly 100% of the natural elemental abundance, and both have a nuclear spin (I) of 3/2. Thus, the electron spin couples to the nuclear spin to produce a hyperfine splitting of the spectrum into four lines (2I+1), and the resultant coupling constants may also be anisotropic ($A \perp$ and $A \parallel$). Additionally, the electron spin may be delocalized onto the ligand, further splitting each hyperfine line into 2I+1 superhyperfine lines. For some compounds, such as Cu(II) porphyrins and corroles, superhyperfine splitting is readily observed under typical experimental conditions at X-band (\sim 9 GHz). Generally, superhyperfine coupling is very small and requires advanced pulsed EPR techniques, such as electron-nuclear double resonance (ENDOR) or electron spin echo envelope modulation (ESEEM), to detect it. 4

2.1.3 Cu(III): d8

High-valent copper species have been increasingly proposed as oxidants and intermediates in cross-coupling reactions, leading to greater interest in Cu(III) chemistry. Several reviews have cataloged examples of small molecule Cu(III) complexes¹⁵ and described their role in organometallic catalysis (e.g., C—C bond coupling)^{19,22–24} and oxidation chemistry.^{25–27} A useful starting point for discussing the chemistry of Cu(III) is to draw comparisons with the isoelectronic Ni(II) ion. Based on this analogy, it is expected that high-spin paramagnetic octahedral complexes will be obtained with weak-field ligands. Upon increasing the ligand field strength, diamagnetic square planar and five-coordinate species would be preferred. Since ligand field strength increases with oxidation state, it is expected that diamagnetic square planar Cu(III) complexes would predominate, and this is what has been observed experimentally.¹⁵ However, five-coordinate examples with square pyramidal²⁸ and trigonal bipyramidal²⁹ geometries have been reported.

Only a few examples of high spin Cu(III) exist, with the $[CuF_6]^{3-}$ anion as the first³⁰ and most well-characterized example. The magnetic moment ranges from 2.91 to 3.03 μ_B for a variety of alkali salts,³¹ which is slightly larger than the spin-only value of 2.83 μ_B . Similar magnetic properties are observed for the octahedral Cu(III) oxides YCuO₃ and LaCuO₃ (3.01 and 3.05 μ_B , respectively).³² Another notable example of high spin Cu(III) is an octahedral copper complex in an S₆ ligand field that bridges two thiol-functionalized Co(III) triazacyclononane units, furnishing a heteronuclear Co(III)–Cu(II)–Co(III) complex. Oxidation by one electron (+0.35 V vs. Fc⁺/Fc or 0.75 V vs. SHE) gives the corresponding Cu(III) complex. This species exhibits a magnetic moment between 2.4 and 2.6 μ_B (20–300 K) and a triplet (S=1) EPR spectrum, consistent with the high-spin d⁸ formulation.³³

One historical class of Cu(III) species is oligo-peptide complexes, which serves as an N₄ or N₃O chelating ligand using nitrogen atoms of the peptide backbone, N-terminus, C-terminus, and/or nitrogen-containing side chains (e.g., histidine). 34-37 The starting Cu(II) complex is oxidized electrochemically or with a chemical oxidant (e.g., IrCl₆²⁻) to yield the Cu(III) derivative, which is EPR silent and less prone to ligand substitution than the Cu(II) analog. Peptide complexes of Cu(III) can oxidize $[Fe(CN)_6]^{4-}$, Γ , and SO_3^{2-} . The first solid-state structure of a Cu(III) peptide was with tri- α -aminoisobutyric acid. ³⁸ The N-terminal nitrogen, C-terminal oxygen, and two backbone nitrogen atoms comprise the nearly coplanar N₃O ligand field with average bond angles of 87.3° at the copper center. The bond lengths are 0.12–0.17 Å shorter than the analogous Cu(II) derivative, suggestive of metal-based oxidation. However, it is worth noting that bond lengths are non-necessarily a convincing metric for oxidation state, as observed in the case of copper corroles (Section 2.2.1). The formal Cu(II)/Cu(III) couple extends over an extremely wide potential window, ranging from 0.45 to 1.02 V vs. NHE.^{32,39} However, similar ligand scaffolds exhibit small differences in potential. For example, tripeptide derivatives of Gly-Gly-His with an N₄ ligand field consisting of the N-terminus, two backbone nitrogens, and histidine exhibit Cu(II)/Cu(III) couples in the 0.92-0.98 V vs. SHE. 36 Since the identity of the peptide scaffold has a profound effect on the putative Cu(II)/Cu(III) couple, it may be that ligand oxidations are occurring, giving rise to the large potential range. With the prevalence of ligand non-innocence in copper chemistry (see Section 2.2), it would be worthwhile to re-examine the electronic structure of these complexes using advanced spectroscopic and computational methods. It is conceivable that there exists a continuum, where easily oxidized complexes are Cu(II) complexes with non-innocent ligands, while derivatives with high potentials are authentic Cu(III)

In neutral aqueous solution, the speciation of the Cu(III) ion is $[CuOH]^{2+}$ or $[Cu(OH)_2]^+$ and decays in a bimolecular fashion to produce two Cu(II) ions and H_2O_2 , as determined by pulse radiolysis. ⁴⁰ Under acidic conditions, Cu(III) generates hydroxyl radicals. ⁴⁰ One example of a powerful oxidant in aqueous solution is Cu(III) periodate, $[Cu(HIO_6)_2]^{5-}$, ⁴¹ which has been used in water treatment research to degrade persistent organic contaminants, such as antibiotics and other drugs. ^{42,43} The Cu(III)/Cu(III) couple for this compound is 0.37 V vs. SCE (or 0.61 vs. SHE), ⁴⁴ this somewhat low value, relative to other Cu(III) species, could suggest that the periodate anion may also serve as an oxidant in these reactions.

2.1.4 Cu(IV): d⁷

Given the relative inaccessibility of Cu(III), complexes containing a Cu(IV) are exceptionally rare. In many cases, purported examples are poorly characterized or lack definitive data to unambiguously assign an authentic Cu(IV) center, including mixed-valent copper oxides^{27,45} and purported Cu(IV) corroles⁴⁶ (see Section 2.2.1). Cu(IV) intermediates have been proposed in water oxidation electrocatalysis.⁴⁷⁻⁴⁹ However, it has been demonstrated that in some cases, the ligand becomes oxidized to avoid this

high energy intermediate. Examples of non-innocent ligands in copper-catalyzed water oxidation include an N_4 amidate ligand, ⁵⁰ bipyridine, ⁵¹ and carbonate. ⁵²

The only compelling example of a Cu(IV) species is the $[CuF_6]^{2-}$ anion. The Cs₂[CuF₆] salt, which is prepared by high pressure fluorination (350 atm F₂) of CsCuCl₃ and CsCl, is a red-orange solid that vigorously decomposes with water.⁵³ The compound has a magnetic moment of 1.5 μ_B , which is lower than the expected spin-only value of 1.73 μ_B for a low-spin d⁷ ion. The compound exhibits a characteristic EPR spectrum that is consistent with a $t_{2g}^6 e_g^1$ electron configuration.⁵⁴ Given that ligand non-innocence may be observed for $[Cu(CF_3)_4]^-$ (see Section 2.2.2), it is conceivable that a similar phenomenon may exist for $[CuF_6]^{2-}$. However, the difficulty in preparing the compound and the inherent instability likely hamper the spectroscopic studies necessary to definitively assign the electronic structure of this anion.

2.2 Caveats in the Electronic Structure of Copper Complexes

The electronic structure of a metal complex describes the distribution of electrons in the molecule. While this may seem inconsequential, it is profoundly important in determining the redox properties of a compound. The orbital character in which an electron resides could be localized on the metal center, the ligand, or delocalized over both. This has critical implications for the reactivity of a complex and governs the molecular mechanism of a chemical transformation. The determination of electronic structure is often nontrivial and can be complicated by ligand-based redox processes (i.e., non-innocent ligands). While this phenomenon is encountered in molecular complexes, it has also been observed in metalloenzymes. One prominent example is the copper center in galactose oxidase; oxidation of the modified tyrosine residue, rather than the metal, generates the active form of the enzyme. In order to assign the electronic structure of a metal complex, a variety of complementary spectroscopic techniques are utilized. These experimental techniques are often supplemented by theoretical calculations to predict transient or reactive intermediates. It is important to ground any theoretical calculation in experimental results to make meaningful predictions.

Determining the oxidation state of the metal center is key to accurately describing the electronic structure of a coordination complex or metalloenzyme active site. One particularly useful technique is X-ray absorption near-edge spectroscopy (XANES) and is often diagnostic for metal oxidation states. For copper complexes, the K-edge spectrum ($1s \rightarrow valence$ transition) is a primary technique to identify the physical oxidation state of the metal. It has long been considered that a distinctive pre-edge feature ($1s \rightarrow 3d$ transition) centered at 8981 eV is indicative of the Cu(III) oxidation state. However, this dogma has been reevaluated in light of ligand non-innocence, which is common in complexes with a high degree of covalent character in the metal-ligand bonds. By analyzing a series of structurally related complexes, Wieghardt and co-workers demonstrated that complexes that exhibit pre-edge features consistent with Cu(III) centers are instead best described as Cu(II) species. These results were bolstered by high-level multi-reference ab initio calculations. The unexpected shift to higher energies arises from metal-to-ligand charge transfer (MLCT) rather than the traditional $1s \rightarrow 3d$ transition. This study demonstrates that one spectroscopic technique alone is insufficient to make definitive assignments of oxidation state or electronic structure. A similar XAS study by Lancaster and coworkers demonstrated that a series of formally Cu(III) complexes have low Cu d-character in the lowest unoccupied molecular orbital. Instead, the hole is significantly localized on the supporting ligands. Since Cu has limited capacity to reach the 3+ oxidation state, the authors speculate that d⁸ Cu(III) does not exist. Sea

Multi-reference and multi-configurational computational methods are necessary in order to accurately describe the electronic structure of copper complexes. Indeed, the results of computational studies of copper complexes are highly dependent on the methods that are utilized. 59,60 It has been demonstrated that single-reference DFT methods give rise to significant errors when determining the energetics of potential PMO active site oxidants. This reflects the multiconfigurational nature of these catalytic intermediates and the necessity of using higher level multi-reference computational methods. 60a When examining structures without corroborating experimental data, benchmarking studies should be performed to ensure that the selected methods can reasonably recapitulate known results from structurally related compounds. Consequently, care must be exercised in interpreting the results of ab initio calculations with respect to the electronic structure of protein active sites and computationally derived reaction mechanisms, especially in the absence of corroborating experimental data. These caveats of electronic structure determination are illustrated using two examples with a rich history of debate and revision in the literature: copper corroles and the tetrakis(trifluoromethyl)cuprate anion, $[Cu(CF_3)_4]^-$. In the case of copper corroles, it is noteworthy that density functional theory (DFT) calculations were used to support each description of the electronic structure. Moreover, these examples underscore the difficulty in accurately determining the electronic structure of copper complexes and highlight the need for several complementary spectroscopic techniques to provide a precise description of electronic structure.

2.2.1 Copper corroles

Corrole (A) is a tetrapyrrole macrocycle with 18 π -electrons, akin to porphyrin (B), but with a contracted 23-atom core as a result of a direct pyrrole-pyrrole linkage (Fig. 2). Copper corrole complexes were reported with the original synthesis of the macrocycle in 1965. Since then, the electronic structure and oxidation state of the copper center in these compounds has been a topic of debate. Initially, the complex was formulated as a Cu(II) center with a dianionic ligand (C), where one of the pyrrole nitrogen atoms retains a proton. This assignment was based on several observations: broad 1 H signals in nuclear magnetic resonance (NMR) spectra, shifts in the UV-vis absorption spectrum upon removal of the "extra" hydrogen by a base, and an EPR signal.

In 1997, these complexes were re-formulated as a fully deprotonated corrole ligand containing a Cu(III) center (\mathbf{D}). This was supported by the lack of an N-pyrrole proton by infrared spectroscopy and crystallography, and the diamagnetic nature of the

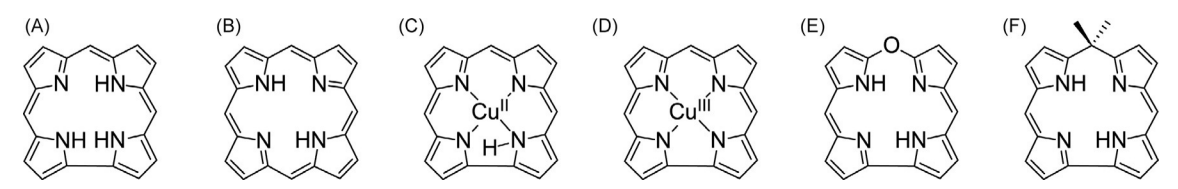


Fig. 2 Chemical structures of corroles and related macrocycles. Corrole (A), porphyrin (B), the initial formulation of copper corroles (C), revised formulation of copper corroles (D), 10-oxacorrole (E), and isocorrole (F).

compound, which exhibited well-resolved 1H NMR lines at room temperature and was EPR silent. 67 These early structural studies contended that the shorter Cu—N bonds of the corrole complexes relative to the porphyrin (by \sim 0.1 Å) support the Cu(III) formulation. Variable temperature (VT) 1H NMR studies demonstrated that the proton signals broaden at elevated temperatures, suggesting that there was a thermally accessible triplet state arising from an equilibrium between a Cu(III) and a Cu(II) corrole radical cation:

$$Cu(III)[Cor] \rightleftharpoons Cu(II)[Cor^{\bullet +}] \tag{1}$$

Later, DFT calculations suggested these complexes have a Cu(III) ground state with two Cu(II) radical cation states 0.161 and 0.354 eV higher in energy.⁶⁸ Other computational,^{69–71} structural,^{72,73} and electrochemical^{74–76} studies supported this formulation.

In 2007, a comparison between the solid-state structure of a copper corrole and an isostructural 10-oxacorrole (E), a nonaromatic dianionic ligand, showed that the structural metrics for the CuN_4 fragments were nearly identical, suggesting that a Cu(II) center was present in both compounds. Complementary DFT calculations demonstrated that a broken symmetry singlet with a Cu(II) center and a ligand-based radical was lower in energy than the Cu(II) triplet and Cu(III) singlet states. These studies led to the conclusion that the Cu(III) formalism is not fully satisfying and a Cu(III) corrole radical cation is a better description of the electronic structure. Subsequently, there have been many structural and computational studies of copper corroles with a myriad of meso and β substituents. Together, these studies have shown that saddling distortions are inherent to copper corroles as a consequence of significant overlap between the $Cu d_{x^2-y^2}$ orbital and the corrole π HOMO. Considering the corrole ligand as redox non-innocent in these complexes, 59,81 the ground state of copper corroles is best described as an antiferromagnetically coupled Cu(II) corrole radical cation. Consistent with the VT NMR experiments, there is a thermally accessible triplet state: the ferromagnetically coupled Cu(II) corrole radical cation.

$$[Cu(II) \uparrow [Cor^{\bullet +}] \downarrow] \rightleftharpoons [Cu(II) \uparrow [Cor^{\bullet +}] \uparrow]$$
(2)

However, the electronic structure of copper corroles remained an unresolved issue, as a 2015 report of a one-electron oxidized Cu corrole derivative claimed to be the first example of a discrete molecular Cu(IV) species. ⁴⁶ This conclusion was derived from the assignment that the neutral corrole complex contains a Cu(III) center, exhibiting a pre-edge feature at 8980.5 eV in the copper K-edge XANES spectrum. Other evidence for the Cu(III) assignment were the diamagnetic nature of the compound (EPR silent) and the Cu—N bond lengths; these observations are consistent with previously reported copper corroles. Upon oxidation, spin density on the metal center with superhyperfine coupling to the corrole nitrogen atoms was observed in the EPR spectrum and corroborated by DFT calculations. As a result, the authors concluded that the oxidized corrole complex contained a Cu(IV) center to account for the metal-centered spin density, which was absent for the neutral complex. The one-electron reduced complex exhibited a similar EPR spectrum and DFT calculations generated a spin density plot nearly identical to that of the oxidized species. Thus, the authors claimed to produce Cu(II), Cu(III), and Cu(IV) complexes within a single ligand framework. ⁴⁶

A subsequent study by Nocera and coworkers re-evaluated the electronic structure of copper corroles. ⁸³ DFT calculations, using both single (B3LYP) and multi-reference (CASSCF) methods, predict that the broken symmetry singlet (i.e., the antiferromagnetically coupled Cu(II) corrole radical cation singlet state) is the lowest energy electronic configuration (Fig. 3B). The energy gap between the singlet and triplet states was measured by both VT 1 H NMR and superconducting quantum interference device (SQUID) magnetometry which gave values of 0.144 ± 0.007 and 0.153 ± 0.005 eV, respectively, and is consistent with early theoretical predictions (0.161 eV). ⁶⁸ The one-electron reduced and oxidized corroles were compared to a copper isocorrole (F), an authentic Cu(II) species in a nearly identical ligand field. Interestingly, the EPR spectra of these three molecules are all characteristic of an axial doublet (S = 1/2) exhibiting hyperfine coupling to the 65 Cu/ 63 Cu nucleus and superhyperfine coupling to the four 14 N nuclei. These results are corroborated by DFT-calculated spin density plots, which show electron density in the Cu $d_{x^2-y^2}$ orbital (Fig. 3C and D). Additionally, all three corrole derivatives and the analogous isocorrole complex display identical XPS spectra, indicating that a Cu(II) center is present in each of these species. Together, these experiments confirm that the ground state of copper corroles is best described as an antiferromagentically coupled Cu(II) corrole radical cation. ⁸³ This formulation has recently been corroborated by Cu K-edge XAS experiments. ⁸⁴ Upon oxidation or reduction, the Cu(II) center is preserved and the redox load is borne by the ligand, underscoring the non-innocent nature of the corrole ligand in these complexes. ⁸³

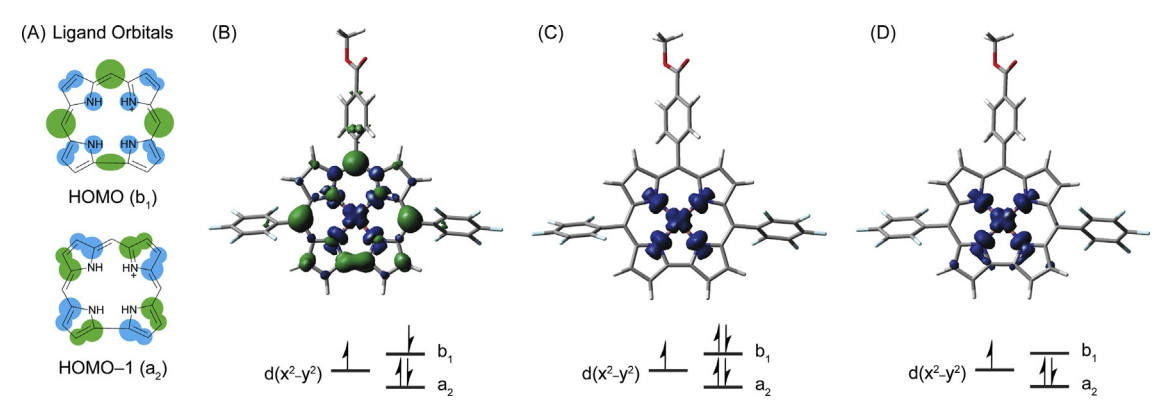


Fig. 3 Summary of the electronic structure of copper corroles. (A) Canonical occupied corrole ligand orbitals. Calculated spin density plots and qualitative molecular orbital diagrams for (B) the neutral corrole complex, (C) the reduced complex, and (D) the oxidized complex. Adapted with permission from Lemon, C.M.; Huynh, M.; Maher, A.G.; Anderson, B.L.; Bloch, E.D.; Powers, D.C.; Nocera, D.G. Electronic Structure of Copper Corroles. *Angew. Chem. Int. Ed.* 2016, *55*, 2176–2180. Copyright 2016 Wiley-VCH Verlag GmbH & Co. KGaA.

2.2.2 The tetrakis(trifluoromethyl)cuprate anion: [Cu(CF₃)₄]

The tetrakis(trifluoromethyl)cuprate anion was first reported by Naumann and co-workers in 1993. An ill-defined mixture of Cu(I)– CF_3 compounds were oxidized (using XeF_2 , I_2 , Br_2 , CI_2 , or ICI) then treated with a salt containing a bulky cation (e.g., $[Bu_4N]^+$ or $[Ph_4P]^+$) to give the corresponding $[Cu(CF_3)_4]^-$ salt as a colorless compound. Unlike the Cu(I)– CF_3 starting material, the $[Cu(CF_3)_4]^-$ salts are soluble in most organic solvents and are insensitive to light, air, and moisture. On the basis of the ligands and charge of the anion, a metal oxidation state of 3 + was assigned. The crystal structure exhibits nearly square planar geometry, albeit with a slight D_{2d} distortion, consistent with the d^8 configuration. Well-defined 1H and ^{19}F NMR spectra were recorded, confirming the diamagnetic nature of the compound.

Given the rarity of the Cu(III) oxidation state, Snyder postulated that an alternative bonding situation may arise in $[Cu(CF_3)_4]^{-.86}$ Computational analysis revealed that the atomic charge on the Cu center is ~ 1 and the Wiberg Cu—C bond orders are modest (0.29 or 0.38, depending on the level of theory) and deviate from the expected value of ~ 1 for a single bond. Additionally, a natural population analysis indicates that 9.7 (or 9.4, depending on the level of theory) electrons reside in the 3d orbitals, suggestive of a Cu(I) center. Given these results, Snyder proposed that the bonding is principally ionic and may be considered a $[Cu(CF_3)_2]^-$ unit with a CF_3^+/CF_3^- ion pair (i.e., $[CF_3^{-0.5}]_4$), resulting in two delocalized five-center, two-electron bonds and two non-bonding electron pairs. If this bonding picture were correct, then oxidation of the Cu(I)– CF_3 starting material effectively removed electrons from a CF_3 ligand rather than the copper center. This non-canonical bonding scenario was met with sharp criticism. However, Snyder defended his formulation by performing a similar analysis with $[Cu(CH_3)_2]^{-.88}$ which contains an obvious Cu(I) center. For both compounds, the bonding is highly ionic (80-95%), which implies that the valance electrons primarily reside in pairs either at the copper center or the $-CF_3/-CH_3$ ligand. Moreover, the d orbital populations are nearly identical $(9.7 \text{ for } [Cu(CF_3)_4]^{-}$ and $9.6 \text{ for } [Cu(CH_3)_2]^{-}$ at the MP2 level of theory), leading to the conclusion that both compounds contain a Cu(I) center with a d^{10} configuration.

While $[Cu(CF_3)_4]^-$ continued to be examined computationally, $^{89-91}$ no experimental studies had been performed to elucidate the electronic structure of this anion. Lancaster and co-workers performed a comprehensive spectroscopic study of this anion in conjunction with multi-reference ab initio calculations. ⁹² The K-edge XAS (1s \rightarrow valance) spectrum exhibited a feature at 8982.0 eV, which had long been considered diagnostic for Cu(III),⁵⁷ but has been re-interpreted to involve MLCT character as well (see Section 2.2). ⁵⁸ In light of this ambiguity, the authors turned to $K\alpha$ X-ray emission ($2p \rightarrow 1s$) because different final electronic states would be obtained for d¹⁰ Cu(I) and d⁸ Cu(III), giving rise to distinct spectral signatures. Such transitions are usually accessed with L-edge XAS (2p -valance), but this soft X-ray technique often leads to photodegradation of the sample, which would lead to difficulties in definitively assigning spectral bands. As a result, 1s2p resonant inelastic X-ray scattering (RIXS) was utilized as a facsimile for L-edge XAS and the resultant data is consistent with the d¹⁰ configuration. DFT calculations reveal that the frontier molecular orbitals are in line with the qualitative molecular orbital (MO) diagram proposed by Snyder. Together, these experimental and computational results demonstrate that the $[Cu(CF_3)_4]^-$ is best described as a Cu(I) complex with an inverted ligand field, where the lowest unoccupied molecular orbital (LUMO) is ligand-centered rather metal-centered (i.e., Cu d_{x²- y²}). ⁹² Additional structural and computational results have supported this conclusion. 93 Snyder made this profound statement about the d¹⁰ configuration of $[Cu(CF_3)_4]^-$: "The apparent willingness of a powerful electronegative moiety such as CF_3 to undergo oxidation in preference to Cu(I) underscores both the importance of the role of [the] ligand in assessing oxidation pathways in metal complexes and the resistance of copper to assume the Cu(III) state. "86 This example demonstrates that even seemingly simple, innocent ligands like –CF₃ can exhibit cryptic, non-innocent behavior.

However, the electronic structure of $[Cu(CF_3)_4]^-$ remains a contentious, unresolved issue. A recent study compared $[M(CF_3)_4]^-$ complexes for the coinage metals (M = Cu, Ag, Au) and determined that homolytic M–C bond cleavage is favored in the gas phase, suggesting that there is a large degree of covalent character in the metal-ligand bonds. ⁹⁴ This is in stark contrast to the ionic bonding scenario proposed by Snyder. ^{86,88} The authors emphasize that CF_3^+ and CF_3^- were not observed in the ionic dissociation of $[Cu(CF_3)_4]^-$, as might be expected if Snyder's formulation were correct. The similar behavior of the three anions indicates that the oxidation state is the same in all cases. While the $[M(CF_3)_4]^-$ complexes do exhibit an inverted ligand field, these compounds are best described as high-valent (i.e., M(III)) species with covalent M–C bonds, rather than M(I) species with ionic M–C bonds.

2.3 Prototypical Mononuclear Copper Proteins

Here, the geometric and spectroscopic properties of canonical mononuclear copper sites, type 1 blue copper and type 2 normal copper centers, are described. Additionally, peptidylglycine α -hydroxylating monooxygenase (PHM) is discussed as a prototypical example of catalysis at a mononuclear copper center. Together, spectroscopic and biochemical studies have provided a rather complete understanding of this enzyme.

2.3.1 Type 1: Blue copper sites

Cupredoxins, also known as blue copper proteins, are a family of electron transfer proteins that are involved in respiration and photosynthesis; prominent examples include plastocyanin in plants and azurin in bacteria. The canonical mononuclear type 1 copper site is ligated by one methionine, one cysteine, and two histidine residues in a distorted tetrahedral geometry, as found in plastocyanin. This unusual coordination sphere represents an intermediate between the ligand and geometric preferences for Cu(I) and Cu(II) in order to minimize reorganization energy upon electron transfer. Indeed, little structural change is observed between the oxidized and reduced forms of the protein. In other cupredoxins, such as azurin, there is a fifth oxygen ligand from a backbone amide to give a five-coordinate trigonal bipyramidal coordination sphere, where the oxygen and methionine sulfur form long (~3 Å) axial bonds. Type 1 copper sites are also present in multicopper oxidases, such as ascorbate oxidase and laccase. ^{5,95,96}

As the name suggests, the copper center exhibits an intense blue color due to an absorption band around 600 nm with a sizable extinction coefficient (\sim 5000 M⁻¹ cm⁻¹), which is significantly higher than d–d transitions (5–10 M⁻¹ cm⁻¹). This feature arises from a charge transfer transition from the cysteine sulfur to the Cu(II) center. The EPR spectrum of type 1 copper centers is distinctive, exhibiting high g values ($g_x = 2.047$, $g_y = 2.059$, $g_z = 2.226$) and low A values (63×10^{-4} cm⁻¹). These features suggest that the unpaired electron is more delocalized than other Cu(II) complexes, which indicates that the bonding situation is highly covalent. Finally, the Cu(I)/Cu(II) couple for typical blue copper proteins ranges from 0.25 to 0.35 V vs. NHE, which is higher than that of the aqueous Cu(I)/Cu(II) couple of 0.16 V vs. NHE. The potential is highly dependent on the identity of the axial amino acid ligand at the copper center, which can tune the potential from 0.16 to 0.8 V vs. NHE.

2.3.2 Type 2: "Normal" copper sites

Type 2, or "normal" copper centers are found in a variety of enzymes including oxygenases, nitrite reductase, and Cu/Zn superoxide dismutase. These mononuclear sites are often involved in the activation of molecular oxygen. This type of copper site is also involved in the synthesis of internal enzymatic cofactors, as in the case of topaquinone in amine oxidase and the cysteine-tyrosine cross-link in galactose oxidase. Like small molecule copper complexes, the Cu(II) center prefers to adopt four-coordinate square planar or five-coordinate square pyramidal geometry. One coordination site is vacant for oxygen binding. The amino acid ligands are variable, including histidine (most abundant), tyrosine (or modified derivatives), methionine, and cysteine (least abundant). The spectroscopic properties of type 2 copper sites are consistent with those of Cu(II) coordination complexes, thus the "normal" designation, and are exemplified by D_{4h} [CuCl₄]²⁻. Normal copper centers have no observable absorption in the visible region. EPR spectra are axially symmetric with $g|| = 2.221 > g \bot = 2.040 > 2.0023$ and sizable coupling constants $(A|| = 164 \times 10^{-4} \text{ cm}^{-1})$, which are significantly higher than type 1 copper centers; the indicated values are for [CuCl₄]²⁻.

2.3.3 Peptidylglycine α -hydroxylating monooxygenase (PHM)

The enzyme peptidylglycine α -hydroxylating monooxygenase, or PHM, is a eukaryotic protein that promotes hydrolytic amidation of peptide hormones. More specifically, it oxidizes C-terminal glycine-extended peptides to produce the corresponding α -hydroxylated derivative (Fig. 4A). PHM can also perform alternative monooxygenase reactions that include N- and O-deal-kylation, as well as sulfoxidation. The enzyme requires copper, oxygen, and ascorbate for catalysis. In this overall four-electron process, two electrons come from the substrate and two electrons are obtained from an external reducing agent, which is generally ascorbate for in vitro assays. PHM possesses two non-coupled copper centers, designated Cu_H and Cu_M , that are separated by ~ 11 Å; Cu_H serves as an electron transfer site, while O_2 activation and substrate binding occur at Cu_M . The Cu_H site is ligated by three histidine residues and the Cu_M site is ligated by one methionine and two histidine residues (Fig. 4B).

The reduced Cu(I) form of the enzyme was examined by EXAFS to determine the primary coordination sphere for the enzyme, ¹⁰¹ which is consistent with crystallographic studies. ^{98,102} Upon oxidation, the two Cu(II) sites are indistinguishable by EPR, giving a single signal with g||=2.288 and $A||=157\times10^{-4}$ cm⁻¹ that is similar to type 2 copper centers. Additionally, the d-d transitions were examined by magnetic circular dichroism (MCD) spectroscopy, and showed that the two copper centers were indistinguishable. EXAFS studies demonstrate that the methionine residue is elongated or dissociated from the Cu_M site in oxidized PHM. Subsequent structural studies confirm that the Cu(II)_M site exhibits square pyramidal geometry with a long axial methionine, two

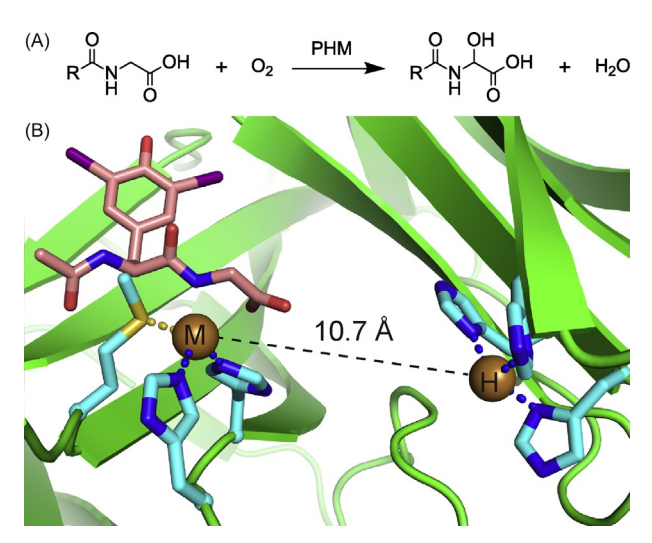


Fig. 4 Active site of rat PHM. (A) Chemical reaction catalyzed by PHM. (B) Solid-state structure of PHM (PDB 10PM)⁹⁸ showing the non-coupled copper centers (brown spheres, M and H), the primary coordination sphere (cyan), and bound substrate (magenta).

histidines, one hydroxide, and one water ligand. The $Cu(II)_H$ site was observed as a distorted square planar geometry (D_{2d}) with three histidine residues and one water ligand. Thus, it is interesting that such different structures can give rise to nearly identical spectroscopic properties. It has been proposed that the square pyramidal distortion and axial methionine ligand of the Cu_M center counteract the effects due to the strong hydroxide ligand, resulting in a ligand field that resembles the Cu_H site.⁴

Kinetic studies by Klinman and co-workers have revealed the molecular mechanism of PHM. ⁹⁹ Both electrons needed for substrate hydroxylation can be stored on the enzyme, such that the electron on Cu_H can be transferred to the Cu_M at a rate compatible with turnover. Substrate binding to the reduced enzyme follows an equilibrium-ordered mechanism, where substrate binding precedes O₂ binding to form the ternary complex. Next, O₂ activation occurs to form a putative Cu(II)–O₂ ^{•-} that performs H-atom abstraction from the substrate to from a Cu(II)–OOH. These intermediates have been directly observed crystallographically, ^{102,103} and have also been inferred from kinetic studies, ¹⁰⁴ the chemistry of model complexes, ^{3,105} and ab initio calculations. ¹⁰⁶ The subsequent electron transfer steps are not entirely clear and have been the subject of debate. In one proposed mechanism, homolytic O—O bond cleavage occurs to form HO•, which then combines with the substrate radical to from the protein-bound hydroxylated product. Subsequent electron transfer from Cu_H reduces the Cu(II)–O• intermediate to Cu(II)–OH. Alternatively, reductive, heterolytic O—O bond cleavage can occur to form water and a Cu(II)–O• that couples with the substrate radical, resulting in a Cu-bound product. In either case, product dissociation from the enzyme is believed to be the rate-determining step. ^{4,99}

3 Introduction to Polysaccharide Monooxygenases

In 2010, oxidative activity of chitin-binding protein 21 (CBP21) from Serratia marcescens was reported (SmLPMO10A), identifying a new paradigm in polysaccharide degradation.⁷ Oxidative activity of related proteins in fungi were subsequently reported and showed that these enzymes possess a mononuclear copper active site. 107-109 Homologous enzymes have since been identified in plants, 110 and viruses, 111 as well as insects, mollusks, algae, and arthropods. 112 Archaea is the only domain of life for which a putative homolog has not been identified. These enzymes are now known to be part of superfamily of enzymes known as polysaccharide monooxygenases (PMOs) or lytic PMOs (LPMOs). Individual fungal genomes have been found to encode large numbers of putative PMOs (>30), whereas bacterial genomes typically have far fewer (2-4). 113 PMOs play important roles in catabolism, specifically in cellulose and hemicellulose degradation, as PMOs are found in the genomes of plant detritivores including filamentous fungi and many bacteria. 114 PMOs are thought to work in concert with glycoside hydrolases (GHs) to facilitate biomass degradation by providing new chain ends and disrupting substrate crystallinity to increase the accessibility of hydrolytic enzymes. 115 The resulting soluble products from polysaccharide degradation can be readily taken up and utilized, 116 leading to an obvious role of PMOs in nutrition. PMOs have also been implicated in the virulence of pathogenic organisms, endosymbiosis, 117-119 and, most recently, development. 112 Bacterial PMOs have been implicated in endosymbiotic relationships with bark beetles, wood wasps, and bivalves to help these organisms break down recalcitrant polysaccharides. 120-122 Viral PMOs, that are part of the fusolin spindle protein family, in addition to a subset of bacterial PMOs, serve as a virulence factors. Activated upon release from the crystalline spindle, these PMOs weaken the chitinous exoskeleton of insects to facilitate infection of the host. 118,123-125

3.1 PMO Classification

The European Bioinformatics Institute (EMBL-EBI) groups PMOs into two unique protein families (Pfams) under accession numbers PF03067 and PF03443. 126,127 From the EMBL database UniProt, there are >16,500 predicted PMO sequences with >80 different annotated domain architectures (see Section 4.1). The carbohydrate active enzyme (CAZy) database is a comprehensive resource for genomic and biochemical information for carbohydrate-active enzymes. 113,128 CAZy currently classifies PMOs into seven auxiliary activity (AA) families based on the amino acid sequence: AA9, AA10, AA11, AA13, AA14, AA15, and AA16 (Table 1). The grouping of AA families also coincides with substrate specificity and taxonomic origin. A PMO-like family, X325, has recently been discovered, but no polysaccharide substrates have yet been identified. 128a Enzymes in five of these families (AA9, AA11, AA13, AA14, and AA16) are found only in fungal organisms. The AA9 family is active on cellulose and/or hemicelluloses and is further divided into four groups based on the oxidative regioselectivity (see Section 4.3): PMO1 (C1 oxidizing), PMO2 (C4 oxidizing), PMO3 (C1/C4 oxidizing), and PMO3* (C1 oxidizing). Chitin-, starch-, and xylan-active fungal PMOs belong to the AA11, AA13, and AA14 families, respectively. The majority of AA11 and all AA14 PMOs are currently not found in either Pfam, as they are not found by the hidden Markov model search by the Pfam database. AA13 is the only known family that can oxidize $\alpha(1 \rightarrow 4)$ glycosidic linkages found in starch. The AA16 family has recently been characterized as a cellulose-active class that is phylogenetically distinct from AA9. 131 While AA10 PMOs are predominately chitin-active enzymes of bacterial origin, this family also contains chitin-active viral enzymes. In addition, there are also distinct clades of cellulose and xylan-active bacterial enzymes within in the AA10 family. 132 Discovery of the AA15 family expanded the phylogenic diversity of PMO-containing organisms to arthropods, algae and oomycetes, 112 and these enzymes are active on chitin or cellulose. One member of the X325 protein family has been proposed to play a role in Cu acquisition during pathogenesis. 132a Several nomenclature styles have been used to identify specific PMOs. The general naming convention uses the first letter of the genus and species of the host organism, followed by either AA and the family number or (L)PMO, and then a letter to identify the specific PMO when multiple PMOs are encoded in the genome (e.g., NcAA9A for an AA9 PMO from Neurospora crassa). In this article, we will refer to specific PMOs as they are referenced in the literature.

Sequence similarity networks (SSNs) are an instructive way to visualize bioinformatic analyses of large sets of protein sequences 133,134 and can be useful for understanding the functional diversity within the large PMO superfamily. 135 SSNs group proteins into clusters based on sequence similarity. An important parameter in analysis is the alignment value or threshold value used to separate sequences. Based on the e-value from a pairwise BLAST analysis, a higher threshold is directly correlated with more stringently defined clusters. When an appropriate threshold value is used to construct the SSN, each resulting cluster represents a distinct group within the analyzed sequences and can provide insight into the origin, substrate specificity, and reaction mechanism of the constituent enzymes. A SSN of all predicted PMOs shows numerous distinct clusters (Fig. 5). Each AA family has its own cluster(s) within the SSN, indicating that this technique may be useful in identifying novel PMOs; it may be that some tight clusters without biochemically-validated examples represent unique AA families. Additional bioinformatic analysis of AA9 sequences showed these PMOs can be divided into 64 unique clusters. Although not every cluster could be associated with a distinctive feature, unique clusters were identified that exhibit specific regioselectivity and taxonomy. Similarly, phylogenetic trees can be used to depict the same bioinformatic information, but these can be more challenging to quickly interpret for large data sets. A phylogenetic tree of PMOs shows distinct clades that correlate with AA family and polysaccharide substrate preference (Fig. 6). Bioinformatic approaches will continue to be instrumental in the discovery of new PMO families and the identification of new polysaccharide substrates.

3.2 Diversity of Polysaccharide Substrates

Polysaccharides are the most abundant and diverse class of biomolecules on Earth. Perhaps the most obvious role of carbohydrates in Nature is as the primary currency in the carbon cycle. These complex biopolymers are comprised of various six- and five-membered cyclic sugars linked by glycosidic bonds, and incorporate significantly more distinct monomeric units (i.e., >40 hexoses,

Tubic I				
Family	Sub-family	Substrate	Regioselectivity	Origin
AA9	PM01	Cellulose	C1	Fungi
	PM02	Cellulose	C4	Fungi
	PMO3	Cellulose, Hemicellulose	C1/C4	Fungi
	PM03*	Cellulose	C1	Fungi
AA10		Chitin, Cellulose, Xylan	C1, C4, C1/C4	Bacteria, Viruses
AA11		Chitin	C1	Fungi
AA13		Amylose	C1	Fungi
AA14		Xylan	C1/C4	Fungi
AA15		Chitin, Cellulose	C1	Arthropods
AA16		Cellulose	C1	Fungi

 Table 1
 Substrate specificity and regioselectivity of PMO families

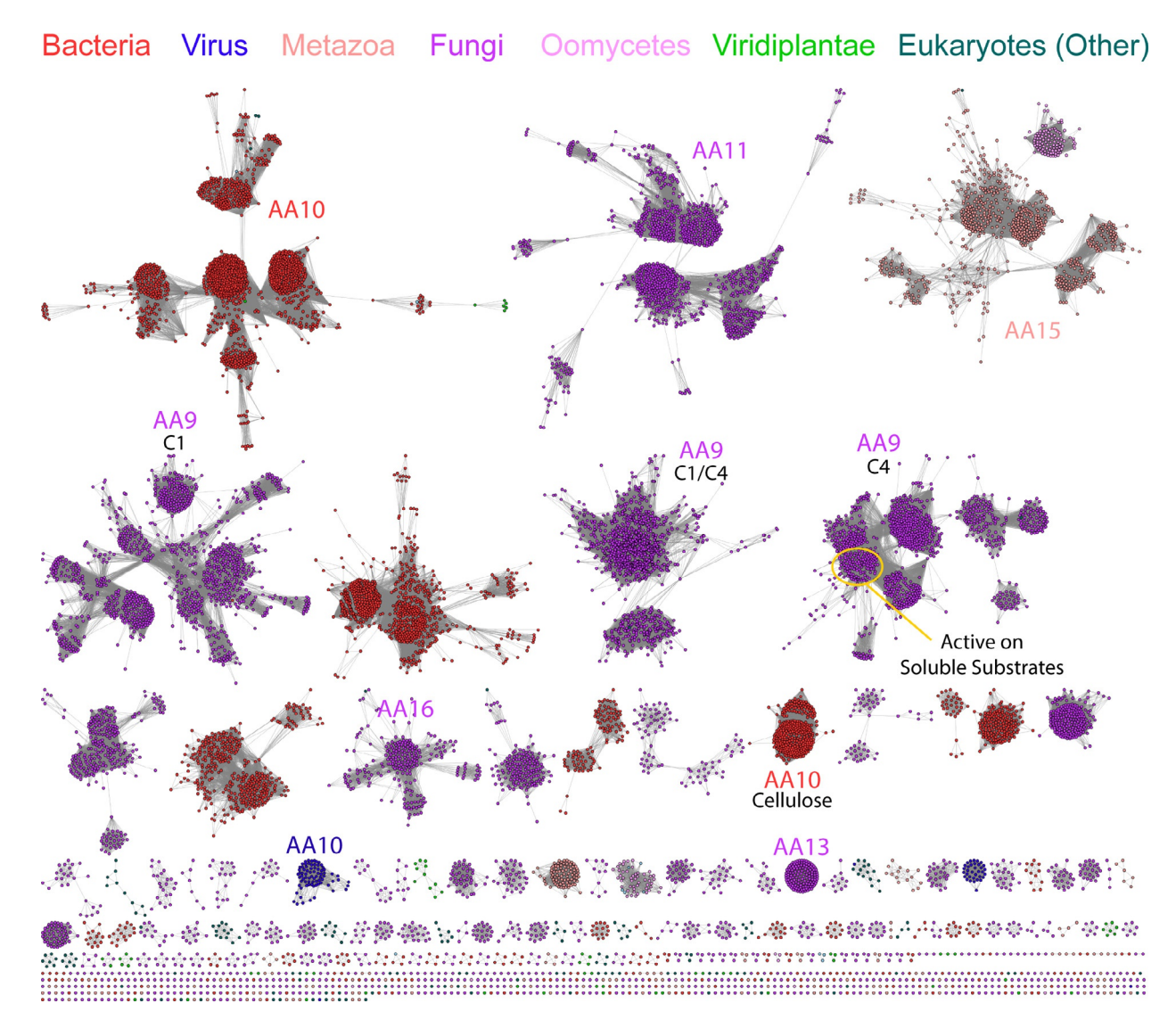


Fig. 5 Sequence similarity network of PMOs. The SSN is comprised of sequences found in Pfams PF03067 and PF03443. Clusters are colored based on the taxonomic origin. Clusters with characterized PMOs are labeled with the appropriate AA family and unique identifying characteristics (i.e., regioselectivity or substrate preference). Soluble-substrate active PMOs form a tight cluster within C4 oxidizing AA9 PMOs (yellow circle). Since AA14 PMOs are not found in either PF03067 or PF03443, they are not included in this SSN. The AA11 sequences have been manually added by including the 2000 most similar sequences through the "Sequence BLAST" option in the EFI-EST software. The SNN was generated using EFI-EST software¹³³ using an alignment score of 65 and was visualized in Cytoscape.

pentoses, and modified derivatives) than both proteins (20 amino acids) and DNA (4 nucleotide bases). The entire polysaccharide make-up of an organism, termed the glycome, has been historically difficult to study, but is becoming increasingly important in understanding fundamental biological processes, such as cell-cell communication. The diversity of polysaccharides is due to numerous combinations of repeating sugar units with various motifs. Common homogenous polysaccharides include starch, cellulose, and chitin. Since these carbohydrates are extremely stable and resistant to hydrolysis, they are used to provide structure (e.g., cellulose and chitin) and store energy (e.g., starch). Polysaccharides decorate the outside of cells and can facilitate cell self-recognition and signaling, as well as stabilize proteins and enhance their function in many organisms. Plant cell walls utilize a complex matrix to provide structural support and to protect the intracellular environment. This matrix is composed of large cellulose microfibers, hemicelluloses, mannans, pectins, lignin, and various proteins. Similarly, chitin is a major component of arthropod exoskeletons and the fungal cell wall. These heterogeneous structures rely on the crystallinity and tensile strength of the polymer to provide a protective external barrier for the organism.

Degradation of polysaccharides is important in numerous cellular processes, including cell division, growth, and response to harsh environmental stimuli. ¹⁴² The recalcitrant nature of these polysaccharides provides a particularly important, but challenging,

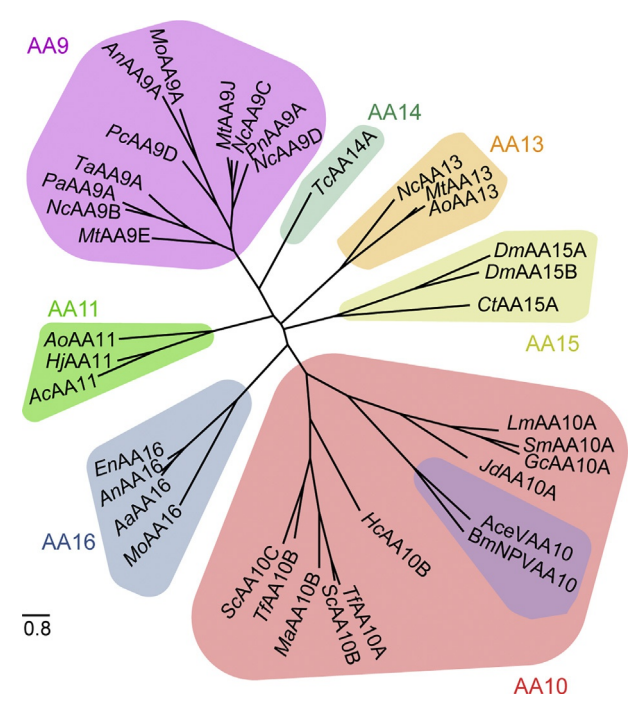


Fig. 6 Phylogenetic tree of PMOs. Representative sequences from each AA family were selected from the CAZy database to show phylogenetic relationships between families. Individual families are colored. The viral PMOs found in the AA10 family are colored purple. Sequences were aligned using ClustalOmega and the phylogenetic tree was generated using PhyML¹³⁷ and visualized with DrawTree in Phylogeny.fr.¹³⁸

landscape for enzymatic processes. In this regard, PMOs are a fascinating family of enzymes, not only for the reaction they catalyze, but also because of the diversity of polysaccharides they can degrade. PMOs oxidize many different carbohydrates, and are not strictly limited to crystalline substrates (Fig. 7). With the exception of starch, all known PMO substrates contain a $\beta(1 \rightarrow 4)$ linkage that is oxidized either at the C1 or C4 position. This section describes the structures and properties of carbohydrates that are known substrates of PMOs.

3.2.1 Cellulose

Cellulose is comprised of $\beta(1 \rightarrow 4)$ linked glucosyl units and is often found as a crystalline polymer. All organisms in the kingdom viridiplantae use this polymer as the primary cell wall constituent, while some larger organisms also use it to support tissues. 144 Cellulose is naturally found in plants in microfibril-like bundles of cellulose I. 145 Cellulose naturally occurs in two polymorphs, cellulose Ia and IB, which are primarily found in bacteria and plants, respectively, although both forms can be found in these organisms. 146,147 Both polymorphs consist of chains that are stacked in parallel bundles. The Ia form contains sheets that are directly stacked on top of each other, whereas the Iß from has stacked sheets that are offset between alternating layers. 148-150 Hydrogen bonds form between intra-layer chains in both cellulose Iα and Iβ, but only van der Waals contacts occur between sheets. For industrial applications of cellulose degradation, cellulose I is treated with either sodium hydroxide or liquid ammonia to produce non-natural cellulose II and cellulose III, 151 respectively. Cellulose III can also be produced by treating cellulose II with liquid ammonia. Cellulose II contains antiparallel bundles of cellulose chains that are stacked, whereas cellulose III forms more staggered layers and does not pack as tightly as cellulose I. While cellulose II and III contain more inter-sheet hydrogen bonds than cellulose I, they are generally more amenable to GH degradation. 152 A fourth, non-naturally-occurring polymorph, cellulose IV, can be produced from cellulose III by high temperature treatment in glycerol. 153,154 While this form has not been extensively characterized, it appears to share many similarities with cellulose IB. 155,156 The most common forms of cellulose used in biochemical assays are Avicel and phosphoric acid swollen cellulose (PASC). Avicel is a common, commercially-available form of microcrystalline cellulose that has been purified from wood and acid treated. In this way, the amorphous regions of bulk cellulose have been hydrolyzed, forming small crystalline particles that closely resemble cellulose Iα. PASC is prepared by treating Avicel with phosphoric acid to swell the material and disrupt tiny crystallites, thereby increasing enzyme accessibility.

3.2.2 Hemicellulose

Hemicelluloses are a highly heterogeneous group of polysaccharides 157 that are comprised of various carbohydrates, including xyloglucans, xylans, and glucomannans. 158,159 These non-crystalline polysaccharides contain primarily $\beta(1 \rightarrow 4)$ backbone linkages. Hemicelluloses play a role in signaling during plant growth, particularly when the cell wall needs to be expanded. 160

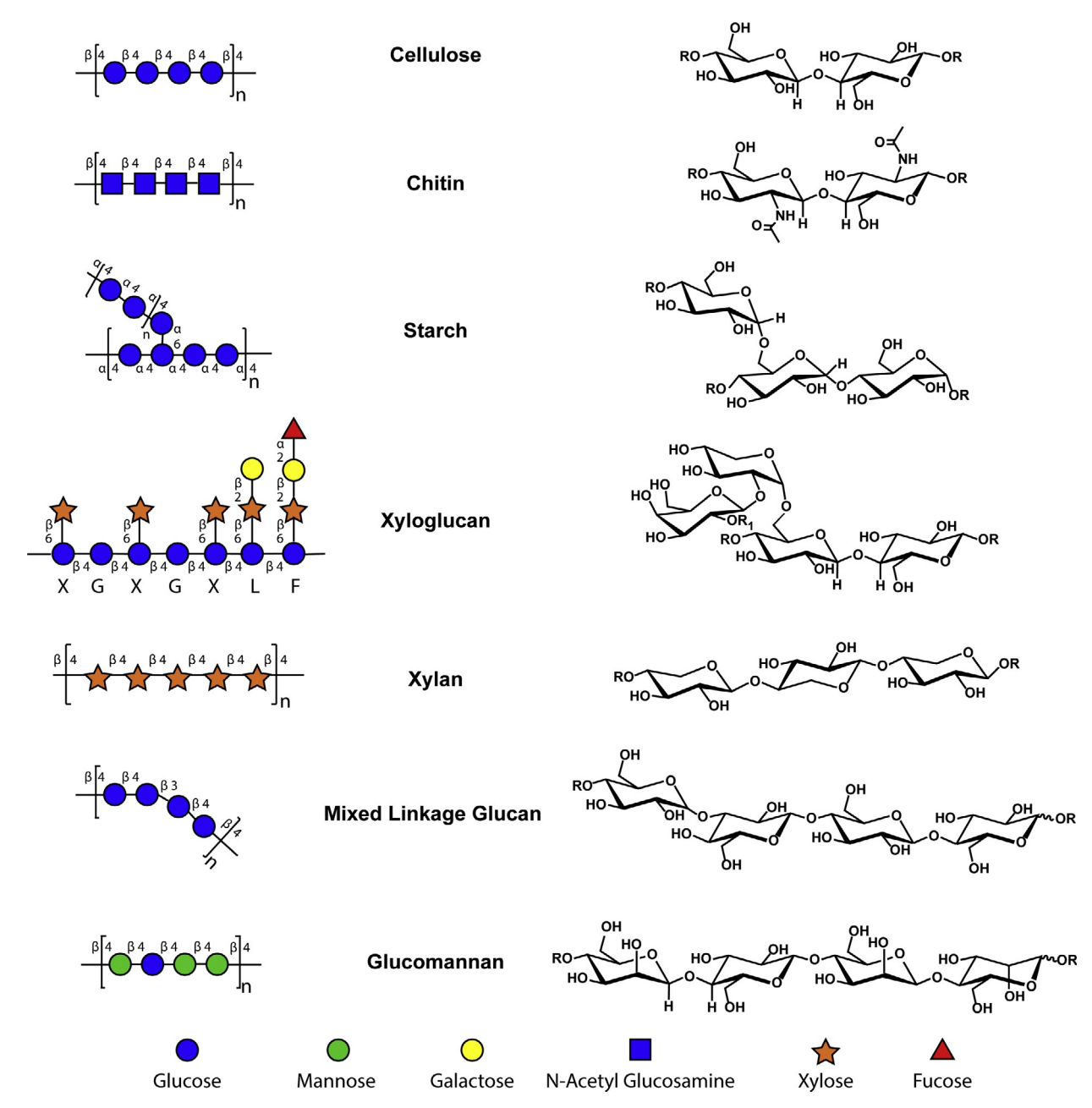


Fig. 7 Known polysaccharide substrates of PMOs. Chemical structure and schematic representation of known polysaccharide substrates of PMOs. Symbols in the schematic representation are based on recommendations from *Essentials of Glycobiology*. ¹⁴³ For the schematic of xyloglucan, G-, X-, L-, and F-type monomeric units are shown, where G is glucose, X is glucose with a linkage to xylose, and L and F represent a galactose unit on the xylose in which the R₁ substituent represents either a H or a fucose sugar, respectively. For xyloglucan and glucomannan, representative examples are depicted; the specific pattern of the interspersed glucose units can vary. For all polysaccharides shown, R represents the repeating unit or the end of the carbohydrate chain (R=H).

Hemiceulluloses also improve cell wall flexibility and can serve as crosslinks between cellulose microfibrils. ¹⁶¹ PMO activity on these polymers likely serves as another way in which polysaccharides can be modified to increase the efficiency of hydrolases.

Xyloglucans are the most abundant form of hemicellulose. The backbone of xyloglucan is comprised of repeating glucosyl units; several of the glucose (G) rings are attached to xylose (X) through a $\beta(1\to2)$ linkage. Xyloglucans are classified by the repeating pattern of the sugars, with XXGG, XGXG, and XXXG as the most common patterns. The xylose units may be further connected to other sugars like fucose or galactose. Xylans are the most abundant non-cellulosic oligosaccharide present in plant cell walls. Xylans are heterogeneous polymers of $\beta(1\to4)$ linked xylose that are stochastically decorated with α-glucuronic acids, α-arabinofuranose, and acetyl groups. Xylan modified with ferulic acid can also be cross-linked with lignin. Glucomannans are

 $\beta(1\rightarrow4)$ linked mannose residues with randomly interspersed glucosyl units. ¹⁶⁶ These may be further decorated by $\beta(1\rightarrow6)$ branching with glucose, galactose, or mannose (Fig. 7). Similar to xylans, glucomannans are often partially acetylated. Mixed-linkage β -glucans are comprised of glucose units linked with alternating $\beta(1\rightarrow3)$ and $\beta(1\rightarrow4)$ glycosidic bonds. ^{167,168} Unlike the linear backbones of other hemicelluloses, this class of oligosaccharides exhibits a bent geometry. It has been suggested that mixed-linked glucans play a role in cell expansion during the development of certain plants. ¹⁶⁹

3.2.3 Chitin

Chitin, the second most abundant polysaccharide, is a linear polymer comprised of N-acetyl-D-glucosamine units linked through $\beta(1\to 4)$ glycosidic bonds. If the residues on the chain are not N-acetylated, then the polysaccharide is referred to as chitosan. ^{170,171} As the range of deacetylated residues is quite large (20–100%), chitosan represents a large class of polysaccharides. ¹⁷² Chitin is found in the shells of many animals including crustaceans, insects, and other arthropods, as well as the cell walls of fungi. ¹⁷³ Similar to cellulose, the linear polymer packs to form a tight crystalline microstructure, thereby providing structure and protection. Chitin itself is polymorphic and can be grouped into three different forms: alpha, beta, and gamma. Alpha chitin is found in the exterior shells of arthropods, sponges, and fungi. ^{174–176} Strands of alpha chitin are arranged in an antiparallel manner. It is the most stable form of chitin and is thought to have the most inter-sheet hydrogen bonding contacts. ^{170,177} Beta chitin, which is found in squid, ¹⁷⁶ is made up of parallel chitin strands and does not have as many hydrogen bonds as crystalline forms of chitin. Found in fungi, gamma chitin is comprised of two parallel strands with alternating antiparallel strands. Given the structural similarity, this may just be a variant of alpha chitin. ^{175,176}

3.2.4 Starch

Since starch induces negligible osmotic pressure, it is advantageous for organisms to store glucose in this form. To date, starch-active PMOs have only been shown to be active on two types of starch: amylose and amylopectin. Both of these polysaccharides have repeating units of $\alpha(1 \rightarrow 4)$ linked glucose, but amylopectin also contains repeating branch points at the C6 carbon of the amylose chain. Plant-based starch is generally comprised of 15–35% amylose and 65–85% amylopectin. Amylose is a crystalline helical bundle tightly packed in a double helix; small molecules, such as lipids, may be present in the central cavity of the helix. Amylopectin is an amorphous branched $\alpha(1 \rightarrow 4)$ linked glucose polymer with dispersed $\alpha(1 \rightarrow 6)$ linkages to other starch chains.

3.3 Methods to Characterize PMO Activity

An intrinsic challenge in studying the reactivity of PMOs is the insolubility of polysaccharide substrates. Advanced imaging techniques, such as scanning electron microscopy (SEM) and atomic force microscopy (AFM), have observed gross changes in the morphology of the polysaccharide nanostructure. ^{186–188} Imaging techniques including synchrotron-based UV imaging and infrared spectroscopy, which monitor real-time interactions between a PMO and its polysaccharide substrate, as well as SEM and AFM measurements, have provided insight into the physiological action of these enzymes on recalcitrant polysachcarides. ^{189–191}

Spectroscopic techniques are commonly employed to probe the geometric and electronic environment of the PMO copper active site. The d⁹ configuration of the Cu(II) ion, which has a single unpaired electron, is amenable to EPR spectroscopy (see Section 2.1.2). This technique has been used to extensively study the Cu(II) form of the enzyme and elucidate changes in the coordination environment of the copper center upon substrate binding.²⁰³ Moreover, insoluble substrates do not interfere with EPR, making this an advantageous technique to understand the Cu(II) active site. X-ray absorption spectroscopy (XAS) (see Sections 2.1.1, 2.2, and 2.2.2) has also been employed to understand the geometry and electronic structure of the PMO active site.^{204,205} One pitfall of this method is that the Cu(II) center is susceptible to photo-reduction by the X-ray beam. Since these spectroscopic properties are dependent on oxidation state, it can be difficult to interpret data and make unequivocal assignments, as the data may reflect heterogeneous mixtures of the Cu(I) and Cu(II) forms of the enzyme.

Determination of structures for every AA family has been accomplished with the exception of the AA16 family (see Section 4.2.). These structures have provided insight into the overall tertiary and active site structure of PMOs; they have also revealed the molecular details of substrate binding and protein-protein interactions (see Section 4.3). NMR has been successfully employed to determine a solution structure of a PMO and to map binding interactions with substrate and cellobiose dehydrogenase (CDH). ^{197,206}

New chemical tools are being developed that provide faster ways to study PMO reactivity. Specifically, methods that enable multiplexing or high-throughput screening are of interest, particularly those that utilize fluorogenic- and chromogenic-based methods. Glycan arrays are promising technologies that will aid in the determination of polysaccharide specificity and potentially identify new polysaccharide substrates. ^{207,208} In the absence of a polysaccharide substrate, the Cu(I) PMO reacts with H₂O₂ and subsequently oxidizes 2,6-dimethoxyphenol to form the colored product coerulignone. ²⁰⁹ This assay not only aids in the identification and purification of PMOs, but can also be used to monitor enzyme activity. Alternatively, strategies that label C1 oxidized sites on insoluble substrates ²¹⁰ or soluble oxidized products ²¹¹ have been employed to identify products from PMO reactivity, thereby increasing the rate of product identification and quantification and simplifying data analysis. A related method non-reductively labels C4 oxidized products with 2-aminobenzamide and these products are identified by reversed-phase high performance liquid chromatography using a UV-vis detector coupled with electron spray ionization mass spectrometry (ESI-MS). ²¹² This method removes the mobile phase buffer required for HPAEC-PAD and enables in-line detection of soluble C4 oxidized products.

4 Structure of PMOs

In this section, the overall structure and domain architecture of PMOs are discussed. The understanding of PMO-polysaccharide binding contacts and the formation of the active site oxidant are discussed in terms of conveying regionselective oxidation of the glycosidic bond.

4.1 Domain Architecture of PMOs

PMOs are globular proteins that have a central β-sandwich fold with loops and helices that contain the active site and provide contacts for substrate binding. This structure is similar to the fibronectin III (FNIII) fold and, by extension, immunoglobulin domains. PMOs are targeted for secretion into the extracellular space via a cleavable N-terminal signal peptide, where the fold of the protein and post-translational glycosylation provides overall stability of the enzyme. While PMOs are often thought to freely diffuse in the extracellular space, bioinformatics analysis has identified some PMO sequences with glycosylphosphatidylinositol (GPI) anchors, which fuse the enzyme to the cell wall. The domain architecture of PMOs is highly modular, ranging from single catalytic domains (most common) to large multi-domain polypeptides (Fig. 8). These proteins are active as monomers with only a single mononuclear copper center and no other redox cofactors in the protein, making PMOs distinct from other copper-containing monooxygenases.

The next most common architecture consists of a catalytic domain and a C-terminally fused carbohydrate binding module (CBM) or another type of polysaccharide-binding domain (e.g., WSC or GbpA domain). The presence of these domains can help guide substrate identification. For example, starch-active fungal PMOs were discovered, in part, by identifying the starch-specific CBM20 domain. Functional differences between single domain PMOs and CBM-containing PMOs are apparent from extensive biochemical analysis. While it appears that single domain PMOs have evolved to efficiently bind polysaccharide substrates, the non-catalytic CBM domains increase polysaccharide binding affinity and specificity. Several studies have demonstrated that a CBM assists catalytic efficiency by conferring polysaccharide specificity and enhancing binding affinity.

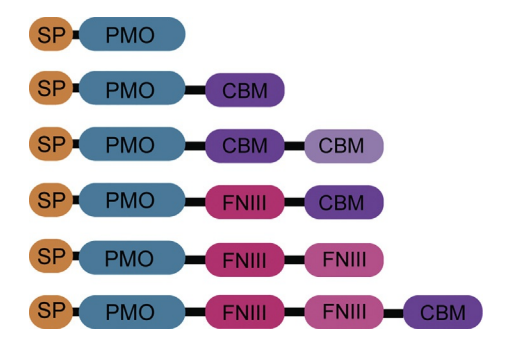


Fig. 8 Representative modular domain architectures of PMOs. The N-terminal signal peptide (SP, orange) is cleaved to generate a free amine and His1 of the catalytic PMO domain (teal). A variety of different carbohydrate-binding module (CBM, purple) families may be appended to PMOs and include CBM1 (chitin specific), CBM2 (cellulose, chitin, or xylan binding), CBM5/12 (chitin specific), CBM14 (chitin specific), CBM19 (chitin specific) and CBM20 (starch specific). Domain architectures are not drawn to scale and linker sequences (black lines) vary in length.

The removal of native CBMs significantly impairs polysaccharide binding. ^{217,221,222} These fused domains may also help protect the enzyme from inactivation. Since the catalytic cycle likely proceeds through a highly reactive oxidizing intermediate, enhanced substrate affinity can limit enzyme inactivation by protecting the active site. The presence of a CBM often alters the product distribution and produces oxidized products of shorter length, suggesting that CBMs may have a role in targeting the crystalline polysaccharide lattice and increasing the binding interaction between the PMO and specific regions of the lattice. Therefore, it is likely that single domain PMOs and PMOs containing at least one polysaccharide-binding domain have evolved for distinct roles in polysaccharide degradation.

PMOs in the PF03067 Pfam are commonly associated with FNIII domains, which are typically located on the C-terminus of the AA10 catalytic domain. Some PMOs have multiple FNIII domains that are often followed by a C-terminal CBM, but other architectures lack a CBM. It has been shown that FNIII domains connected to glycosyl hydrolases help modify the crystalline surface of polysaccharides, facilitating hydrolytic activity. PNIII domains may serve a similar role when fused to PMO catalytic domains, although removal of these domains has not altered catalytic activity or substrate binding. Other, less frequently encountered domains identified in the polypeptide sequence with either fungal or bacterial PMO catalytic domains include: glycoside hydrolases (GH), polycystic kidney disease (PKD) domains, extracellular membrane protein CFEM domains, cytochrome *b* domains, short chain dehydrogenase domains, and dopamine β-monooxygenase (DβM) N-terminal domains (DOMON). DOMON domains are capable of binding heme, which may serve as an electron source for PMOs, analogous to their role in DβM catalysis. The biochemical characterization of PMOs with these domain architectures and their functional relevance has yet to be reported.

4.2 Active Site Contributions to Reactivity

PMOs contain a N-terminal signal peptide that targets the enzyme for secretion, and subsequent cleavage yields the N-terminal histidine residue required for activity. All PMOs bind the active site copper ion through a unique histidine brace motif in a planar T-shape, leaving an open coordination site for co-substrate binding (Fig. 9). The brace consists of two histidines in a *trans* arrangement and the N-terminal amine. The first histidine residue in the canonical sequence serves as a bidentate ligand, where the N-terminal amine and His1-N $_{\delta}$ coordinate to the copper center. Consequently, the binding affinity for Cu(II) is very tight, with a $K_{\rm D}$ typically in the low nanomolar range (0.8–62.5 nM).

Early studies identified differences in both the primary and secondary copper coordination spheres of bacterial and fungal PMOs. 107,228,233 This may reflect differences in reactivity, substrate specificity, and potentially the active site oxidant. The His1 is Nɛmethylated in nearly all fungal PMOs, whereas bacterial PMOs lack this post-translational modification (PTM). Since the histidine brace is central to the oxidative activity of the enzyme, the copper coordination chemistry has been intensely studied. There have been conflicting reports on the protonation state of the N-terminal amine, which impacts the accessibility of various oxidizing intermediates (see Section 5.4). $^{234-236}$ The role of histidine methylation, which is likely significant for PMO function, is also debated. The electron donating nature of the methyl group could increase electron density on the copper, thereby tuning co-substrate binding at the metal center and modulating enzyme reactivity. 206 Indeed, histidine methylation (Nɛ or Nô) increases H_2O_2 production in amyloid- β peptides, 237 and increases reactivity of de novo designed copper nitrite reductase peptides. 238 Conversely, computational studies suggest that this PTM has little influence on PMO reactivity. 239 It is possible that methylation helps lock the His brace into one tautomeric form, thereby increasing rigidy. 227 Experimental studies indicate that His methylation has little influence on PMO reactivity and was proposed to help protect the PMO from inactivation by \bullet OH. 240 Although the effect

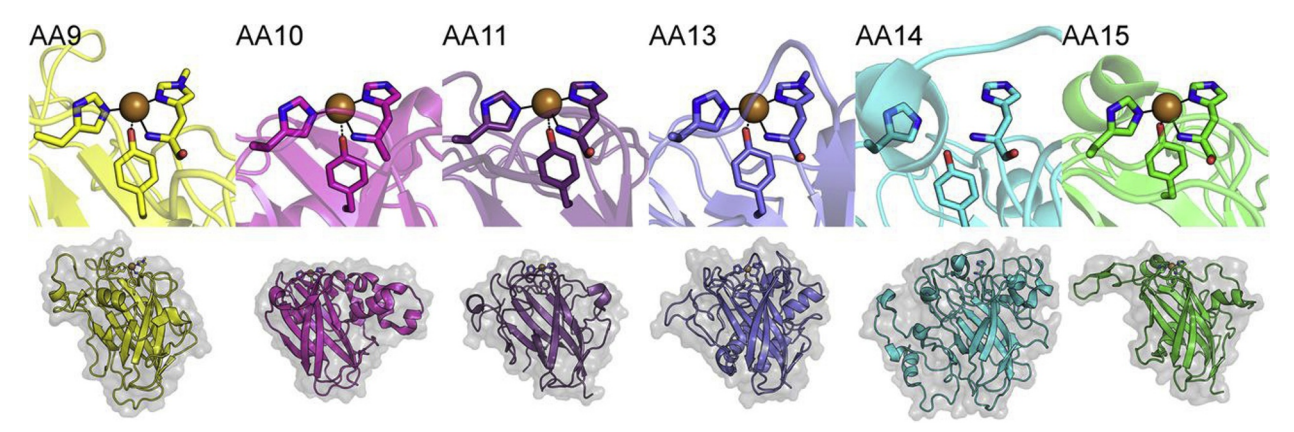


Fig. 9 Overall fold and active site structure of PMO families. All PMO families coordinate a copper center through a conserved histidine brace motif. Methylation of His1 is observed in AA9 and AA13 structures. All natively expressed fungal PMOs likely contain this post-translational modification. While the AA14 PMO structure was obtained without copper, the metal center is still required for activity. A representative structure for the AA16 family has not yet been reported. Reproduced with permission from, Tandrup, T.; Frandsen, K.E.H.; Johansen, K.S.; Berrin, J.-G.; Lo Leggio, L. Recent Insights Into Lytic Polysaccharide Monooxygenases (LPMOs). Biochem. Soc. Trans. 2018, 46, 1431–1447.

of *N*-methylation remains ambiguous, the significant question that remains unresolved is why this PTM is absent in bacterial PMOs, but present in all fungal PMOs.

Fungal PMOs have a tyrosine (Tyr) residue located in close proximity to the copper center, axial to the histidine brace. Conversely, most bacterial PMOs, including the AA10 family, have a phenylalanine (Phe) in this position, although a subset of cellulose-active bacterial PMOs have an axial Tyr. Structures of AA9 PMOs indicate this Tyr is often too far away to directly coordinate, but it may be sufficiently close in AA13²⁴¹ and AA15¹¹² structures. However, there are substantially fewer structures for these families, so this may not be a general phenomenon. Cautious interpretation of bond lengths surrounding the active site is necessary because the enzyme can potentially be photo-reduced during data collection, and Cu(I) and Cu(II) have different coordination preferences. Since the EPR spectra of AA14 and AA9 PMOs are quite similar, it is likely that the active sites of these enzymes are quite similar. The neutral axial tyrosine plays a key role in PMO reactivity by tuning the electronic structure of the active site and influencing O₂ reduction activity.²⁴² Conversely, bacterial PMOs with a native Phe exhibit extremely low O₂ reduction activity; mutations of native Tyr residues to Phe also decrease O₂ reduction activity.^{225,243} These findings suggest that the tyrosine influences the kinetically and thermodynamically challenging step of O₂ reduction at the copper active site. In AA9 PMOs, this Tyr and nearby electron wire comprised of aromatic residues have been proposed to serve as a means of protecting the protein from oxidative damage from catalytic intermediates^{243a} (see Section 5.5).

An extensive hydrogen bonding network in the secondary coordination sphere also influences PMO activity. 244,245 The number of hydrogen bonding residues varies with AA family, and has been partially attributed to the presence (or absence) of the axial Tyr. 246 Perturbation of this network diminishes the activity of the enzyme. 244,245,247 Of particular interest is a conserved Gln (or Glu in some PMOs) that occupies a similar position in proximity to the active site in all PMOs. 248 Mutation of the glutamine led to the release of $O_2^{\bullet-}$ and a decrease in product formation, suggesting that this residue stabilizes a Cu-superoxo intermediate. 245 Additionally, this residue could provide the protons necessary to reduce oxygen to hydrogen peroxide. 235,245 While chitin-active bacterial PMOs do not have this H-bonding network, 130 the conserved glutamate (Glu) is located in a similar position and may hydrogen bond with an active site water molecule. Molecular dynamics (MD) simulations suggest the Glu serves as a gate, controlling co-substrate access to the active site. 249 This subtle difference in the second coordination sphere of PMOs may point to differences in co-substrate reactivity and the molecular mechanisms between families of PMOs (see Section 5).

4.3 Substrate Binding and Regioselective Oxidation

Both the solvent-exposed active site and the substrate-binding surface vary among PMO families. AA9, AA10, and AA11 PMOs have a relatively flat substrate-binding surface that is ideal for the active site to interact with the crystalline lattice of cellulose or chitin. Conversely, AA15 PMOs do not have a flat polysaccharide-binding surface, although they are active on chitin and cellulose. Instead, a β -tongue-like motif extends between two loops with a surface-exposed Tyr residue that could be involved in substrate binding. While this is a unique structural motif within the PMO superfamily, the sequence that comprises this protrusion is not strictly conserved across the family and thus may not be a representative characteristic of all AA15 PMOs. Nonetheless, the relevance of this motif and functional significance in substrate recognition and binding is of interest. The AA13 family also has a distinct binding surface compared to cellulose and chitin active PMOs. The AA13 family has a groove in the substrate binding surface that conforms to the helical starch substrate amylose, and is thought to help confer substrate specificity. 241,250 The structure of a protein, LaX325 (UniProtKB A0A4P918G4, PDB 6IBI), from the X325 family has also been reported. While sharing an overall similar fold to PMOs, X325 proteins possess an axial Asp ligand at the Cu and lack a flat polysaccharide binding surface.

A limited number of PMO structures have been reported with a soluble polysaccharide substrate bound at the active site. While these static structures represent thermodynamically favorable conformations of the PMOs and do not capture the dynamic flexibility of the protein, they do provide insight into enzyme-substrate contacts. *Ls*AA9A (UniProtKB A0A0S2GKZ1) is the only PMO for which structures have been obtained with bound oligosaccharide substrates: xylose, glucomannan, or cellulose. ^{195,251} These structures suggest that the co-substrate coordination site, and perhaps the chemical mechanism, is dependent on the identity of the polysaccharide substrate. Crystal structures with bound cellohexaose suggest that the most likely position for the co-substrate (O₂ or H₂O₂) to bind is in the equatorial plane, *trans* to the N-terminal amine (PDB 5ACI, 5NLS). A structure of a similar PMO, *Nc*PMO-2 (UniProtKB Q8WZQ2, PDB 5TKF), contains density consistent with a reduced O₂ adduct in the equatorial plane in the absence of substrate. The equatorial positioning of the co-substrate suggests that the O—O bond would need to be cleaved in order to generate an active site oxidant (i.e., Cu-oxyl) with the spatial orientation necessary for hydrogen atom abstraction (HAA).²³⁶

In contrast to the cellulose-bound structure, structures with bound oligo-xylose exhibit a distortion in the polysaccharide chain, which forces axial coordination of the co-substrate (PDB 5NLO). In this orientation, a Cu/O_2 adduct with an intact O—O bond (i.e., Cu-superoxo or Cu-peroxo) has the appropriate spatial positioning to abstract a hydrogen atom from xylose. In the absence of substrate, reduced O_2 species have been observed crystallographically in the axial position (PDB 4EIR), indicating the feasibility of O_2 reduction in this coordination mode. A computational study has suggested that molecular oxygen can bind in the axial position and found the most favorable oxidant is a species with a cleaved O—O bond (i.e., Cu-oxyl, see Section 5.4.4). Experimental biochemical evidence will help resolve the differences in substrate positioning between computational studies and crystal structures.

Contacts between the polysaccharide substrate and PMO at the substrate-binding interface confer regioselectivity in substrate oxidation. ^{129,243,252,253} Since the core fold of PMOs is conserved, the loops on the substrate-binding surface are primarily responsible for substrate recognition and binding, and, by extension, oxidation regioselectivity. MD simulations, using elastic network models, show that these loops are flexible, ²⁵⁴ and the movements vary among AA families. For example, the molecular

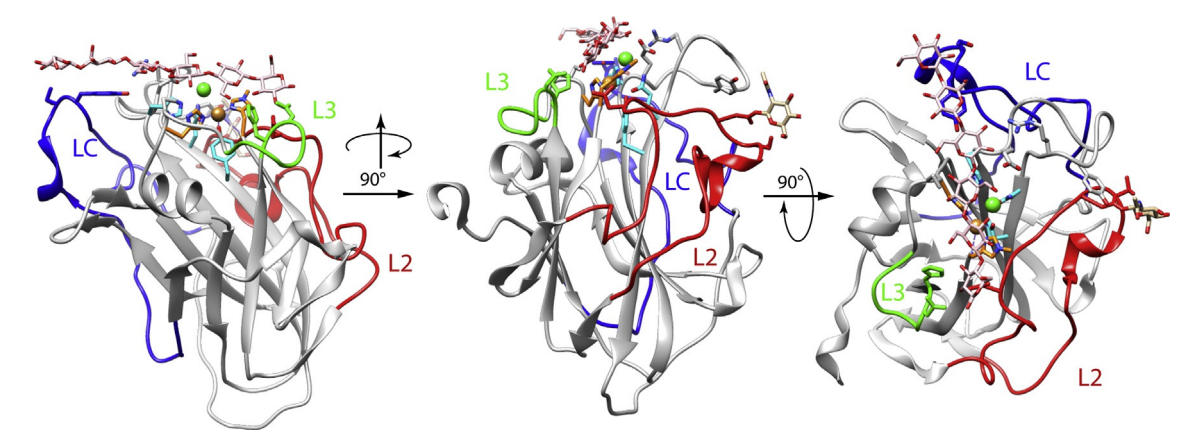


Fig. 10 Representative tertiary structure of an AA9 PMO. The illustrated structure is LsAA9A in complex with cellohexaose (PDB 5ACl). Loops that are important to oxidative regioselectivity are labeled: LC (blue), L3 (green), L2 (red).

motions of AA10 PMOs differ from those of fungal AA9 and AA11 PMOs. In general, these loops contain hydrogen bonding residues (e.g., asparagine and glycosylated asparagine) and aromatic residues (e.g., tyrosine and tryptophan) that can participate in carbohydrate stacking interactions with the polysaccharide substrate. Deletion or insertion of loops in fungal PMOs first indicated that these structures play a key role in regioselectivity of substrate oxidation. In particular, the L2 loop is important for regioselectivity in both bacterial and fungal PMOs (Fig. 10). ^{243,252} Mutations along the LC and L3 loops demonstrate that these regions confer some control over regioselectivity. ²⁵² However, mutations on the substrate-binding surface of *SmLPMO10A* (UniProtKB O83009) did not alter regioselectivity, but had a significant impact on overall substrate conversion. ²⁵⁵ Ultimately, these residues, which are distant from the active site, have a profound effect on the positioning of the glycosidic bond with respect to the oxidizing intermediate. ^{129,243,252,253}

Regioselective C1 or C4 hydroxylation of the polysaccharide substrate is achieved by positioning the glycosidic bond in proximity of a reactive Cu/O_2 based oxidant resulting from the activation of the co-substrate (O_2 or H_2O_2) (see Section 5.4). Hydroxylation of the C1 or C4 position of the glycosidic linkage generates an inherently unstable hemiketal intermediate that spontaneously eliminates to generate unique regiospecific oxidized products. C1 hydroxylation results in the formation of aldonolactone products, which subsequently hydrolyze to form aldonic acids, while C4 hydroxylation yields 4-ketoaldoses and the hydrated *gem*-diol as products (Fig. 11).^{7,108,256} Oxidation of the C6 position in non-branched cellodextrins has also been observed.¹⁹⁹ While most chitin-active PMOs form C1 oxidized products, some can generate both C1 and C4 oxidized products.²²⁹ Table 1 shows the C—H regioselectivity for each PMO family. The AA9 family contains three subclasses based on the primary sequence that are categorized by regioselectivity: PMO1, PMO2 and PMO3, which are C1, C4, and C1/C4 oxidizing enzymes, respectively. In the PMO3 subclass, there is a distinct subset of PMOs, denoted as PMO3*, that only oxidize the C1 position. Starchactive PMOs (AA13) only oxidize the C1 position of $\alpha(1 \rightarrow 4)$ linkages. Although $\alpha(1 \rightarrow 6)$ linkages are present in amylopectin, it seems unlikely that the PMO can position this branch point in the active site for hydroxylation.

The observed regioselective oxidation of hemicelluloses is more complicated than homogeneous substrates. With the exception of xylan, these polysaccharides are hydroxylated at unmodified glucose residues in the backbone that are connected through $\beta(1\rightarrow 4)$ linkages. As in the case of other substrates, the L3 loop has been implicated in hemicellulose recognition based on crystal structures of NcPMO9C (UniProtKB Q7SH18, PDB 4D7V, 4D7U). However, the hemicellulose-active PMO GtLPMO9A-2 (GenBank BAV57612.1) lacks this loop and, unlike NcPMO9C, can cleave any position of xyloglucans, suggesting this loop may help confer selectivity for the XG motif. Although the AA14 active site is not flat, it contains a clamp comprised of two loops, corresponding to the L2 and L3 loops in other PMOs, that likely enhances binding to the xylan substate. As the only characterized AA14, PcAA14 is active on xylans, but only if the xylose chain is linked to cellulose. In addition to cellulose, NcA9C hydroxylates xyloglucans with XGXG and XXXG motifs at the C4 position to give XXXG–OH or XG–OH. This PMO oxidizes any unsubstituted glucose unit in the xyloglycan backbone, regardless of the surrounding substitution pattern. PaLPMO9H (UniProtKB B2ADG1) and GtLPMO9A-2 both have similar activity and can hydroxylate substrates at both the C1 and C4 positions. Struck and XXGG type xyloglycans, oxidizing any position along the backbone.

Although NcAA9C is active on glucomannans, it does not oxidize pure oligo-mannan substrates. The product profiles from glucomannan oxidation indicate that the enzyme can only cleave $\beta(1 \rightarrow 4)$ glucose linkages. Similarly, both LsAA9A and CvAA9A (GenBank AST24379.1) exhibit low activity when cleaving glucomannans at the mannose residues, but no activity is observed with pure mannose. LsAA9A and CvAA9A oxidatively cleave mixed-linkage glucans and glucomannan, but these PMOs only modify the $\beta(1 \rightarrow 4)$ sites. These results suggest that PMOs have some promiscuity in substrate recognition, enabling other substrates to be cleaved. Overall, these observations are consistent for many AA9 PMOs that are active on both cellulose and various hemicelluloses,

Fig. 11 Regioselective oxidation of polysaccharide substrates. Hydroxylation of the C1–H or C4–H (black filled 0-atom) and subsequent nonenzymatic elimination of the glycosidic bond forms aldonolactone and 4-ketoaldose products, respectively. Aldonolactones and 4-ketoaldose products can hydrate to form aldonic acids and *gem*-diols, respectively. R = glycosyl unit.

suggesting that they may serve a more general purpose, namely to increase the accessibility of hydrolases, the workhorses of cellulolytic degradation.

NcAA13 (UniProtKB Q7SCE9), the first PMO discovered to oxidize starch, has a C-terminal starch-specific carbohydrate binding domain (CBM20) and oxidizes amylose, amylopectin, and cornstarch. Other characterized AA13 PMOs do not yield detectable oxidized products when incubated with amylopectin or cornstarch, which primarily consists of amylopectin. Therefore, it seems that PMO-mediated starch degradation is specific to crystalline amylose. The enzyme creates new chain ends on the helical bundle for exo-amylases, facilitating the synergistic degradation of amylose into soluble glucose fragments. Branching in the amylopectin substrate may prevent the detection of soluble fragments, or may inhibit the enzyme. De-branching enzymes that hydrolyze both $\alpha(1 \rightarrow 4)$ and $\alpha(1 \rightarrow 6)$ linkages likely work synergistically with AA13 PMOs to degrade starch. Indeed, two AA13 PMOs (NcAA13 and MtAA13 [UniprotKB G2QP40]) show \sim 100-fold more soluble products when incubated with amylose, relative to amylopectin or cornstarch.

5 Catalytic Mechanism of PMOs

PMOs are isolated in the Cu(II) oxidation state, exhibiting EPR-derived g values ($g_x \sim g_y = 2.02-2.05 < g_z = 2.25$) that are consistent with mononuclear type 2 copper species (see Section 2.3.2). The metal center exhibits trigonal bipyramidal or distorted square pyramidal geometry in almost all AA10 PMOs, whereas fungal PMOs adopt an elongated octahedral geometry. Neither co-substrate (O_2 or O_2 reacts productively with the oxidized form of the enzyme. Reduction of the PMO active site is an absolute requirement for catalysis and also increases the binding affinity for the polysaccharide substrate (O_2 or O_2 mM). Initial reduction of the active site is rapid (faster than enzyme turnover). Upon reduction, the coordination geometry of the copper active site changes, elongating the Cu—Tyr bond (if present) and releasing water/hydroxide ligands, to give a 3-coordinate T-shaped Cu(I) center. This geometry leaves an open equatorial coordination site for co-substrate binding, giving the expected square planar geometry for a Cu(I) center (see Section 2.1.1). This coordination change is a driving force for the increase in polysaccharide binding affinity. Occupancy of the polysaccharide substrate at the active site is important to maximize productive turnover and minimize the decoupling of O_2 reduction and substrate oxidation, which can lead to oxidative inactivation of the enzyme. Binding of the polysaccharide and co-substrate (O_2 or O_2) forms the ternary enzyme complex, which serves as the key intermediate from which all mechanistic pathways emanate.

Initial $^{18}O_2$ -labeling studies with bacterial and fungal PMOs confirmed the monooxygenase activity of these proteins. 7,108 Upon reduction of $^{18}O_2$, one ^{18}O -atom was incorporated into the polysaccharide substrate and led to cleavage of the glycosidic bond. In light of PMO reactivity with H_2O_2 , these experiments could instead generate $H_2^{18}O_2$ in situ, followed by ^{18}O incorporation into

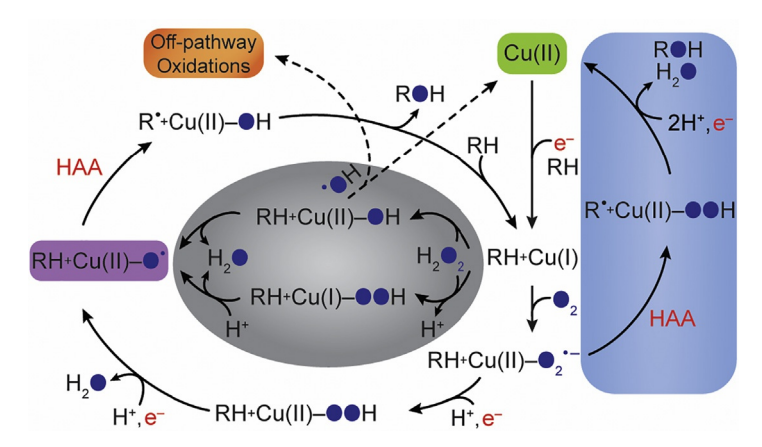


Fig. 12 General chemical mechanism of PMOs. PMOs begin in the Cu(II) resting state (green box). Reduction to Cu(I) increases polysaccharide (RH) binding affinity and enables co-substrate reactivity. Binding of 0_2 to Cu(I) PMO forms the Cu-superoxo intermediate. Following prototypical copper monooxygenase reactivity (blue box), the Cu-superoxo performs hydrogen atom abstraction (HAA). The two electron, reductive heterolytic cleavage of the Cu-superoxo (outer oval) generates a Cu(II)-oxyl (purple box), which can perform HAA. Peroxide reactivity (gray oval) can proceed through two mechanistic routes to generate the Cu(II)-oxyl. H_2O_2 reactivity with Cu(I) is reminiscent of Fenton chemistry (upper route) and can generate the Cu(II)-oxyl, but is also prone to off-pathway oxidations (orange box). H_2O_2 reactivity can also proceed through a Cu(I)-OOH intermediate (lower route). Reproduced with permission from, Hangasky, J.A.; Detomasi, T.C.; Marletta, M.A. Glycosidic Bond Hydroxylation by Polysaccharide Monooxygenases. *Trends Chem.* **2019**, *1*, 198–209.

the substrate. $H_2^{18}O_2$ labeling studies indicated that only ^{18}O is incorporated into the oxidized products, even in the presence of $^{16}O_2$. 266 However, reaction mixtures were analyzed after only 4 min and contained a low, "priming" amount of reductant (10 μ M); these constraints could have limited the ability of $^{16}O_2$ to react in these experiments. The exact identity of the intermediate responsible for hydrogen atom abstraction (HAA) is not known. The potential catalytic mechanisms involving O_2 and O_2 give rise to several distinct possibilities (Fig. 12). O_2 Reactions involving O_2 require the O_2 require the O_2 form of the enzyme, analogous to Fenton chemistry with iron, O_2 and likely generates a Cu-oxyl intermediate that performs HAA. Conversely, two predominant oxygenase mechanisms have emerged that differ in the identity of the oxidant, as well and the oxidation state in the initial and final forms of the enzyme. O_2 In the first mechanism, which is drawn from previous studies of copper monooxygenase activity (see Section 2.3.3), the enzyme starts and ends in the O_2 Cu(II) form, and HAA occurs prior to scission of the O_2 Dond. The second proposed mechanism enters the catalytic cycle after reduction by one electron. Subsequent delivery of two electrons and two protons cleaves the O_2 Dond and yields a Cu-oxyl as the HAA species. In this case, each catalytic cycle regenerates the O_3 Cu(I) form of the enzyme. If this second mechanism were operative, it is likely that O_3 reactivity serves as a shunt for oxygenase activity, circumventing the need for additional reducing equivalents.

A number of studies have reported pH-dependent activity of PMOs, demonstrating that optimal activity typically occurs between pH 6 and 8, but decreases below pH 6. The pK_a of histidine ($pK_a = 6.00$) and carboxylate sidechains ($pK_a = 3.65-4.25$) fall within this pH range, suggesting that decreased activity may reflect the protonation of one of these key residues. Similarly, pH-dependent rotation of a copper-coordinating His has been observed crystallographically, suggesting that altered ligand coordination at the copper center may be responsible for loss in activity at low pH.²⁷¹ At low pH, substrate binding rotates the His back into in the equatorial plane to coordinate the copper, yet the enzyme remains inactive, ^{193,271} suggesting that other factors influence activity. In light of reactivity with H_2O_2 , pH activity profiles should be revisited using H_2O_2 to distinguish pH-dependent O_2 reduction from H_2O_2 -mediated glycosidic bond hydroxylation. While the most common reductant used in biochemical PMO assays is ascorbic acid, other reductants, such as gallic acid and cysteine, are increasingly being used due to their stability and limited reactivity with O_2 . The reduction potential of the chosen reducing agent and the pH of the assay are important factors when choosing reductants, given that the reduction potential of most small molecules is pH dependent (\sim 60 mV per pH unit, assuming Nernstian behavior for a reversible one-electron transfer). This is a direct consequence of changes in the hydronium ion concentration and a change in the conjugate acid/base stability of the reductant.²⁷³

5.1 Details of 02 Reactivity

Upon reduction of the active site to Cu(I), O_2 binds to the copper and the affinity for the polysaccharide substrate increases. Detailed steady-state kinetic studies indicated that random-sequential binding of O_2 and the polysaccharide substrate (RH) form a ternary enzyme complex: RH Cu(II)– $O_2^{\bullet-}$. 193,204 It is likely that O_2 initially binds to the copper in an η^1 fashion (i.e., end-on) and the Cu(II)– $O_2^{\bullet-}$ is stabilized by a conserved glutamine in fungal PMOs. 245 Formation and stabilization of this intermediate is known for AA10 PMOs. Crystal structures of fungal PMOs with bound cellodextrin substrates indicate that no other residues are

able to provide hydrogen-bonding contacts, although water molecules are present. Chemical steps after the formation of the ternary complex are not clear, but O_2 reduction ultimately leads to product formation. The precise timing and delivery of electrons and protons is required to reduce O_2 and form the active site oxidant capable of HAA from the C—H of the glycosidic bond, without dissociating to form H_2O_2 . Unlike most other copper monooxygenases, $Cu(II)-O_2^{\bullet -}$ is frequently dismissed as the oxidant in PMOs because it is presumed to be insufficiently potent to perform HAA from a glycosidic C—H bond (see Section 5.4.1).

A subset of PMOs has been identified that oxidize soluble polysaccharide substrates, enabling homogenous reaction mixtures to be studied using standard enzymological techniques. While it is unclear if these PMOs encounter or act on these substrates in a physiological setting, a distinct cluster is observed in the SSN, suggesting a unique characteristic that sets them apart from other PMOs (Fig. 5). Steady-state kinetic characterization of the fungal PMO MtPMO9E with a soluble substrate has provided insight into the oxygenase mechanism. The turnover number for MtPMO9E ($k_{cat} = 0.28 \text{ s}^{-1}$) is comparable to the timescale on which PMOs interact with substrate. The catalytic efficiency is low ($k_{cat}/K_{M(O_2)} = 0.074 \text{ µM}^{-1}\text{min}^{-1}$), which could allow polysaccharide binding to occur prior to formation of the active site oxidant, thereby minimizing non-productive O_2 reduction and ultimately avoiding off-pathway oxidations that could lead to enzyme inactivation. Indeed, both single-turnover and steady-state kinetics with oxygen as the co-substrate did not show enzyme inactivation or off-pathway oxidations of the PMO. 193,267 At saturating concentrations of the soluble polysaccharide substrate (1 mM), the $K_{M(O_2)}$ is 235 µM, which is similar to dissolved O_2 concentrations (at 42°C) and is consistent with the extracellular function of the enzyme. With mounting evidence favoring a reduced O_2 currentation of kinetic data. To date, experiments cannot separate pure oxygenase activity from in situ generation of O_2 and subsequent reactivity.

The kinetics of the oxygenase reaction is similar to that of particulate methane monooxygenase (pMMO), which has a similar copper active site and oxidizes the strong C—H bond of methane (BDE \sim 105 kcal mol⁻¹). Although numerous studies have provided significant insight into the mechanism of pMMO, the exact mechanism remains unclear. Additionally, the metal stoichiometry of the pMMO active site has been also debated. However, quantum mechanical enhanced refinement of crystal structures and advanced spectroscopic techniques suggest a mononuclear copper active site. Since both enzymes have similar active site architectures and perform challenging transformations in oxidizing strong C—H bonds, it is possible that similar oxidants are employed with analogous mechanisms of activation.

5.2 Uncoupled 0₂ Reduction: Oxidase Activity

In the absence of polysaccharide substrate and presence of reductant, PMOs are able to reduce O_2 to H_2O_2 .¹⁹² This is not an uncommon occurrence with oxygenases, as many will reduce oxygen in the absence of substrate in vitro (e.g., cytochrome P450s). This activity, decoupled from substrate oxidation, can lead to inactivation of the enzyme and is always a concern when highly reactive, oxidizing intermediates are involved. In general, oxidase function is regulated by pH, which is consistent with the pH-dependent activity of PMOs. ^{193,278,279} There are several plausible explanations for this oxidase function in PMOs. This activity may simply be due to the combination of a surface-exposed active site, a poorly accessible insoluble substrate, and excess reducing equivalents. Alternatively, oxidase function may prevent off-pathway oxidations by •OH from Fenton-like chemistry, as PMOs do not have an enclosed active site to sequester active site oxidants. "Pre-processing" of O_2 into the more reactive co-substrate H_2O_2 to drive peroxidase reactions has also been proposed. ²⁸⁰ Finally, oxidase function may have a specific role in signaling pathways, as low H_2O_2 concentrations are known to serve as signaling molecules in various physiological pathways. ^{281–283}

5.3 Details of H₂O₂ Reactivity

Numerous reports have demonstrated that PMOs can use H_2O_2 as the co-substrate for polysaccharide oxidation. An attractive feature of H_2O_2 reactivity is that the mechanism only requires an initial pre-reduction of the active site, from Cu(II) to Cu(I), to enter the catalytic cycle, and each turnover returns the enzyme to the Cu(I) form. Therefore, no additional reducing equivalents are necessary, as H_2O_2 is reduced by two electrons relative to O_2 .

A compulsory-ordered ternary mechanism, a strict requirement that the polysaccharide substrate bind prior to H_2O_2 , has been proposed to form the ternary enzyme complex. ²⁶⁸ This is intriguing, since the rate of polysaccharide binding to the Cu(I) form of the enzyme would always need to exceed that of co-substrate binding in order to prevent the formation of deleterious •OH from Fenton-like chemistry and subsequent enzyme inactivation. Two computational studies suggest that an outer-sphere mechanism is used to activate H_2O_2 in a way that does not require binding to the copper center, ^{284,285} while another study proposed direct H_2O_2 coordination to the Cu(I) active site. ²⁸⁶ Computational studies predict that a Cu-oxyl is generated through hydroxyl radical chemistry. Homolysis of the O—O bond would generate •OH that is effectively 'caged' by the polysaccharide substrate and positioned for HAA from the Cu(II)–OH to generate a Cu(II)-oxyl (Fig. 12). ²⁸⁴ There is experimental evidence for the formation of •OH, as both non-specific oxidation of the enzyme and polysaccharide substrate have been reported. Since saccharides, such as mannitol, are efficient •OH scavengers, polysaccharides bound at the active site would likely serve a protective role. Nevertheless, oxidative damage and irreversible inactivation of the PMO highlights the deleterious effects of generating a hydroxyl radical in the enzyme active site.

Steady-state kinetics for the H_2O_2 -driven reaction have been reported for AA10 PMOs, using chitin nanowhiskers as a substrate. ^{268,287} The turnover number ($k_{cat} = 6.7 \text{ s}^{-1}$) and catalytic efficiency ($k_{cat}/K_{M(H_2O_2)} = 2 \times 10^6 \text{M}^{-1} \text{s}^{-1}$) are significantly faster

than for the O_2 -driven reaction. The estimated $K_{M(H_2O_2)}$ (2.8 μ M), combined with oxidative enzyme inactivation, indicates that PMOs would operate best with nanomolar concentrations of H_2O_2 . Steady-state kinetics of the AA9 PMO MtPMO9E with H_2O_2 and a soluble substrate were too fast to be accurately determined, but k_{cat} was estimated to be >15 s⁻¹. Biologically relevant H_2O_2 concentrations have been reported that span many orders of magnitude, making it difficult to interpret the relevance of $K_{M(H_2O_2)}$. Both the extracellular H_2O_2 concentration and the concentration of other peroxide-utilizing enzymes (e.g., catalase) will direct PMO reactivity either toward enzyme inactivation or productive turnover.

5.4 Potential Intermediates in Catalysis

Although oxygen is a potent oxidant, the triplet ground state provides kinetic stability toward most biological molecules, which are ground state singlets. Consequently, this presents a significant challenge for chemical reactions that use oxygen. To overcome this, Nature utilizes metals and other redox-active cofactors to reduce O_2 through readily accessible one-electron chemistry, which enables a wide range of biochemical transformations.

The mononuclear copper center, combined with the high bond dissociation energy (BDE) of the glycosidic C—H bonds they activate (\sim 96 kcal mol⁻¹), ^{288,289} makes PMOs an intriguing system to understand. The high BDE creates a significant reaction barrier, suggesting that a powerful oxidant must be generated, and/or the protein structure modulates the substrate C—H bond strength. Crystal structures of PMOs with bound cellulosic substrates suggest the enzyme does not modulate the substrate conformation to lower the strength of the C—H bond. Conversely, a kink in the glycosidic bond of bound hemicellulose substrates is observed by crystallography (PDB 5NLO); this may decrease the C—H bond strength and thereby lower the activation barrier for catalysis. Therefore, the identity of the active site oxidant is of considerable interest. One primary focus has been to identify the activated Cu/O₂ or Cu/H₂O₂ intermediate that performs HAA, which may depend on the combination of the co-substrate and polysaccharide. Potential intermediates in PMO catalysis are discussed below in the context of their ability to perform HAA (Fig. 13).

Fig. 13 Potential intermediates in the reaction mechanism of PMOs. Note: Nε-methylation of the coordinating histidine is not observed in AA10 PMOs. The color of the Cu center is based on the oxidation state (Cu(III), red; Cu(II), blue) (see Section 2 for a discussion of copper oxidation states). Cu/O₂ species with intact 0–0 bonds are illustrated with end-on (η^1) coordination, but side-on coordination (η^2) has not been ruled out experimentally.

5.4.1 Copper-superoxo: Cu(II)-02°-

Oxygen binds to copper centers either in an end-on (η^1) or side-on (η^2) fashion. Oxygen coordination is typically end-on for mononuclear metals, whereas side-on binding is usually observed in multinuclear copper centers, bridging the metal centers. In the absence of substrate, crystal structures of PMOs have exhibited a variety of reduced oxygen species $(O_2^{\bullet}$ and O_2°) in the active site, although the exact assignment of these species is ambiguous (PDB 4EIR, 4EIS, 5TKH). An X-ray crystal structure of PHM (PDB 1SDW, see Section 2.3.3) in complex with substrate and O_2 demonstrates end-on O_2 binding for this mononuclear copper enzyme. Computational studies suggest that molecular oxygen preferentially binds end-on in PMOs rather than side-on.

In the absence of a polysaccharide substrate, oxygen rapidly oxidizes the Cu(I) center in TaAA9 PMO to regenerate the Cu(II) form. This process proceeds through an inner sphere mechanism, indicating that O_2 binds to the copper center and is subsequently released as the superoxide anion. In the presence of a cellulosic substrate, the equatorial plane trans to the N-terminal amine is the most likely coordination site for O_2 . Binding at this site enables π back-bonding between an interaxial copper orbital (e.g., d_{xz}) and a π^* orbital of O_2 . This interaction increases the strength of the Cu—O bond and consequently weakens the O—O bond, increasing its oxidizing strength. The protein environment and hydrogen bonding networks may also help increase the oxidizing power of the Cu(II)-superoxo. Intra- and inter-molecular hydrogen bonds, as well as orbital overlap between the copper center and O_2 , contribute to the stability and reactivity of this intermediate. A Cu(II)- $O_2^{\bullet-}$ is the generally accepted oxidant in copper monooxygenases such as PHM and D β M, which oxidize C—H bonds with BDEs < 90 kcal mol⁻¹. She glycosidic C—H bond strength creates a formable barrier that must be overcome, suggesting that a more powerful oxidant is needed. Indeed, multiple computational studies have proposed that Cu(II)- $O_2^{\bullet-}$ is not potent enough to perform HAA from the glycosidic bond.

5.4.2 Copper-peroxo: $Cu(II)-O_2^{2-}$

Since PMOs produce H_2O_2 in the absence of substrate, it is possible that a $Cu(II)-O_2^{2-}$ could form. Addition of a single electron to $Cu(II)-O_2^{\bullet-}$ would generate this intermediate. However, this peroxo species would likely serve as an intermediate in the catalytic cycle rather than the oxidizing species because it is a relatively poor oxidant, comparable to the Cu-superoxo complex. ^{285,286}

5.4.3 Copper-hydroperoxo: Cu(II)-00H

The Cu(II)–OOH can be formed by the delivery of a proton to Cu(II)– O_2^{2-} or through proton-coupled electron transfer (PCET) to the Cu(II)-superoxo. Computations have shown the singlet spin state is more stable than the triplet. ²⁸⁶ There are three divergent routes through which a Cu(II)–OOH may react. First, Cu(II)–OOH could directly carry out HAA from the substrate. Second, delivery of a second proton generates H_2O_2 , a known product of the uncoupled reaction. Delivery of one or two electrons and a proton would further reduce the Cu(II)–OOH to form a Cu-oxyl species and H_2O . QM/MM calculations suggest that the site of protonation (the distal vs. proximal O-atom) is influenced by the presence of the polysaccharide substrate and the identity of the reductant, leading either to the release of H_2O_2 or the formation of a Cu(I)– H_2O_2 species. ²⁹³ Another study proposes that a conserved His in the second coordination sphere is involved in proton transfer. ²³⁵ Regardless, PCET to the Cu(II)–OOH can form a Cu-oxyl, which is a common intermediate in the chemical mechanisms for both proposed co-substrates.

Like $Cu(II)-O_2^{\bullet-}$, the -OOH unit can bind either side-on (η^2) or end-on (η^1) . Side-on coordination would position the glycosidic bond over the Cu(II)-OOH moiety. For many of the other possible oxidizing intermediates, there is a spatial disparity between the glycosidic C—H bond and the oxidant, so it is not clear how the oxidant would abstract a proton from the correct position of the substrate. Regardless of the coordination mode, Cu(II)-OOH is a poor oxidant, making HAA from the polysaccharide unfavorable. However, activation of Cu(II)-OOH could be achieved through H-bonding with the distal oxygen. Hood stabilized by a H-bond to the proximal O-atom has been observed in an artificial metalloprotein that is modeled after the PMO active site. H-bond stabilization may help minimize disproportionation (Cu(II)-OOH $\leftrightarrow Cu(I) + \bullet OOH$) to prevent subsequent Fenton-like chemistry. Similar to cytochrome P450s and peroxidases, H-bonds to the distal O-atom in Cu(II)-OOH may lead to O—O bond scission. He hydrogen bonding network in PMOs (see Section 4.2) has both conserved Gln and His residues that could serve such as role. However, there is a disconnect between computational studies and experimental evidence in the role of the conserved His. His can facilitate proton transfer, and is supported by experiments that show superoxide is released upon mutation of this residue.

5.4.4 Copper-oxyl: Cu(II)-0• or [Cu(III)-0]*+

Cu-oxyl species are potent oxidants that are short-lived in the gas-phase and have yet to be observed in a biological environment. Model complexes and computational studies have provided insight to the electronic structure and reactivity of Cu-oxyl intermedates. Determination of the oxidation state of this intermediate is complicated by the difficulty in unequivocally characterizing Cu(III) complexes (see Section 2.2) and the experimental challenge in sequentially delivering reducing equivalents. A Cu(III)–OH is isoelectronic with a protonated Cu(II)–O• and such species have been observed in synthetic complexes. The electron donating, anionic framework of these ligands helps to stabilize the Cu(III) oxidation state, thereby increasing the reactivity of the hydroxo ligand. It should be noted that formally Cu(III) complexes with extensive π systems and/or a high degree of covalency in the Cu-ligand bonds may be noninnocent (see Section 2.2). Characterization of these synthetic complexes shows that this species is capable of HAA from C—H bonds with BDEs >90 kcal/mol. Analogous to Fe(IV)=O in

 α KG-dependent dioxygenases and P450's, the Cu-oxyl is potent enough to oxidize the strong glycosidic C—H bond. Proposed mechanisms for the reactivity of O_2 and H_2O_2 can both converge on a Cu-oxyl intermediate (Fig. 12). Cu(I) can react with H_2O_2 to generate a Cu(II) $-O_1$ without the need for additional protons or electrons. Oxygen can react with the Cu(I) center to form either a Cu(II) $-O_2$ or Cu(III) $-O_3$ upon the addition of two protons and three or two electrons, respectively. If the Cu-oxyl were responsible for HAA, H_2O_2 reactivity could serve as a shunt for O_2 reactivity, based on the electron and proton stoichiometry.

Several computational studies favor a chemical mechanism that invokes a Cu-oxyl as the HAA species. It has been speculated that the active site of PMOs is well-suited for the stabilization of this highly reactive intermediate. Whereas P450s rely on the electron rich porphyrin to stabilize the ferryl (Fe(IV) = O) intermediate, PMOs may rely on increased electron density at the copper from structural features, such as the deprotonated N-terminus and the *N*-methylated histidine. The Tyr in fungal PMOs may also have a role in stabilizing a Cu-oxyl. Indeed, computational studies have suggested that the axial Tyr influences the reactivity of a protonated Cu(III)-oxyl (i.e., Cu(III)-OH), but not the Cu(II)-oxyl.³⁰⁵ Formally a [Cu-OH]³⁺, the Cu(III)-oxyl could also be described as a Cu(II)-oxyl with a Tyr radical cation. A Cu-Tyr radical cation can be formed by treating the reduced PMO with H_2O_2 . This species is not observed in the presence of substrate, which indicates that, while the radical cation can form, its role during productive catalysis remains unclear.^{243a,305a} Since AA10 PMOs typically have an Phe in the axial position, perhaps [Cu-OH]³⁺ is not the active-site oxidant that performs HAA. Alternatively, different PMO families may have distinct mechanisms that do not share a common oxidant.

5.4.5 Hydroxyl radical: • OH

Hydroxyl radicals are powerful reactive oxygen species with high reduction potentials (1.8–2.7 V vs. NHE), resulting in rate constants that are typically diffusion limited ($10^9-10^{10} \text{ M}^{-1} \text{ s}^{-1}$). While H_2O_2 reactivity is speculated to generate a copper-oxyl through "controlled Fenton-chemistry," there is no evidence that •OH is generated through monooxygenase activity. Confined within the enzyme active site by the polysaccharide substrate, •OH can preferentially perform HAA from Cu(II)–OH to form Cu(II)–O•. Alternatively, •OH may perform HAA from the polysaccharide substrate followed by rebound from the Cu(II)–OH.

5.5 Electron Transfer Mechanisms

PMO activity requires reduction of the copper active site, making electron transfer an essential aspect of PMO catalysis. Bacterial PMOs have reduction potentials that range between 250 and 370 mV vs. SHE, 206,228,229 whereas fungal PMOs have reduction potentials ranging from 155 to 326 mV vs. SHE. 107,196,218 All PMO reduction potentials are higher than the aqueous Cu(I)/Cu(II) couple (160 mV) (Fig. 1) and comparable to the mononuclear copper center in cupredoxins (250–350 mV, see Section 2.3.1). This relatively low potential could account for the ability of various biological, chemical, and photo reductants to reduce the PMO active site. This promiscuity has complicated the interpretation of physiologically relevant electron donors, but has provided flexibility in the types of reductants used in industrial cocktails for cellulolytic degradation. Since H_2O_2 reactivity requires only one initial reducing equivalent to initiate catalysis (see Section 5.3), the identity of the reducing agent should have a minimal effect on H_2O_2 reactivity. Conversely, oxygenase reactivity requires two or three electrons to reduce a copper-superoxo intermediate and complete the catalytic cycle (see Section 5). Delivery of these electrons depends on the reduction potential of the reductant and the Cu/O_2 adduct(s), which will influence the observed rate of turnover. The mechanism of PMO reduction will be fully elucidated by determining the binding sites of the reductant and the delivery mechanism of electrons to the active site.

Physiological electron transfer has been studied most thoroughly in fungi. When fungi are grown on wood, cellobiose dehydrogenase (CDH) is upregulated; 306,307 knock-out of CDH in *N. crassa* drastically impairs oxidative degradation of cellulose. ¹⁰⁹ CDH is an extracellular flavin/heme protein that may be appended to a CBM to help bind polysaccharides. ³⁰⁸ Consequently, this enzyme has been invoked as one of the major biologically-relevant electron donors for PMOs. ^{109,309} CDH uses the flavin-containing domain to oxidize the disaccharide cellobiose to cellobio- δ -lactone, yielding two electrons. The electrons are shuttled to the heme-containing cytochrome domain, which directly interacts with the copper PMO active site and delivers the electrons sequentially. ³¹⁰ While rates as high as 20.6 s⁻¹ have been measured, PMOs typically oxidize CDH at a rate of 0.5–2.4 s⁻¹, which is commensurate with the turnover rate. However, CDH interacts with the same side of the PMO as polysaccharide substrates, ^{197,242,311,312} making the delivery of the second electron physically complicated.

Since not all fungi that contain PMOs encode CDH, other biologically-relevant redox mediators are necessary. One potential enzyme family is the pyrroloquinoline quinone (PQQ)-dependent pyranose dehydrogenases.³¹³ These fungal enzymes have a similar domain architecture to CDH, but contain a PQQ cofactor instead of a flavin.³¹⁴ These enzymes use PPQ to catalyze the two-electron oxidation of various sugars. Intramolecular electron transfer to a heme enables sequential one-electron reductions of suitable acceptors. Fungal PQQ-dependent dehydrogenases are able to reduce PMOs and drive oxidative activity.³¹⁵ Although the mechanism of electron transfer is unknown, it is likely similar to that of CDH.³¹⁵

Long-range electron transfer mechanisms have also been proposed for PMOs. This is an attractive model because substrate binding occludes the copper active site. PMOs lack a second redox site to store an additional electron, as opposed to other copper monooxygenases, such as PHM (see Section 2.3.3). There is a chain of aromatic residues that would be suitable to facilitate electron transfer from the surface of the protein to the active site. ^{130,290,316} In this way, an electron carrier can bind to the PMO far from the active site and shuttle electrons to the copper center, rather than through direct electron transfer (ET). Long-range electron transfer from lignin can effectively reduce PMOs and promote oxidative activity; this process is mediated by low molecular weight lignin-derived compounds. ^{317,318} Metabolites including 3-hydroxyanthranilic acid, catechin, ferulic acid, and sinapic acid, as well as

plant-derived quinones, can also provide the reducing equivalents for PMO activity. 317,319 Some of these molecules can be regenerated by extracellular GMC oxidoreductases, creating a redox cycle that can help sustain enzyme catalysis. An analysis of LsAA9 identifies an electron hopping pathway that may directly supply electrons from solvent to prevent oxidative protein damage during catalysis. Each of these residues, which are conserved in the AA9 family, was oxidatively modified, enabling the buildup and observation of the Try radical cation. 243a The exact mechanism involved in long-range ET still remains to be elucidated for PMOs, and may be the key to understand the discrete steps in PMO catalysis and the overall function of these enzymes.

Conversely, bacteria lack CDH and it is unclear if bacterial PQQ-dependent dehydrogenases can drive PMO activity. External oxidoreductases, analogous to CDH, may be operative and could provide electrons for bacterial PMOs. It has been shown that two genes in *Cellvibrio japonicus* (*cbp2D* and *cbp2E*) are important for Avicel degradation. Both of the proteins encoded by these genes contain a domain that can bind a redox-active cofactor. CBP2E contains a Ycel domain, which is known to bind ubiquinone in other proteins. And one recently it has been shown that *cbp2D*, which contains a predicted cytochrome domain, is co-regulated with PMOs in *C. japonicas*. And one studies are needed to fully understand the molecular details surrounding these proteins and their potential role in electron transfer for PMO activity.

5.6 Biological Co-Substrate Availability: H₂O₂ vs. O₂

Brown rot fungi exploit Fenton chemistry to depolymerize and degrade biomass.³²³ Both small molecule Fe complexes and H₂O₂-generating enzymes are secreted to generate •OH. A multi-stage decay mechanism is employed to protect carbohydrate-active enzymes; H₂O₂-generating enzymes in conjunction with small molecule Fe complexes are utilized in early stages of decay to spatiotemporally separate them from the majority of CAZy enzymes, which are expressed in later stages of decay.^{324–326} This spatially-resolved multi-stage protein expression protects susceptible enzymes from ROS, where enzymes expressed at earlier stages likely have a higher tolerance to ROS. This spatiotemporal separation also addresses one of the main issues surrounding the use of Fenton chemistry in biology. Spatially-resolved gene expression has also been observed for other filamentous fungi,³²⁵ suggesting this may be a common strategy that Nature employs to minimize the deleterious side effects of ROS.

PMOs are expressed in later stages of degradation in conjunction with known ROS scavengers, including superoxide dismutase, catalase, and glutathione S-transferase, which are all involved in ROS detoxification. The central role of these detoxification enzymes in maintaining low H_2O_2 concentrations is highlighted by the requirement of catalase for fungal growth and the nanomolar H_2O_2 concentrations found in later stages of decay. The low H_2O_2 concentration, combined with the catalytic efficiency of H_2O_2 vs. O_2 , suggests that there is a competition between H_2O_2 and O_2 ($\sim 250 \,\mu\text{M}$) for the PMO active site.

6 Conclusions and Outlook

The widespread distribution of PMOs in bacterial and eukaryotic genomes, combined with the challenging chemistry these enzymes mediate, has focused attention on these proteins. The diverse physiological functions of PMOs and variety of polysaccharides that can be oxidized have further deepened interest. The multiplicity of PMOs in fungal genomes suggests that there is functional diversity among PMOs, which may point to widespread roles that go beyond polysaccharide degradation. Future research will expand the portfolio of PMO substrates to potentially include many other classes of polysaccharides and even non-carbohydrate substrates. Continued research will determine how PMOs fit into the complex mechanisms involved in biomass degradation and host-microbe interactions to unravel new physiological roles for PMOs.

A major focal point has been the copper active site that is shared across all PMO families. The histidine brace provides a unique framework that could support a Cu-oxyl intermediate to carry out HAA. If this were the case, PMO oxygenase activity would deviate from known copper monooxygenases. Moreover, this mechanism would make PMOs more analogous to P450s, and H₂O₂ would shunt the oxygenase reaction, as both co-substrates would converge on the Cu-oxyl (Fig. 12). Also, H₂O₂ reactivity may have profound mechanistic implications. H₂O₂ is two-electrons reduced relative to O₂, such that slow proton and/or electron transfers that are key mechanistic steps in the oxygenase reaction can be bypassed when H₂O₂ serves as the co-substrate. Accurate determination of the electronic structure of the oxidizing intermediate will necessitate a multi-disciplinary approach that requires complementary techniques. Appropriate multi-reference computational methods must be used that can accurately capture the electronic structure of copper centers, which is notoriously difficult to accomplish (see Section 2.2). Moreover, while calculations can describe transient intermediates that are otherwise difficult, or impossible, to detect, these studies must be guided by experiments so that calculated mechanisms are consistent with biochemical data. The combination of rigorous enzymology and spectroscopy, in conjunction with computations, will help to understand the molecular details of PMO activity.

Environmental variables within the biological milieu will have a direct impact on the function of PMOs and the substrates they utilize. It remains unclear if H_2O_2 is the natural co-substrate for PMOs, or if H_2O_2 simply serves as a shunt for oxygenase activity. Altering H_2O_2 concentrations would significantly attenuate H_2O_2 -driven activity. Notably, addition of the peroxide scavenger HRP to the secretome of *N. crassa* has no noticeable effect on cellulose conversion, and the addition of catalase improves PMO-mediated saccharification of lignocellulose. Additionally, neither superoxide dismutase nor catalase impact cellulose oxidation in light-driven systems. While these findings suggest that ROS are not involved in PMO catalysis, low H_2O_2 concentrations can drive PMO reactivity in vitro. It is becoming clear that distinct mechanistic routes may be operative that depend on the active-site

architecture, co-substrate identity, polysaccharide substrate, reductant, and pH of the system. Ultimately, the components in the biological milieu and the identity of the PMO will dictate co-substrate utilization.

Acknowledgments

The authors would like to thank the members of the Marletta lab for insightful feedback and critical reading of the manuscript. CML acknowledges the Miller Institute for Basic Research in Science at UC Berkeley for a postdoctoral fellowship. This work was supported in part by the National Science Foundation (NSF), grant number CHE-1904540.

References

- 1. Lemon, C. M.; Dogutan, D. K.; Nocera, D. G. Porphyrin and Corrole Platforms for Water Oxidation, Oxygen Reduction, and Peroxide Dismutation. In *Handbook of Porphyrin Science*; Kadish, K. M., Smith, K. M., Guilard, R., Eds.; World Scientific Publishing: Singapore, 2012; pp 1–143.
- 2. Solomon, E. I.; Sundaram, U. M.; Machonkin, T. E. Multicopper Oxidases and Oxygenases. Chem. Rev. 1996, 96, 2563-2605.
- 3. Adam, S. M.; Wijeratne, G. B.; Rogler, P. J.; Diaz, D. E.; Quist, D. A.; Liu, J. J.; Karlin, K. D. Synthetic Fe/Cu Complexes: Toward Understanding Heme-Copper Oxidase Structure and Function. Chem. Rev. 2018, 118, 10840–11022.
- 4. Solomon, E. I.; Heppner, D. E.; Johnston, E. M.; Ginsbach, J. W.; Cirera, J.; Qayyum, M.; Kieber-Emmons, M. T.; Kjaergaard, C. H.; Hadt, R. G.; Tian, L. Copper Active Sites in Biology. Chem. Rev. 2014, 114, 3659–3853.
- 5. Messerschmidt, A. In Copper metalloenzymes. Comprehensive Natural Products II; Liu, H., Mander, L., Eds.; Elsevier: Oxford, 2010; pp 489-545.
- 6. Klinman, J. P. Mechanisms Whereby Mononuclear Copper Proteins Functionalize Organic Substrates. Chem. Rev. 1996, 96, 2541–2561.
- Vaaje-Kolstad, G.; Westereng, B.; Horn, S. J.; Liu, Z.; Zhai, H.; Sørlie, M.; Eijsink, V. G. H. An Oxidative Enzyme Boosting the Enzymatic Conversion of Recalcitrant Polysaccharides. Science 2010, 330, 219–222.
- 8. Hangasky, J. A.; Detomasi, T. C.; Marletta, M. A. Glycosidic Bond Hydroxylation by Polysaccharide Monooxygenases. Trends Chem. 2019, 1, 198–209.
- 9. Emsley, J. Nature's Building Blocks: An A-Z Guide to the Elements; Oxford University Press: New York, 2011.
- 10. Cotton, F.; Wilkinson, G. Advanced Inorganic Chemistry, 5th edn.; John Wiley & Sons: New York, 1988.
- 11. Kaplan, J. H.; Maryon, E. B. How Mammalian Cells Acquire Copper: An Essential But Potentially Toxic Metal. Biophys. J. 2016, 110, 7-13.
- 12. Rae, T. D.; Schmidt, P. J.; Pufahl, R. A.; Culotta, V. C.; O'Halloran, T. V. Undetectable Intracellular Free Copper: The Requirement of a Copper Chaperone for Superoxide Dismutase. Science 1999, 284, 805–808.
- 13. Bandmann, O.; Weiss, K. H.; Kaler, S. G. Wilson's Disease and Other Neurological Copper Disorders. Lancet Neurol. 2015, 14, 103-113.
- 14. Denoyer, D.; Masaldan, S.; La Fontaine, S.; Cater, M. A. Targeting Copper in Cancer Therapy: "Copper that Cancer" Metallomics 2015, 7, 1459-1476.
- 15. Levason, W.; Spicer, M. D. The Chemistry of Copper and Silver in Their Higher Oxidation States. Coord. Chem. Rev. 1987, 76, 45-120.
- 16. Huheey, J. E.; Keiter, E. A.; Keiter, R. L. Inorganic Chemistry: Principles of Structure and Reactivity, 4th edn.; HarperCollins College Publishers: New York, 1993.
- 17. Raciti, D.; Wang, C. Recent Advances in CO₂ Reduction Electrocatalysis on Copper. ACS Energy Lett. 2018, 3, 1545-1556.
- 18. Wang, V. C. C.; Maji, S.; Chen, P. P. Y.; Lee, H. K.; Yu, S. S. F.; Chan, S. I. Alkane Oxidation: Methane Monooxygenases, Related Enzymes, and Their Biomimetics. *Chem. Rev.* 2017, 117, 8574–8621.
- Sambiagio, C.; Marsden, S. P.; Blacker, A. J.; McGowan, P. C. Copper Catalysed Ullmann Type Chemistry: From Mechanistic Aspects to Modern Development. Chem. Soc. Rev. 2014, 43, 3525–3550.
- 20. Pearson, R. G. Hard and Soft Acids and Bases. J. Am. Chem. Soc. 1963, 85, 3533-3539.
- 21. Hartwig, J. Organotransition Metal Chemistry: From Bonding to Catalysis; University Science Books: Sausalito, 2010.
- 22. Casitas, A.; Ribas, X. The Role of Organometallic Copper(III) Complexes in Homogeneous Catalysis. Chem. Sci. 2013, 4, 2301–2318.
- 23. Ribas, X.; Güell, I. Cu(I)/Cu(III) Catalytic Cycle Involved in Ullmann-Type Cross-Coupling Reactions. Pure Appl. Chem. 2014, 86, 345-360.
- 24. Esguerra, K.; Lumb, J.-P. Cu(III)-mediated aerobic oxidations. Synthesis-Stuttgart 2019, 51, 334-358.
- 25. Gagnon, N.; Tolman, W. B. [CuO]⁺ and [CuOH]²⁺ complexes: Intermediates in Oxidation Catalysis? Acc. Chem. Res. 2015, 48, 2126–2131.
- Elwell, C. E.; Gagnon, N. L.; Neisen, B. D.; Dhar, D.; Spaeth, A. D.; Yee, G. M.; Tolman, W. B. Copper-Oxygen Complexes Revisited: Structures, Spectroscopy, and Reactivity. Chem. Rev. 2017, 117, 2059–2107.
- 27. Keown, W.; Gary, J. B.; Stack, T. D. P. High-Valent Copper in Biomimetic and Biological Oxidations. J. Biol. Inorg. Chem. 2017, 22, 289-305.
- 28. Speier, G.; Fülöp, V. The Oxidative Addition of Dibenzoyl Peroxide to Copper(I) Chloride. The Crystal and Molecular Structure of [CuCl(PhCO₂)₂(Py)₂] (Py = Pyridine). *J. Chem. Soc. Chem. Commun.* **1990**, 905–906.
- Santo, R.; Miyamoto, R.; Tanaka, R.; Nishioka, T.; Sato, K.; Toyota, K.; Obata, M.; Yano, S.; Kinoshita, I.; Ichimura, A.; et al. Diamagnetic-Paramagnetic Conversion of Tris(2-Pyridylthio)Methylcopper(III) Through a Structural Change From Trigonal Bipyramidal to Octahedral. Angew. Chem. Int. Ed. 2006, 45, 7611–7614.
- 30. Klemm, W.; Huss, E. Fluorokomplexe. I. Eisen-, Kobalt-, Nickel- Und Kupfer-Komplexe. Z. Anorg. Chem. 1949, 258, 221–226.
- 31. Hoppe, R.; Wingefeld, G. Zur kenntnis der hexafluorocuprate(III). Z. Anorg. Allg. Chem. 1984, 519, 195–203.
- 32. Arjomand, M.; Machin, D. J. Oxide Chemistry. Part II. Ternary Oxides Containing Copper in Oxidation States-I, -II, -III, and -IV. J. Chem. Soc. Dalton Trans. 1975, 1061–1066.
- Krebs, C.; Glaser, T.; Bill, E.; Weyhermüller, T.; Meyer-Klaucke, W.; Wieghardt, K. A Paramagnetic Copper(III) Complex Containing an Octahedral Cu^{III}S₆ Coordination Polyhedron.
 Angew. Chem. Int. Ed. 1999. 38, 359–361.
- 34. Margerum, D. W.; Chellappa, K. L.; Bossu, F. P.; Buree, G. L. Characterization of a Readily Accessible Copper(III)-Peptide Complex. J. Am. Chem. Soc. 1975, 97, 6894–6896.
- 35. Bossu, F. P.; Chellappa, K. L.; Margerum, D. W. Ligand Effects on the Thermodynamic Stabilization of Copper(III)-Peptide complexes. J. Am. Chem. Soc. 1977, 99, 2195–2203.
- 36. Neubecker, T. A.; Kirksey, S. T.; Chellappa, K. L.; Margerum, D. W. Amine Deprotonation in Copper(III)-Peptide Complexes. Inorg. Chem. 1979, 18, 444–448.
- 37. Lappin, A.; Youngblood, M.; Margerum, D. Electron-Transfer Reactions of Copper(II) complexes. Inorg. Chem. 1980, 19, 407–413.
- 38. Diaddario, L.; Robinson, W.; Margerum, D. Crystal and Molecular Structure of the Copper (III)-Tripeptide Complex of Tri-. Alpha.-Aminoisobutyric Acid. *Inorg. Chem.* 1983, 22, 1021–1025.
- 39. Pap, J.; Szyrwiel, L. On the Cu(III)/Cu(II) Redox Chemistry of Cu-Peptide Complexes to Assist Catalyst Design. Comments Inorg. Chem. 2017, 37, 59-77.
- 40. Meyerstein, D. Trivalent Copper. I. A Pulse Radiolytic Study of the Chemical Properties of the Aquo Complex. Inorg. Chem. 1971, 10, 638-641.
- 41. Balikungeri, A.; Pelletier, M.; Monnier, D. Contribution to the Study of the complexes Bis(Dihydrogen Tellurato)Cuprate(III) and Argentate(III), Bis(Hydrogen Periodato)Cuprate(III) and Argentate(III). Inorg. Chim. Acta 1977, 22, 7–14.
- 42. Bolattin, M. B.; Meti, M. D.; Nandibewoor, S. T.; Chimatadar, S. A. Oxidative Degradation of the Antihypertensive Drug Losartan by Alkaline Copper(III) Periodate Complex in the Presence and Absence of Ruthenium(III) Catalyst: A Kinetic and Mechanistic Study of Losartan Metabolite. *Monatsh. Chem.* 2015, 146, 1649–1663.

- 43. Feng, Y.; Qing, W.; Kong, L.; Li, H.; Wu, D.; Fan, Y.; Lee, P. H.; Shih, K. Factors and Mechanisms That Influence the Reactivity of Trivalent Copper: A Novel Oxidant for Selective Degradation of Antibiotics. *Water Res.* 2019, 149, 1–8.
- 44. Wu, Z.; Zhang, Z.; Liu, L. Electrochemical Studies of a Cu(II)-Cu(III) Couple: Cyclic Voltammetry and Chronoamperometry in a Strong Alkaline Medium and in the Presence of Periodate Anions. *Electrochim. Acta* 1997, 42, 2719–2723.
- 45. Darracq, S.; Kang, S. G.; Choy, J. H.; Demazeau, G. Stabilization of the Mixed Valence Cu(III)/Cu(IV) in the Perovskite Lattice of La_{1-x}Sr_xCuO₃ Under High Oxygen Pressure. J. Solid State Chem. **1995**, 114, 88–94.
- 46. Sinha, W.; Sommer, M. G.; Deibel, N.; Ehret, F.; Bauer, M.; Sarkar, B.; Kar, S. Experimental and Theoretical Investigations of the Existence of Cu^{II}, Cu^{III}, and Cu^{IV} in Copper Corrolato Complexes. *Angew. Chem. Int. Ed.* **2015**, *54*, 13769–13774.
- 47. Zhang, M. T.; Chen, Z.; Kang, P.; Meyer, T. J. Electrocatalytic Water Oxidation With a Copper(II) Polypeptide Complex. J. Am. Chem. Soc. 2013, 135, 2048–2051.
- 48. Coggins, M. K.; Zhang, M. T.; Chen, Z.; Song, N.; Meyer, T. J. Single-Site Copper(II) Water Oxidation Electrocatalysis: Rate Enhancements With HPO₄²⁻ as a Proton Acceptor at pH 8. *Angew. Chem. Int. Ed.* **2014**, *53*, 12226–12230.
- 49. Du, J.; Chen, Z.; Ye, S.; Wiley, B. J.; Meyer, T. J. Copper as a Robust and Transparent Electrocatalyst for Water Oxidation. Angew. Chem. Int. Ed. 2015, 54, 2073–2078.
- 50. Garrido-Barros, P.; Funes-Ardoiz, I.; Drouet, S.; Benet-Buchholz, J.; Maseras, F.; Llobet, A. Redox Non-Innocent Ligand Controls Water Oxidation Overpotential in a New Family of Mononuclear Cu-Based Efficient Catalysts. *J. Am. Chem. Soc.* 2015, *137*, 6758–6761.
- 51. Zhang, T.; Wang, C.; Liu, S.; Wang, J. L.; Lin, W. A Biomimetic Copper Water Oxidation Catalyst With Low Overpotential. J. Am. Chem. Soc. 2014, 136, 273–281.
- 52. Mizrahi, A.; Maimon, E.; Cohen, H.; Kornweitz, H.; Zilbermann, I.; Meyerstein, D. Mechanistic Studies on the Role of [Cu^{III}(CO₃)_n]²⁻²ⁿ as a Water Oxidation Catalyst: Carbonate as a Non-Innocent Ligand. *Chem. Eur. J.* **2018**, *24*, 1088–1096.
- 53. Harnischmacher, W.; Hoppe, R. Tetravalent Copper: Cs₂[CuF₆]. Angew. Chem. Int. Ed. Engl. 1973, 12, 582–583.
- 54. Hoppe, R. Recent Progress in Oxo- and Fluorometalate Chemistry. Angew. Chem. Int. Ed. Engl. 1981, 20, 63-87.
- 55. Kaim, W. Manifestations of Noninnocent Ligand Behavior. *Inorg. Chem.* **2011**, *50*, 9752–9765.
- 56. Heims, F.; Ray, K. Multiple Spin Scenarios in Transition-Metal Complexes Involving Redox Non-Innocent Ligands. In *Spin States in Biochemistry and Inorganic Chemistry*, Swart, M., Costas, M., Eds.; John Wiley & Sons: Chichester, 2016; pp 229–262.
- 57. DuBois, J. L.; Mukherjee, P.; Stack, T. D. P.; Hedman, B.; Solomon, E. I.; Hodgson, K. O. A Systematic K-Edge X-Ray Absorption Spectroscopic Study of Cu(III) Sites. J. Am. Chem. Soc. 2000. 122. 5775–5787.
- 58. Tomson, N. C.; Williams, K. D.; Dai, X.; Sproules, S.; Debeer, S.; Warren, T. H.; Wieghardt, K. Re-Evaluating the Cu K Pre-Edge XAS Transition in Complexes With Covalent Metal-Ligand Interactions. *Chem. Sci.* 2015, *6*, 2474–2487.
- 58a. DiMucci, I. M.; Lukens, J. T.; Chatterjee, S.; Carsch, K. M.; Titus, C. J.; Lee, S. J.; Nordlund, D.; Betley, T. A.; MacMillan, S. N.; Lancaster, K. M. The Myth of d⁸ Copper(III). J. Am. Chem. Soc. 2019, 141, 18508–18520.
- 59. Pierloot, K.; Zhao, H.; Vancoillie, S. Copper Corroles: The Question of Noninnocence. Inorg. Chem. 2010, 49, 10316–10329.
- 60. Dereli, B.; Ortuño, M. A.; Cramer, C. J. Accurate Ionization Energies for Mononuclear Copper Complexes Remain a Challenge for Density Functional Theory. *ChemPhysChem* **2018**, *19*, 959–966.
- 60a. Larsson, E. D.; Dong, G.; Veryazov, V.; Ryde, U.; Hedegård, E. D. Is Density Functional Theory Accurate for Lytic Polysaccharide Monooxygenase Enzymes? Dalton Trans. 2020, 49. 1501–1512.
- 61. Johnson, A. W.; Kay, I. T. Corroles. Part I. Synthesis. J. Chem. Soc. 1965, 1620-1629
- 62. Grigg, R.; Johnson, A. W.; Shelton, G. The Structures and Thermal Rearrangements of Alkylated Palladium and Copper Corroles. J. Chem. Soc. C 1971, ;2287–2294.
- 63. Johnson, A. W. Aromaticity in Macrocyclic Polypyrrolic Ring Systems. Pure Appl. Chem. 1971, 28, 195–217.
- 64. Hush, N. S.; Dyke, J. M. A Polarographic Investigation of Some Metal Tetradehydrocorrins. J. Inorg. Nucl. Chem. 1973, 35, 4341–4347.
- 65. Hush, N. S.; Dyke, J. M.; Williams, M. L.; Woolsey, I. S. Electronic Spectra of Metal Corrole Anions. J. Chem. Soc. Dalton Trans. 1974, 395–399.
- 66. Murakami, Y.; Matsuda, Y.; Sakata, K.; Yamada, S.; Tanaka, Y.; Aoyama, Y. Transition-Metal Complexes of Pyrrole Pigments. XVII. Preparation and Spectroscopic Properties of Corrole Complexes. *Bull. Chem. Soc. Jpn.* **1981**, *54*, 163–169.
- 67. Will, S.; Lex, J.; Vogel, E.; Schmickler, H.; Gisselbrecht, J. P.; Haubtmann, C.; Bernard, M.; Gross, M. Nickel and Copper Corroles: Well-Known Complexes in a New Light. Angew. Chem. Int. Ed. Engl. 1997, 36, 357–362.
- 68. Ghosh, A.; Wondimagegn, T.; Parusel, A. B. J. Electronic Structure of Gallium, Copper, and Nickel complexes of Corrole. High-Valent Transition Metal Centers Versus Noningnocent Ligands. J. Am. Chem. Soc. 2000, 122, 5100–5104
- 69. Wasbotten, I. H.; Wondimagegn, T.; Ghosh, A. Electronic Absorption, Resonance Raman, and Electrochemical Studies of Planar and Saddled Copper(III) Meso-Triarylcorroles. Highly Substituent-Sensitive Soret Bands as a Distinctive Feature of High-Valent Transition Metal Corroles. J. Am. Chem. Soc. 2002, 124, 8104–8116.
- Thomas, K. E.; Wasbotten, I. H.; Ghosh, A. Copper β-Octakis(Trifluoromethyl)Corroles: New Paradigms for Ligand Substituent Effects in Transition Metal Complexes. *Inorg. Chem.* 2008, 47, 10469–10478.
- 71. Steene, E.; Dey, A.; Ghosh, A. β-Octafluorocorroles. J. Am. Chem. Soc. 2003, 125, 16300–16309.
- 72. Brückner, C.; Briñas, R. P.; Krause Bauer, J. A. X-Ray Structure and Variable Temperature NMR Spectra of [meso-triarylcorrolato]Copper(III). Inorg. Chem. 2003, 42, 4495–4497.
- 73. Luobeznova, I.; Simkhovich, L.; Goldberg, I.; Gross, Z. Electronic Structures and Reactivities of Corrole-Copper complexes. Eur. J. Inorg. Chem. 2004, 1724–1732.
- 74. Kadish, K. M.; Adamian, V. A.; Van Caemelbecke, E.; Gueletii, E.; Will, S.; Erben, C.; Vogel, E. Electrogeneration of Oxidized Corrole Dimers. Electrochemistry of (OEC)M Where M = Mn, Co, Ni, or Cu and OEC is the Trianion of 2,3,7,8,12,13,17,18-Octaethylcorrole. *J. Am. Chem. Soc.* 1998, *120*, 11986–11993.
- 75. Guilard, R.; Gros, C. P.; Barbe, J. M.; Espinosa, E.; Jérôme, F.; Tabard, A.; Latour, J. M.; Shao, J.; Ou, Z.; Kadish, K. M. Alkyl- and Aryl-Substituted Corroles. 5. Synthesis, Physicochemical Properties, and X-Ray Structural Characterization of Copper Biscorroles and Porphyrin-Corrole Dyads. *Inorg. Chem.* **2004**, *43*, 7441–7455.
- 76. Ou, Z.; Shao, J.; Zhao, H.; Ohkubo, K.; Wasbotten, I. H.; Fukuzumi, S.; Ghosh, A.; Kadish, K. M. Spectroelectrochemical and ESR Studies of Highly Substituted Copper Corroles. J. Porphyrins Phthalocyanines 2004, 8, 1236–1247.
- 77. Bröring, M.; Brégier, F.; Cónsul Tejero, E.; Hell, C.; Holthausen, M. C. Revisiting the Electronic Ground State of Copper Corroles. Angew. Chem. Int. Ed. 2007, 46, 445–448.
- 78. Alemayehu, A. B.; Gonzalez, E.; Hansen, L. K.; Ghosh, A. Copper Corroles are Inherently Saddled. Inorg. Chem. 2009, 48, 7794–7799.
- 79. Thomas, K. E.; Conradie, J.; Hansen, L. K.; Ghosh, A. A Metallocorrole With Orthogonal Pyrrole Rings. Eur. J. Inorg. Chem. 2011, 1865–1870.
- 80. Thomas, K. E.; Alemayehu, A. B.; Conradie, J.; Beavers, C. M.; Ghosh, A. The Structural Chemistry of Metallocorroles: Combined X-Ray Crystallography and Quantum Chemistry Studies Afford Unique Insights. *Acc. Chem. Res.* 2012, *45*, 1203–1214.
- 81. Alemayehu, A. B.; Hansen, L. K.; Ghosh, A. Nonplanar, Noninnocent, and Chiral: A Strongly Saddled Metallocorrole. Inorg. Chem. 2010, 49, 7608–7610.
- 82. Alemayehu, A.; Conradie, J.; Ghosh, A. A First TDDFT Study of Metallocorrole Electronic Spectra: Copper Meso-Triarylcorroles Exhibit Hyper Spectra. Eur. J. Inorg. Chem. 2011, 1857–1864.
- 83. Lemon, C. M.; Huynh, M.; Maher, A. G.; Anderson, B. L.; Bloch, E. D.; Powers, D. C.; Nocera, D. G. Electronic Structure of Copper Corroles. *Angew. Chem. Int. Ed.* 2016, *55*, 2176–2180.
- 84. Lim, H.; Thomas, K. E.; Hedman, B.; Hodgson, K. O.; Ghosh, A.; Solomon, E. I. X-Ray Absorption Spectroscopy as a Probe of Ligand Noninnocence in Metallocorroles: The Case of Copper Corroles. *Inorg. Chem.* 2019, *58*, 6722–6730.
- 85. Naumann, D.; Roy, T.; Tebbe, K.-F.; Crump, W. Synthesis and Structure of Surprisingly Stable Tetrakis(Trifluoromethyl)Cuprate(III) Salts. *Angew. Chem. Int. Ed. Engl.* **1993**, *32*, 1482–1483.
- 86. Snyder, J. P. Elusiveness of Cu^{III} Complexation; Preference for Trifluoromethyl Oxidation in the Formation of [Cu^I(CF₃)₄]⁻ Salts. Angew. Chem. Int. Ed. Engl. 1995, 34, 80–81.

- 87. Kaupp, M.; von Schnering, H. G. Formal Oxidation State Versus Partial Charge—A Comment, Angew. Chem. Int. Ed. Engl. 1995, 34, 986.
- 88. Snyder, J. P. Distinguishing Copper d⁸ and d¹⁰ Configurations in a Highly Ionic Complex; A Nonformal metal Oxidation State. *Angew. Chem. Int. Ed. Engl.* **1995**, *34*, 986–987.
- 89. Preiss, U.; Krossing, I. A Computational Study of [M(CF₃)₄]⁻ (M = Cu, Ag, Au) and Their Properties as Weakly Coordinating Anions. *Z. Anorg. Allg. Chem.* **2007**, *633*, 1639–1644.
- 90. Aullón, G.; Alvarez, S. Oxidation States, Atomic Charges and Orbital Populations in Transition Metal Complexes. Theor. Chem. Accounts 2009, 123, 67–73.
- 91. Hoffmann, R.; Alvarez, S.; Mealli, C.; Falceto, A.; Cahill, T. J.; Zeng, T.; Manca, G. From Widely Accepted Concepts in Coordination Chemistry to Inverted Ligand Fields. *Chem. Rev.* 2016, *116*, 8173–8192.
- 92. Walroth, R. C.; Lukens, J. T.; MacMillan, S. N.; Finkelstein, K. D.; Lancaster, K. M. Spectroscopic Evidence for a 3d¹⁰ Ground State Electronic Configuration and Ligand Field Inversion in [Cu(CF₃)₄]¹⁻. *J. Am. Chem. Soc.* 2016, *138*, 1922–1931.
- 93. Gao, C.; Macetti, G.; Overgaard, J. Experimental X-Ray Electron Density Study of Atomic Charges, Oxidation States, and Inverted Ligand Field in Cu(CF₃)⁴⁻. *Inorg. Chem.* **2019**, *58*, 2133–2139.
- 94. Baya, M.; Joven-Sancho, D.; Alonso, P. J.; Orduna, J.; Menjón, B. M–C Bond Homolysis in Coinage-Metal [M(CF₃)₄]⁻ Derivatives. *Angew. Chem. Int. Ed.* **2019**, *58*, 9954–9958.
- 95. Solomon, E. I.; Szilagyi, R. K.; DeBeer George, S.; Basumallick, L. Electronic Structures of metal Sites in Proteins and Models: Contributions to Function in Blue Copper Proteins. Chem. Rev. 2004. 104. 419–458.
- 96. Lippard, S. J.; Berg, J. M. Principles of Bioinorganic Chemistry, University Science Books: Mill Valley, 1999.
- 97. Solomon, E. I.; Baldwin, M. J.; Lowery, M. D. Electronic Structures of Active Sites in Copper Proteins: Contributions to Reactivity. Chem. Rev. 1992, 92, 521-542.
- 98. Prigge, S. T.; Kolhekar, A. S.; Eipper, B. A.; Mains, R. E.; Mario Amzel, L. Substrate-Mediated Electron Transfer in Peptidylglycine α-Hydroxylating Monooxygenase. *Nat. Struct. Biol.* **1999**. *6*. 976–983.
- 99. Klinman, J. P. The Copper-Enzyme Family of Dopamine β-Monooxygenase and Peptidylglycine α-Hydroxylating Monooxygenase: Resolving the Chemical Pathway for Substrate Hydroxylation. *J. Biol. Chem.* **2006**, *281*, 3013–3016.
- 100. Katopodis, A. G.; May, S. W. Novel Substrates and Inhibitors of Peptidylglycine α-Amidating Monooxygenase. *Biochemistry* **1990**, *29*, 4541–4548.
- 101. Chen, P.; Bell, J.; Eipper, B. A.; Solomon, E. I. Oxygen Activation by the Noncoupled Binuclear Copper Site in Peptidylglycine α-Hydroxylating Monooxygenase. Spectroscopic Definition of the Resting Sites and the Putative Cull—OOH Intermediate. Biochemistry 2004, 43, 5735–5747.
- 102. Prigge, S. T.; Eipper, B. A.; Mains, R. E.; Amzel, L. M. Dioxygen Binds End-on to Mononuclear Copper in a Precatalytic Enzyme Complex. Science 2004, 304, 864–867.
- 103. Rudzka, K.; Moreno, D. M.; Eipper, B.; Mains, R.; Estrin, D. A.; Amzel, L. M. Coordination of Peroxide to the Cu_M Center of Peptidylglycine α-Hydroxylating Monooxygenase (PHM): Structural and Computational Study. *J. Biol. Inorg. Chem.* 2013, 18, 223–232.
- 104. Francisco, W. A.; Knapp, M. J.; Blackburn, N. J.; Klinman, J. P. Hydrogen Tunneling in Peptidylglycine α-Hydroxylating Monooxygenase. J. Am. Chem. Soc. 2002, 124, 8194–8195
- 105. Bhadra, M.; Lee, J. Y. C.; Cowley, R. E.; Kim, S.; Siegler, M. A.; Solomon, E. I.; Karlin, K. D. Intramolecular Hydrogen Bonding Enhances Stability and Reactivity of Mononuclear Cupric Superoxide complexes. J. Am. Chem. Soc. 2018, 140, 9042–9045.
- 106. Meliá, C.; Ferrer, S.; Řezáč, J.; Parisel, O.; Reinaud, O.; Moliner, V.; De La Lande, A. Investigation of the Hydroxylation Mechanism of Noncoupled Copper Oxygenases by *ab initio* Molecular Dynamics Simulations. *Chem. Eur. J.* 2013, *19*, 17328–17337.
- 107. Quinlan, R. J.; Sweeney, M. D.; Lo Leggio, L.; Otten, H.; Poulsen, J.-C.; Johansen, K. S.; Krogh, K. B.; Jørgensen, C. I.; Tovborg, M.; Anthonsen, A.; et al. Insights Into the Oxidative Degradation of Cellulose by a Copper Metalloenzyme That Exploits Biomass Components. *Proc. Natl. Acad. Sci.* 2011, 108, 15079–15084.
- Beeson, W. T.; Phillips, C. M.; Cate, J. H. D.; Marletta, M. A. Oxidative Cleavage of Cellulose by Fungal Copper-Dependent Polysaccharide Monooxygenases. J. Am. Chem. Soc. 2012, 134, 890–892.
- 109. Phillips, C. M.; Beeson, W. T.; Cate, J. H.; Marletta, M. A. Cellobiose Dehydrogenase and a Copper-Dependent Polysaccharide Monooxygenase Potentiate Cellulose Degradation by *Neurospora crassa*. *ACS Chem. Biol.* 2011, *6*, 1399–1406.
- 110. Yadav, S. K.; Archana; Singh, R.; Singh, P. K.; Vasudec, P. G. Insecticidal Fern Protein Tma12 is Possibly a Lytic Polysaccharide Monooxygenase. *Planta* 2019, 249, 1987–1996.
- 111. Chiu, E.; Hijnen, M.; Bunker, R. D.; Boudes, M.; Rajendran, C.; Aizel, K.; Oliéric, V.; Schulze-Briese, C.; Mitsuhashi, W.; Young, V.; et al. Structural Basis for the Enhancement of Virulence by Viral Spindles and Their In Vivo Crystallization. *Proc. Natl. Acad. Sci.* 2015, 112, 3973–3978.
- 112. Sabbadin, F.; Hemsworth, G. R.; Ciano, L.; Henrissat, B.; Dupree, P.; Tryfona, T.; Marques, R. D. S.; Sweeney, S. T.; Besser, K.; Elias, L.; et al. An Ancient Family of Lytic Polysaccharide Monooxygenases With Roles in Arthropod Development and Biomass Digestion. *Nat. Commun.* 2018, *9*, 756–767.
- 113. Levasseur, A.; Drula, E.; Lombard, V.; Coutinho, P. M.; Henrissat, B. Expansion of the Enzymatic Repertoire of the CAZy Database to Integrate Auxiliary Redox Enzymes. Biotechnol. Biofuels 2013, 6, 41.
- 114. Johansen, K. S. Discovery and Industrial Applications of Lytic Polysaccharide Mono-Oxygenases. Biochem. Soc. Trans. 2016, 44, 143–149.
- 115. Horn, S. J.; Vaaje-Kolstad, G.; Westereng, B.; Eijsink, V. G. Novel Enzymes for the Degradation of Cellulose. Biotechnol. Biofuels 2012, 5, 45.
- 116. Li, X.; Chomvong, K.; Yu, V. Y.; Liang, J. M.; Lin, Y.; Cate, J. H. D. Cellobionic Acid Utilization: From Neurospora crassa to Saccharomyces cerevisiae. Biotechnol. Biofuels 2015, 8, 120.
- 117. Agostoni, M.; Hangasky, J. A.; Marletta, M. A. Physiological and Molecular Understanding of Bacterial Polysaccharide Monooxygenases. *Microbiol. Mol. Biol. Rev.* 2017, 81, e00015—e00017.
- 118. Johansen, K. S. Lytic Polysaccharide Monooxygenases: The Microbial Power Tool for Lignocellulose Degradation. Trends Plant Sci. 2016, 21, 926–936.
- 119. Berrin, J. G.; Rosso, M. N.; Abou Hachem, M. Fungal Secretomics to Probe the Biological Functions of Lytic Polysaccharide Monooxygenases. *Carbohydr. Res.* **2017**, *448*, 155–160
- 120. Seipke, R. F.; Hutchings, M. I.; Kaltenpoth, M. Streptomyces as Symbionts: An Emerging and Widespread Theme? FEMS Microbiol. Rev. 2012, 36, 862–876.
- 121. Distel, D. L.; Beaudoin, D. J.; Morrill, W. Coexistence of Multiple Proteobacterial Endosymbionts in the Gills of the Wood-Boring Bivalve *Lyrodus pedicellatus* (Bivalvia: Teredinidae). *Appl. Environ. Microbiol.* **2002**, *68*, 6292–6299.
- 122. O'Connor, R. M.; Fung, J. M.; Sharp, K. H.; Benner, J. S.; McClung, C.; Cushing, S.; Lamkin, E. R.; Fomenkov, A. I.; Henrissat, B.; Londer, Y. Y.; et al. Gill Bacteria Enable a Novel Digestive Strategy in a Wood-Feeding Mollusk. *Proc. Natl. Acad. Sci.* 2014, 111, E5096–E5104.
- 123. Mitsuhashi, W. Analysis of the Viral Lytic Polysaccharide Monooxygenase Fusolin and Its Potential Application to Pest Control. In *Trends in Insect Molecular Biology and Biotechnology*, Kumar, D., Gong, C., Eds.; Springer International Publishing AG: Switzerland, 2018; pp 129–142.
- 124. Frederiksen, R. F.; Paspaliari, D. K.; Larsen, T.; Storgaard, B. G.; Larsen, M. H.; Ingmer, H.; Palcic, M. M.; Leisner, J. J. Bacterial Chitinases and Chitin-Binding Proteins as Virulence Factors. *Microbiology* 2013, *159*, 833–847.
- 125. Wong, E.; Vaaje-Kolstad, G.; Ghosh, A.; Hurtado-Guerrero, R.; Konarev, P. V.; Ibrahim, A. F. M.; Svergun, D. I.; Eijsink, V. G. H.; Chatterjee, N. S.; van Aalten, D. M. F. The Vibrio cholerae Colonization Factor GbpA Possesses a Modular Structure That Governs Binding to Different Host Surfaces. PLoS Pathog. 2012, 8, e1002373.
- 126. Finn, R. D.; Coggill, P.; Eberhardt, R. Y.; Eddy, S. R.; Mistry, J.; Mitchell, A. L.; Potter, S. C.; Punta, M.; Qureshi, M.; Sangrador-Vegas, A.; et al. The Pfam Protein Families Database: Towards a More Sustainable Future. *Nucleic Acids Res.* 2016, 44, D279–D285.
- 127. McWilliam, H.; Li, W.; Uludag, M.; Squizzato, S.; Park, Y. M.; Buso, N.; Cowley, A. P.; Lopez, R. Analysis Tool Web Services from the EMBL-EBI. *Nucleic Acids Res.* 2013, 41, W597–W600
- 128. Lombard, V.; Golaconda Ramulu, H.; Drula, E.; Coutinho, P. M.; Henrissat, B. The Carbohydrate-Active Enzymes Database (CAZy) in 2013. *Nucleic Acids Res.* 2014, 42, D490–D495.

- 128a. Labourel, A.; Frandsen, K. E. H.; Zhang, F.; et al. A Fungal Family of Lytic Polysaccharide Monooxygenase-Like Copper Proteins. Nat. Chem. Biol. 2020, 16, 345-350.
- 129. Vu, V. V.; Beeson, W. T.; Phillips, C. M.; Cate, J. H. D.; Marletta, M. A. Determinants of Regioselective Hydroxylation in the Fungal Polysaccharide Monooxygenases. J. Am. Chem. Soc. 2014, 136, 562–565.
- 130. Beeson, W. T.; Vu, V. V.; Span, E. A.; Phillips, C. M.; Marletta, M. A. Cellulose Degradation by Polysaccharide Monooxygenases. Annu. Rev. Biochem. 2015, 84, 923–946.
- 131. Filiatrault-Chastel, C.; Navarro, D.; Haon, M.; Grisel, S.; Herpoël-Gimbert, I.; Chevret, D.; Fanuel, M.; Henrissat, B.; Heiss-Blanquet, S.; Margeot, A.; et al. AA16, a New Lytic Polysaccharide Monooxygenase Family Identified in Fungal Secretomes. *Biotechnol. Biofuels* 2019, 12, 55.
- 132. Correa, T. L. R.; Junior, A. T.; Wolf, L. D.; Buckeridge, M. S.; dos Santos, L. V.; Murakami, M. T. An Actinobacteria Lytic Polysaccharide Monooxygenase Acts on both Cellulose and Xylan to Boost Biomass Saccharification. *Biotechnol. Biofuels* 2019, 12, 117.
- 132a. Garcia-Santamarina, S.; Probst, C.; Festa, R. A.; et al. A Lytic Polysaccharide Monooxygenase-Like Protein Functions in Fungal Copper Import and Meningitis. Nat. Chem. Biol. 2020, 16, 337–344.
- 133. Gerlt, J. A.; Bouvier, J. T.; Davidson, D. B.; Imker, H. J.; Sadkhin, B.; Slater, D. R.; Whalen, K. L. Enzyme Function Initiative-Enzyme Similarity Tool (EFI-EST): A Web Tool for Generating Protein Sequence Similarity Networks. *Biochim. Biophys. Acta Proteins Proteomics* 2015. 1854. 1019–1037.
- 134. Atkinson, H. J.; Morris, J. H.; Ferrin, T. E.; Babbitt, P. C. Using Sequence Similarity Networks for Visualization of Relationships Across Diverse Protein Superfamilies. *PLoS One* **2009**, *4*, e4345.
- 135. Book, A. J.; Yennamalli, R. M.; Takasuka, T. E.; Currie, C. R.; Phillips, G. N.; Fox, B. G. Evolution of Substrate Specificity in Bacterial AA10 Lytic Polysaccharide Monooxygenases. Biotechnol. Biofuels 2014, 7, 109.
- 136. Lenfant, N.; Hainaut, M.; Terrapon, N.; Drula, E.; Lombard, V.; Henrissat, B. A Bioinformatics Analysis of 3400 Lytic Polysaccharide Oxidases From Family AA9. Carbohydr. Res. 2017. 448, 166–174.
- 137. Guindon, S.; Dufayard, J. F.; Lefort, V.; Anisimova, M.; Hordijk, W.; Gascuel, O. New Algorithms and Methods to Estimate Maximum-Likelihood Phylogenies: Assessing the Performance of PhyML 3.0. Syst. Biol. 2010, 59, 307–321.
- 138. Dereeper, A.; Guignon, V.; Blanc, G.; Audic, S.; Buffet, S.; Chevenet, F.; Dufayard, J.-F.; Guindon, S.; Lefort, V.; Lescot, M.; et al. Phylogeny.fr: Robust Phylogenetic Analysis for the Non-Specialist. Nucleic Acids Res. 2008, 36, W465—W469.
- 139. Bard, F.; Chia, J. Cracking the Glycome Encoder: Signaling, Trafficking, and Glycosylation. Trends Cell Biol. 2016, 26, 379–388.
- 140. Beckerman, A. P.; de Roij, J.; Dennis, S. R.; Little, T. J. A Shared Mechanism of Defense Against Predators and Parasites: Chitin Regulation and Its Implications for Life-History Theory. Ecol. Evol. 2013, 3, 5119–5126.
- 141. Aranaz, I.; Mengibar, M.; Harris, R.; Panos, I.; Miralles, B.; Acosta, N.; Galed, G.; Heras, A. Functional Characterization of Chitin and Chitosan. Curr. Chem. Biol. 2012, 3, 203–230.
- 142. Glass, N. L.; Schmoll, M.; Cate, J. H. D.; Coradetti, S. Plant Cell Wall Deconstruction by Ascomycete Fungi. Annu. Rev. Microbiol. 2013, 67, 477-498.
- 143. Varki, A., Cummings, R. D., Esko, J. D., Freeze, H. H., Stanley, P., Bertozzi, C. R., Hart, G. W., Etzler, M. E., Eds.; In *Essentials of Glycobiology*, Cold Spring Harbor Laboratory Press: Cold Spring Harbor, 2009.
- 144. Delmer, D. P. Cellulose Biosynthesis: Exciting Times for a Difficult Field of Study. Annu. Rev. Plant Physiol. Plant Mol. Biol. 1999, 50, 245–276.
- 145. Somerville, C. Cellulose Synthesis in Higher Plants. Annu. Rev. Cell Dev. Biol. 2006, 22, 53-78.
- 146. Atalla, R. H.; VanderHart, D. L. Native Cellulose: A Composite of Two Distinct Crystalline Forms. Science 1984, 223, 283–285
- 147. VanderHart, D. L.; Atalla, R. H. Studies of Microstructure in Native Celluloses Using Solid-State ¹³C NMR. Macromolecules 1984, 17, 1465–1472.
- 148. Nishiyama, Y.; Sugiyama, J.; Chanzy, H.; Langan, P. Crystal Structure and Hydrogen Bonding System in Cellulose Iα From Synchrotron X-Ray and Neutron Fiber Diffraction. *J. Am. Chem. Soc.* **2003**, *125*, 14300–14306.
- 149. Atalla, R. H. The Individual Structures of Native Celluloses. In 10th International Symposium on Wood and Pulping Chemistry, TAPPI Press, 1999; pp 608-614.
- Szymańska-Chargot, M.; Cybulska, J.; Zdunek, A. Sensing the Structural Differences in Cellulose From Apple and Bacterial Cell Wall Materials by Raman and FT-IR Spectroscopy. Sensors 2011, 11, 5543–5560.
- 151. Wada, M.; Chanzy, H.; Nishiyama, Y.; Langan, P. Cellulose III_I Crystal Structure and Hydrogen Bonding by Synchrotron X-ray and Neutron Fiber Diffraction. *Macromolecules* **2004**, *37*, 8548–8555.
- 152. Wood, T. M. Fungal Cellulases. Biochem. Soc. Trans. 2015, 20, 46-53.
- 153. Hayashi, J.; Sufoka, A.; Ohkita, J.; Watanabe, S. The Confirmation of Existences of Cellulose III, III, IV, and IV, by the X-ray Method. J. Polym. Sci., Polym. Lett. Ed. 1975, 23–27
- 154. Hutino, K.; Sakurada, I. Über die existenz einer vierten modifikation der cellulose. Naturwissenschaften 1940, 28, 577-578.
- 155. Gardiner, E. S.; Sarko, A. Packing Analysis of Carbohydrates and Polysaccharides. 16. The Crystal Structures of Celluloses IVI and IVII. Can. J. Chem. 1985, 63, 173–180.
- 156. Al Aiti, M.; Jehnichen, D.; Fischer, D.; Brünig, H.; Heinrich, G. On the Morphology and Structure Formation of Carbon Fibers From Polymer Precursor Systems. *Prog. Mater. Sci.* 2018, *98*, 477–551.
- 157. Scheller, H. V.; Ulvskov, P. Hemicelluloses. Annu. Rev. Plant Biol. 2010, 61, 263–289.
- 158. Popper, Z. A. Evolution and Diversity of Green Plant Cell Walls. *Curr. Opin. Plant Biol.* **2008**, *11*, 286–292.
- 159. Moller, I.; Sørensen, I.; Bernal, A. J.; Blaukopf, C.; Lee, K.; Øbro, J.; Pettolino, F.; Roberts, A.; Mikkelsen, J. D.; Knox, J. P.; et al. High-Throughput Mapping of Cell-Wall Polymers Within and Between Plants Using Novel Microarrays. *Plant J.* 2007, *50*, 1118–1128.
- 160. McDougall, G. J.; Fry, S. C. Xyloglucan Oligosaccharides Promote Growth and Activate Cellulase: Evidence for a Role of Cellulase in Cell Expansion. Plant Physiol. 1990, 93, 1042–1048.
- 161. Caffall, K. H.; Mohnen, D. The Structure, Function, and Biosynthesis of Plant Cell Wall Pectic Polysaccharides. Carbohydr. Res. 2009, 344, 1879-1900.
- 162. Hoffman, M.; Jia, Z.; Peña, M. J.; Cash, M.; Harper, A.; Blackburn, A. R.; Darvill, A.; York, W. S. Structural Analysis of Xyloglucans in the Primary Cell Walls of Plants in the Subclass Asteridae. Carbohydr. Res. 2005, 340, 1826–1840.
- 163. Schultink, A.; Liu, L.; Pauly, M. Structural Diversity and Function of Xyloglucan Sidechain Substituents. Plan. Theory 2014, 3, 526-542.
- 164. Vincken, J. P.; York, W. S.; Beldman, G.; Voragen, A. G. Two General Branching Patterns of Xyloglucan, XXXG and XXGG. Plant Physiol. 1997, 114, 9-13.
- 165. Fry, S. C.; York, W. S.; Albersheim, P.; Darvill, A.; Hayashi, T.; Joseleau, J.-P.; Kato, Y.; Lorences, E. P.; Maclachlan, G. A.; McNeil, M.; et al. An Unambiguous Nomenclature for Xyloglucan-Derived Oligosaccharides. *Physiol. Plant.* **1993**, *89*, 1–3.
- 166. Yui, T.; Ogawa, K.; Sarko, A. Molecular and Crystal Structure of Konjac Glucomannan in the Mannan II Polymorphic Form. Carbohydr. Res. 1992, 229, 41–55.
- 167. Bacic, A., Fincher, G. B., Stone, A. B., Eds.; In Chemistry, Biochemistry, and Biology of 1-3 Beta Glucans and Related Polysaccharides; New York: Academic Press, 2009.
- 168. Woodward, J. R.; Phillips, D. R.; Fincher, G. B. Water-Soluble (1→3), (1→4)-β-D-Glucans From Barley (Hordeum vulgare) Endosperm. I. Physicochemical Properties. Carbohydr. Polym. 1983, 3, 143–156.
- 169. Gibeaut, D. M.; Pauly, M.; Bacic, A.; Fincher, G. B. Changes in Cell Wall Polysaccharides in Developing Barley (Hordeum vulgare) Coleoptiles. Planta 2005, 221, 729–738.
- 170. Kittur, F. S.; Harish Prashanth, K. V.; Udaya Sankar, K.; Tharanathan, R. N. Characterization of Chitin, Chitosan and Their Carboxymethyl Derivatives by Differential Scanning Calorimetry. Carbohydr. Polym. 2002, 49, 185–193.
- 171. Araki, Y.; Ito, E. A. Pathway of Chitosan Formation in Mucor rouxii: Enzymatic Deacetylation of Chitin. Eur. J. Biochem. 1975, 55, 71–78.
- 172. Yuan, Y.; Chesnutt, B. M.; Haggard, W. O.; Bumgardner, J. D. Deacetylation of Chitosan: Material Characterization and *In Vitro* Evaluation via Albumin Adsorption and Pre-Osteoblastic Cell Cultures. *Materials (Basel)* 2011, 4, 1399–1416.
- 173. Davis, L. L.; Bartnicki-Garcia, S. Chitosan Synthesis by the Tandem Action of Chitin Synthetase and Chitin Deacetylase From Mucor rouxii. Biochemistry 1984, 23, 1065–1073.

- 174. Ehrlich, H.; Krautter, M.; Hanke, T.; Simon, P.; Knieb, C.; Heinemann, S.; Worch, H. First Evidence of the Presence of Chitin in Skeletons of Marine Sponges. Part II. Glass Sponges (Hexactinellida: Porifera). J. Exp. Zool. 2007, 308B, 473–483.
- 175. Rudall, K. M. Chitin and Its Association With Other Molecules. J. Polym. Sci., Part C: Polym. Symp. 1969, 28, 83-102.
- 176. Rudall, K. M.; Kenchington, W. The Chitin System. Biol. Rev. 1973, 40, 597-636.
- 177. Grant, S.; Blair, H. S.; Mckay, G. Structural Studies on Chitosan and Other Chitin Derivatives. Makromol. Chem. 1989, 190, 2279-2286.
- 178. Wang, S.; Li, C.; Copeland, L.; Niu, Q.; Wang, S. Starch Retrogradation: A Comprehensive Review. Compr. Rev. Food Sci. Food Sci. Food Sci. 7, 14, 568–585.
- 179. Smith, A. M.; Zeeman, S. C.; Smith, S. M. Starch Degradation. Annu. Rev. Plant Biol. 2005, 56, 73-98.
- 180. Berry, C. S. Resistant Starch: Formation and Measurement of Starch That Survives Exhaustive Digestion With Amylolytic Enzymes During the Determination of Dietary Fibre. J. Cereal Sci. 1986, 4, 301–314.
- 181. Pérez, S.; Bertoft, E. The Molecular Structures of Starch Components and Their Contribution to the Architecture of Starch Granules: A Comprehensive Review. Starch-Starke 2010, 62, 389–420.
- 182. Vamadevan, V.; Bertoft, E. Structure-Function Relationships of Starch Components. Starch-Starke 2015, 67, 55-68.
- 183. Sarko, A.; Wu, H.-C. H. The Crystal Structures of A-, B- and C-Polymorphs of Amylose and Starch. Starch-Starke 1978, 30, 73-78.
- 184. Hsien-Chih, H. W.; Sarko, A. The Double-Helical Molecular Structure of Crystalline a-Amylose. Carbohydr. Res. 1978, 61, 27–40.
- 185. Hsein-Chih, H. W.; Sarko, A. The Double-Helical Molecular Structure of Crystalline b-Amylose. Carbohydr. Res. 1978, 61, 7–25.
- 186. Villares, A.; Moreau, C.; Bennati-Granier, C.; Garajova, S.; Foucat, L.; Falourd, X.; Saake, B.; Berrin, J. G.; Cathala, B. Lytic Polysaccharide Monooxygenases Disrupt the Cellulose Fibers Structure. Sci. Rep. 2017, 7, 40262.
- 187. Eibinger, M.; Ganner, T.; Bubner, P.; Rošker, S.; Kracher, D.; Haltrich, D.; Ludwig, R.; Plank, H.; Nidetzky, B. Cellulose Surface Degradation by a Lytic Polysaccharide Monooxygenase and Its Effect on Cellulase Hydrolytic Efficiency. *J. Biol. Chem.* 2014, *289*, 35929–35938.
- 188. Hu, J.; Tian, D.; Renneckar, S.; Saddler, J. N. Enzyme Mediated Nanofibrillation of Cellulose by the Synergistic Actions of an Endoglucanase, Lytic Polysaccharide Monooxygenase (LPMO) and Xylanase. Sci. Rep. 2018, 8, 3195.
- 189. Song, B.; Li, B.; Wang, X.; Shen, W.; Park, S.; Collings, C.; Feng, A.; Smith, S. J.; Walton, J. D.; Ding, S. Y. Real-Time Imaging Reveals That Lytic Polysaccharide Monooxygenase Promotes Cellulase Activity by Increasing Cellulose Accessibility. *Biotechnol. Biofuels* 2018, 11, 41.
- 190. Eibinger, M.; Sattelkow, J.; Ganner, T.; Plank, H.; Nidetzky, B. Single-Molecule Study of Oxidative Enzymatic Deconstruction of Cellulose. Nat. Commun. 2017, 8, 894.
- 191. Chabbert, B.; Habrant, A.; Herbaut, M.; Foulon, L.; Aguié-Béghin, V.; Garajova, S.; Grisel, S.; Bennati-Granier, C.; Gimbert-Herpoël, I.; Jamme, F.; et al. Action of Lytic Polysaccharide Monooxygenase on Plant Tissue is Governed by Cellular Type. Sci. Rep. 2017, 7, 17792.
- 192. Kittl, R.; Kracher, D.; Burgstaller, D.; Haltrich, D.; Ludwig, R. Production of Four *Neurospora crassa* Lytic Polysaccharide Monooxygenases in *Pichia pastoris* Monitored by a Fluorimetric Assay. *Biotechnol. Biofuels* **2012**, *5*, 79–92.
- 193. Hangasky, J. A.; Marletta, M. A. A Random-Sequential Kinetic Mechanism for Polysaccharide Monooxygenases. Biochemistry 2018, 57, 3191–3199.
- 194. Gusakov, A. V.; Bulakhov, A. G.; Demin, I. N.; Sinitsyn, A. P. Monitoring of Reactions Catalyzed by Lytic Polysaccharide Monooxygenases Using Highly-Sensitive Fluorimetric Assay of the Oxygen Consumption Rate. *Carbohydr. Res.* 2017, 452, 156–161.
- 195. Frandsen, K. E. H.; Simmons, T. J.; Dupree, P.; Poulsen, J.-C. N.; Hemsworth, G. R.; Ciano, L.; Johnston, E. M.; Tovborg, M.; Johansen, K. S.; von Freiesleben, P.; et al. The Molecular Basis of Polysaccharide Cleavage by Lytic Polysaccharide Monooxygenases. *Nat. Chem. Biol.* 2016, *12*, 298–303.
- 196. Garajova, S.; Mathieu, Y.; Beccia, M. R.; Bennati-Granier, C.; Biaso, F.; Fanuel, M.; Ropartz, D.; Guigliarelli, B.; Record, E.; Rogniaux, H.; et al. Single-Domain Flavoenzymes Trigger Lytic Polysaccharide Monooxygenases for Oxidative Degradation of Cellulose; 6, 28276.
- 197. Courtade, G.; Wimmer, R.; Røhr, Å.K.; Preims, M.; Felice, A. K. G.; Dimarogona, M.; Vaaje-Kolstad, G.; Sørlie, M.; Sandgren, M.; Ludwig, R.; et al. Interactions of a Fungal Lytic Polysaccharide Monooxygenase With β-Glucan Substrates and Cellobiose Dehydrogenase. *Proc. Natl. Acad. Sci.* **2016**, *113*, 5922–5927.
- 198. Zouraris, D.; Dimarogona, M.; Karnaouri, A.; Topakas, E.; Karantonis, A. Direct Electron Transfer of Lytic Polysaccharide Monooxygenases (LPMOs) and Determination of Their Formal Potentials by Large Amplitude Fourier Transform Alternating Current Cyclic Voltammetry. *Bioelectrochemistry* **2018**, *124*, 149–155.
- 199. Chen, C.; Chen, J.; Geng, Z.; Wang, M.; Liu, N.; Li, D. Regioselectivity of Oxidation by a Polysaccharide Monooxygenase from *Chaetomium thermophilum. Biotechnol. Biofuels* **2018**, *11*, 155.
- 200. Karnaouri, A.; Muraleedharan, M. N.; Dimarogona, M.; Topakas, E.; Rova, U.; Sandgren, M.; Christakopoulos, P. Recombinant Expression of Thermostable Processive MtEG5 Endoglucanase and Its Synergism With MtLPMO From Myceliophthora thermophila During the Hydrolysis of Lignocellulosic Substrates. Biotechnol. Biofuels 2017, 10, 126.
- 201. Semenova, M. V.; Gusakov, A. V.; Volkov, P. V.; Matys, V. Y.; Nemashkalov, V. A.; Telitsin, V. D.; Rozhkova, A. M.; Sinitsyn, A. P. Enhancement of the Enzymatic Cellulose Saccharification by *Penicillium verruculosum* Multienzyme Cocktails Containing Homologously Overexpressed Lytic Polysaccharide Monooxygenase. *Mol. Biol. Rep.* 2019, 46, 2363–2370.
- 202. Müller, G.; Kalyani, D. C.; Horn, S. J. LPMOs in Cellulase Mixtures Affect Fermentation Strategies for Lactic Acid Production From Lignocellulosic Biomass. *Biotechnol. Bioeng.* 2017, 114, 552–559.
- 203. Hemsworth, G. R.; Ciano, L.; Davies, G. J.; Walton, P. H. Production and Spectroscopic Characterization of Lytic Polysaccharide Monooxygenases. In *Methods in Enzymology*; Academic Press: Cambridge, MA, USA, 2018; vol. 613, pp 61–90.
- 204. Kjaergaard, C. H.; Qayyum, M. F.; Wong, S. D.; Xu, F.; Hemsworth, G. R.; Walton, D. J.; Young, N. A.; Davies, G. J.; Walton, P. H.; Johansen, K. S.; et al. Spectroscopic and Computational Insight Into the Activation of O₂ by the Mononuclear Cu Center in Polysaccharide Monooxygenases. *Proc. Natl. Acad. Sci.* 2014, *111*, 8797–8802.
- 205. Le, C. N.; Phan, H.; Tran-Le, D. P.; Tran, D. H.; Farquhar, E. R.; Vu, V. V. Solution Structure of the Reduced Active Site of a Starch-Active Polysaccharide Monooxygenase From Neurospora crassa. Vietnam J. Sci. Technol. Eng. 2018, 60, 9–12.
- 206. Aachmann, F. L.; Sørlie, M.; Skjåk-Bræk, G.; Eijsink, V. G. H.; Vaaje-Kolstad, G. NMR Structure of a Lytic Polysaccharide Monooxygenase Provides Insight Into Copper Binding, Protein Dynamics, and Substrate Interactions. *Proc. Natl. Acad. Sci.* 2012, 109, 18779–18784.
- 207. Agger, J. W.; Isaksen, T.; Varnai, A.; Vidal-Melgosa, S.; Willats, W. G. T.; Ludwig, R.; Horn, S. J.; Eijsink, V. G. H.; Westereng, B. Discovery of LPMO Activity on Hemicelluloses Shows the Importance of Oxidative Processes in Plant Cell Wall Degradation. *Proc. Natl. Acad. Sci.* 2014, 111, 6287–6292.
- Pedersen, H. L.; Fangel, J. U.; McCleary, B.; Ruzanski, C.; Rydahl, M. G.; Ralet, M. C.; Farkas, V.; Von Schantz, L.; Marcus, S. E.; Andersen, M. C. F.; et al. Versatile High Resolution Oligosaccharide Microarrays for Plant Glycobiology and Cell Wall Research. J. Biol. Chem. 2012, 287, 39429–39438.
- 209. Breslmayr, E.; Hanžek, M.; Hanrahan, A.; Leitner, C.; Kittl, R.; Šantek, B.; Oostenbrink, C.; Ludwig, R. A Fast and Sensitive Activity Assay for Lytic Polysaccharide Monooxygenase. Biotechnol. Biofuels 2018, 11, 79.
- Vuong, T. V.; Liu, B.; Sandgren, M.; Master, E. R. Microplate-Based Detection of Lytic Polysaccharide Monooxygenase Activity by Fluorescence-Labeling of Insoluble Oxidized Products. Biomacromolecules 2017, 18, 610–616.
- 211. Wang, D.; Li, J.; Wong, A. C. Y.; Aachmann, F. L.; Hsieh, Y. S. Y. A Colorimetric Assay to Rapidly Determine the Activities of Lytic Polysaccharide Monooxygenases. *Biotechnol. Biofuels* 2018, *11*, 215.
- 212. Frommhagen, M.; van Erven, G.; Sanders, M.; van Berkel, W. J. H.; Kabel, M. A.; Gruppen, H. RP-UHPLC-UV-ESI-MS/MS Analysis of LPMO Generated C4-Oxidized Gluco-Oligosaccharides After Non-Reductive Labeling With 2-Aminobenzamide. Carbohydr. Res. 2017, 448, 191–199.
- 213. Vu, V. V.; Beeson, W. T.; Span, E. A.; Farquhar, E. R.; Marletta, M. A. A Family of Starch-Active Polysaccharide Monooxygenases. *Proc. Natl. Acad. Sci.* 2014, 111, 13822–13827.
- 214. Boraston, A. B.; Bolam, D. N.; Gilbert, H. J.; Davies, G. J. Carbohydrate-Binding Modules: Fine-Tuning Polysaccharide Recognition. Biochem. J. 2004, 382, 769-781.
- 215. Guillén, D.; Sánchez, S.; Rodríguez-Sanoja, R. Carbohydrate-Binding Domains: Multiplicity of Biological Roles. Appl. Microbiol. Biotechnol. 2010, 85, 1241–1249.

- 216. Cuskin, F.; Flint, J. E.; Gloster, T. M.; Morland, C.; Baslé, A.; Henrissat, B.; Coutinho, P. M.; Strazzulli, A.; Solovyova, A. S.; Davies, G. J.; et al. How Nature Can Exploit Nonspecific Catalytic and Carbohydrate Binding Modules to Create Enzymatic Specificity. *Proc. Natl. Acad. Sci.* 2012, *109*, 20889–20894.
- 217. Crouch, L. I.; Labourel, A.; Walton, P. H.; Davies, G. J.; Gilbert, H. J. The Contribution of Non-Catalytic Carbohydrate Binding Modules to the Activity Lytic Polysaccharide Monooxygenases. J. Biol. Chem. 2016, 291, 7439–7449.
- 218. Borisova, A. S.; Isaksen, T.; Dimarogona, M.; Kognole, A. A.; Mathiesen, G.; Várnai, A.; Røhr, Å.K.; Payne, C. M.; Sørlie, M.; Sørlie, M.; Sandgren, M.; et al. Structural and Functional Characterization of a Lytic Polysaccharide Monooxygenase With Broad Substrate Specificity. *J. Biol. Chem.* 2015, *290*, 22955–22969.
- 219. Hansson, H.; Karkehabadi, S.; Mikkelsen, N.; Douglas, N. R.; Kim, S.; Lam, A.; Kaper, T.; Kelemen, B.; Meier, K. K.; Jones, S. M.; et al. High-Resolution Structure of a Lytic Polysaccharide Monooxygenase From *Hypocrea jecorina* Reveals a Predicted Linker as an Integral Part of the Catalytic Domain. *J. Biol. Chem.* 2017, 292, 19099–19109.
- 220. Courtade, G.; Forsberg, Z.; Heggset, E. B.; Eijsink, V. G. H.; Aachmann, F. L. The Carbohydrate-Binding Module and Linker of a Modular Lytic Polysaccharide Monooxygenase Promote Localized Cellulose Oxidation. *J. Biol. Chem.* 2018, 293, 13006–13015.
- 221. Mutahir, Z.; Mekasha, S.; Loose, J. S. M.; Abbas, F.; Vaaje-Kolstad, G.; Eijsink, V. G. H.; Forsberg, Z. Characterization and Synergistic Action of a Tetra-Modular Lytic Polysaccharide Monooxygenase From *Bacillus cereus. FFBS Lett.* **2018**. *592*. 2562–2571.
- 222. Forsberg, Z.; Nelson, C. E.; Dalhus, B.; Mekasha, S.; Loose, J. S. M.; Crouch, L. I.; Røhr, Å.K.; Gardner, J. G.; Eijsink, V. G. H.; Vaaje-Kolstad, G. Structural and Functional Analysis of a Lytic Polysaccharide Monooxygenase Important for Efficient Utilization of Chitin in *Cellvibrio japonicus*. *J. Biol. Chem.* **2016**, *291*, 7300–7312.
- 223. Manjeet, K.; Purushotham, P.; Neeraja, C.; Podile, A. R. Bacterial Chitin Binding Proteins Show Differential Substrate Binding and Synergy With Chitinases. *Microbiol. Res.* 2013, 168, 461–468.
- 224. Kataeva, I. A.; Seidel, R. D.; Shah, A.; West, L. T.; Li, X. L.; Ljungdahl, L. G. The Fibronectin Type 3-Like Repeat From the Clostridium thermocellum Cellobiohydrolase CbHa Promotes Hydrolysis of Cellulose by Modifying its Surface. Appl. Environ. Microbiol. 2002, 68, 4292–4300.
- 225. Kruer-Zerhusen, N.; Alahuhta, M.; Lunin, V. V.; Himmel, M. E.; Bomble, Y. J.; Wilson, D. B. Structure of a *Thermobifida fusca* Lytic Polysaccharide Monooxygenase and Mutagenesis of Key Residues. *Biotechnol. Biofuels* 2017, 10, 243.
- 226. Manjeet, K.; Madhuprakash, J.; Mormann, M.; Moerschbacher, B. M.; Podile, A. R. A Carbohydrate Binding Module-5 is Essential for Oxidative Cleavage of Chitin by a Multi-Modular Lytic Polysaccharide Monooxygenase From Bacillus thuringiensis Serovar kurstaki. Int. J. Biol. Macromol. 2019, 127, 649–656.
- 227. Ciano, L.; Davies, G. J.; Tolman, W. B.; Walton, P. H. Bracing Copper for the Catalytic Oxidation of C-H Bonds. Nat. Catal. 2018, 1, 571-577.
- 228. Hemsworth, G. R.; Taylor, E. J.; Kim, R. Q.; Gregory, R. C.; Lewis, S. J.; Turkenburg, J. P.; Parkin, A.; Davies, G. J.; Walton, P. H. The Copper Active Site of CBM33 Polysaccharide Oxygenases. J. Am. Chem. Soc. 2013, 135, 6069–6077.
- 229. Forsberg, Z.; Mackenzie, A. K.; Sorlie, M.; Rohr, A. K.; Helland, R.; Arvai, A. S.; Vaaje-Kolstad, G.; Eijsink, V. G. H. Structural and Functional Characterization of a Conserved Pair of Bacterial Cellulose-Oxidizing Lytic Polysaccharide Monooxygenases. *Proc. Natl. Acad. Sci.* 2014, 111, 8446–8451.
- 230. Hemsworth, G. R.; Henrissat, B.; Davies, G. J.; Walton, P. H. Discovery and Characterization of a New Family of Lytic Polysaccharide Monooxygenases. *Nat. Chem. Biol.* 2014, 10, 122–126.
- 231. Gregory, R. C.; Hemsworth, G. R.; Turkenburg, J. P.; Hart, S. J.; Walton, P. H.; Davies, G. J. Activity, Stability and 3-D Structure of the Cu(II) Form of a Chitin-Active Lytic Polysaccharide Monooxygenase From Bacillus amyloliquefaciens. Dalton Trans. 2016, 45, 16904—16912.
- 232. Chaplin, A. K.; Wilson, M. T.; Hough, M. A.; Svistunenko, D. A.; Hemsworth, G. R.; Walton, P. H.; Vijgenboom, E.; Worrall, J. A. R. Heterogeneity in the Histidine-Brace Copper Coordination Sphere in Auxiliary Activity Family 10 (AA10) Lytic Polysaccharide Monooxygenases. J. Biol. Chem. 2016, 291, 12838–12850.
- 233. Hemsworth, G. R.; Davies, G. J.; Walton, P. H. Recent Insights Into Copper-Containing Lytic Polysaccharide Mono-Oxygenases. Curr. Opin. Struct. Biol. 2013, 23, 660-668.
- 234. Bacik, J.-P.; Mekasha, S.; Forsberg, Z.; Kovalevsky, A. Y.; Vaaje-Kolstad, G.; Eijsink, V. G. H.; Nix, J. C.; Coates, L.; Cuneo, M. J.; Unkefer, C. J.; et al. Neutron and Atomic Resolution X-ray Structures of a Lytic Polysaccharide Monooxygenase Reveal Copper-Mediated Dioxygen Binding and Evidence for N-Terminal Deprotonation. *Biochemistry* 2017, *56*, 2529–2532.
- 235. Caldararu, O.; Oksanen, E.; Ryde, U.; Hedegård, E. D. Mechanism of Hydrogen Peroxide Formation by Lytic Polysaccharide Monooxygenase. Chem. Sci. 2019, 10, 576-586.
- 236. O'Dell, W. B.; Agarwal, P. K.; Meilleur, F. Oxygen Activation at the Active Site of a Fungal Lytic Polysaccharide Monooxygenase. Angew. Chem. Int. Ed. 2017, 56, 767–770.
- 237. Tickler, A. K.; Smith, D. G.; Ciccotosto, G. D.; Tew, D. J.; Curtain, C. C.; Carrington, D.; Masters, C. L.; Bush, A. I.; Cherny, R. A.; Cappai, R.; et al. Methylation of the Imidazole Side Chains of the Alzheimer Disease Amyloid-β Peptide Results in Abolition of Superoxide Dismutase-Like Structures and Inhibition of Neurotoxicity. *J. Biol. Chem.* 2005, *280*, 13355–13363.
- 238. Koebke, K. J.; Yu, F.; Van Stappen, C.; Pinter, T. B. J.; Deb, A.; Penner-Hahn, J. E.; Pecoraro, V. L. Methylated Histidines Alter Tautomeric Preferences That Influence the Rates of Cu Nitrite Reductase Catalysis in Designed Peptides. J. Am. Chem. Soc. 2019, 141, 7765–7775.
- 239. Kim, S.; Ståhlberg, J.; Sandgren, M.; Paton, R. S.; Beckham, G. T. Quantum Mechanical Calculations Suggest That Lytic Polysaccharide Monooxygenases Use a Copper-Oxyl, Oxygen-Rebound Mechanism. *Proc. Natl. Acad. Sci.* 2014, 111, 149–154.
- 240. Petrović, D. M.; Bissaro, B.; Chylenski, P.; Skaugen, M.; Sørlie, M.; Jensen, M. S.; Aachmann, F. L.; Courtade, G.; Várnai, A.; Eijsink, V. G. H. Methylation of the N-Terminal Histidine Protects a Lytic Polysaccharide Monooxygenase From Auto-Oxidative Inactivation. *Protein Sci.* 2018, *27*, 1636–1650.
- 241. Lo Leggio, L.; Simmons, T. J.; Poulsen, J.-C. N.; Frandsen, K. E. H.; Hemsworth, G. R.; Stringer, M. A.; von Freiesleben, P.; Tovborg, M.; Johansen, K. S.; De Maria, L.; et al. Structure and Boosting Activity of a Starch-Degrading Lytic Polysaccharide Monooxygenase. *Nat. Commun.* 2015, *6*, 5961.
- 242. Bodenheimer, A. M.; O'Dell, W. B.; Stanley, C. B.; Meilleur, F. Structural Studies of Neurospora crassa LPMO9D and Redox Partner CDHIIA Using Neutron Crystallography and Small-Angle Scattering. Carbohydr. Res. 2017, 448, 200–204.
- 243. Forsberg, Z.; Bissaro, B.; Gullesen, J.; Dalhus, B.; Vaaje-Kolstad, G.; Eijsink, V. G. H. Structural Determinants of Bacterial Lytic Polysaccharide Monooxygenase Functionality. J. Biol. Chem. 2018, 293, 1397–1412.
- 243a. Paradisi, A.; Johnston, E. M.; Tovborg, M.; Nicoll, C. R.; Ciano, L.; Dowle, A.; McMaster, J.; Hancock, Y.; Davies, G. J.; Walton, P. H. Formation of a Copper(II)–Tyrosyl Complex at the Active Site of Lytic Polysaccharide Monooxygenases Following Oxidation by H₂O₂. *J. Am. Chem. Soc.* 2019, *141*, 18585–18599.
- 244. Harris, P. V.; Welner, D.; McFarland, K. C.; Re, E.; Navarro Poulsen, J.-C.; Brown, K.; Šalbo, R.; Ding, H.; Vlasenko, E.; Merino, S.; et al. Stimulation of Lignocellulosic Biomass Hydrolysis by Proteins of Glycoside Hydrolase Family 61: Structure and Function of a Large, Enigmatic Family. *Biochemistry* 2010, 49, 3305–3316.
- 245. Span, E. A.; Suess, D. L. M.; Deller, M. C.; Britt, R. D.; Marletta, M. A. The Role of the Secondary Coordination Sphere in a Fungal Polysaccharide Monooxygenase. *ACS Chem. Biol.* 2017. 12, 1095–1103.
- 246. Span, E. A.; Marletta, M. A. The Framework of Polysaccharide Monooxygenase Structure and Chemistry. Curr. Opin. Struct. Biol. 2015, 35, 93–99.
- 247. Vaaje-Kolstad, G.; Horn, S. J.; Van Aalten, D. M. F.; Synstad, B.; Eijsink, V. G. H. The Non-Catalytic Chitin-Binding Protein CBP21 From Serratia marcescens is Essential for Chitin Degradation. J. Biol. Chem. 2005, 280, 28492–28497.
- 248. Vaaje-Kolstad, G.; Forsberg, Z.; Loose, J. S.; Bissaro, B.; Eijsink, V. G. Structural Diversity of Lytic Polysaccharide Monooxygenases. Curr. Opin. Struct. Biol. 2017, 44, 67–76.
- 249. Bissaro, B.; Isaksen, I.; Vaaje-Kolstad, G.; Eijsink, V. G. H.; Røhr, Å.K. How a Lytic Polysaccharide Monooxygenase Binds Crystalline Chitin. Biochemistry 2018, 57, 1893–1906.
- 250. Vu, V. V.; Marletta, M. A. Starch-Degrading Polysaccharide Monooxygenases. Cell. Mol. Life Sci. 2016, 73, 2809–2819.
- 251. Simmons, T. J.; Frandsen, K. E. H.; Ciano, L.; Tryfona, T.; Lenfant, N.; Poulsen, J. C.; Wilson, L. F. L.; Tandrup, T.; Tovborg, M.; Schnorr, K.; et al. Structural and Electronic Determinants of Lytic Polysaccharide Monooxygenase Reactivity on Polysaccharide Substrates. *Nat. Commun.* 2017, 8, 1064.
- 252. Danneels, B.; Tanghe, M.; Desmet, T. Structural Features on the Substrate-Binding Surface of Fungal Lytic Polysaccharide Monooxygenases Determine Their Oxidative Regioselectivity. *Biotechnol. J.* 2019, *14*, 1800211.
- 253. Liu, B.; Kognole, A. A.; Wu, M.; Westereng, B.; Crowley, M. F.; Kim, S.; Dimarogona, M.; Payne, C. M.; Sandgren, M. Structural and Molecular Dynamics Studies of a C1-Oxidizing Lytic Polysaccharide Monooxygenase From Heterobasidion irregulare Reveal Amino Acids Important for Substrate Recognition. FEBS J. 2018, 285, 2225–2242.

- Arora, R.; Bharval, P.; Sarswati, S.; Sen, T. Z.; Yennamalli, R. M. Structural Dynamics of Lytic Polysaccharide Monoxygenases Reveals a Highly Flexible Substrate Binding Region.
 J. Mol. Graph. Model. 2019. 88. 1–10.
- 255. Loose, J. S. M.; Arntzen, M.; Bissaro, B.; Ludwig, R.; Eijsink, V. G. H.; Vaaje-Kolstad, G. Multipoint Precision Binding of Substrate Protects Lytic Polysaccharide Monooxygenases From Self-Destructive Off-Pathway Processes. *Biochemistry* 2018, *57*, 4114–4124.
- 256. Isaksen, T.; Westereng, B.; Aachmann, F. L.; Agger, J. W.; Kracher, D.; Kittl, R.; Ludwig, R.; Haltrich, D.; Eijsink, V. G. H.; Horn, S. J. A C4-Oxidizing Lytic Polysaccharide Monooxygenase Cleaving Both Cellulose and Cello-Oligosaccharides. *J. Biol. Chem.* 2014, 289, 2632–2642.
- 257. Kojima, Y.; Várnai, A.; Ishida, T.; Sunagawa, N.; Petrovic, D. M.; Igarashi, K.; Jellison, J.; Goodell, B.; Alfredsen, G.; Westereng, B.; et al. A Lytic Polysaccharide Monooxygenase With Broad Xyloglucan Specificity From the Brown-Rot Fungus Gloeophyllum trabeum and Its Action on Cellulose-Xyloglucan Complexes. Appl. Environ. Microbiol. 2016, 82, 6557–6572.
- 258. Couturier, M.; Ladevèze, S.; Sulzenbacher, G.; Ciano, L.; Fanuel, M.; Moreau, C.; Villares, A.; Cathala, B.; Chaspoul, F.; Frandsen, K. E.; et al. Lytic Xylan Oxidases From Wood-Decay Funqi Unlock Biomass Degradation. *Nat. Chem. Biol.* 2018, 14, 306.
- 259. Nekiunaite, L.; Isaksen, T.; Vaaje-Kolstad, G.; Abou Hachem, M. Fungal Lytic Polysaccharide Monooxygenases Bind Starch and β-Cyclodextrin Similarly to Amylolytic Hydrolases. *FEBS Lett.* **2016**, *590*, 2737–2747.
- 260. Møller, M. S.; Henriksen, A.; Svensson, B. Structure and Function of α-Glucan Debranching Enzymes. Cell. Mol. Life Sci. 2016, 73, 2619–2641.
- 261. Vu, V. V.; Hangasky, J. A.; Detomasi, T. C.; Henry, S. J. W.; Ngo, S. T.; Span, E. A.; Marletta, M. A. Substrate Specificity in Starch Active Polysaccharide Monooxygenases. J. Biol. Chem. 2019, 294, 12157–12166.
- 262. Vu, V. V.; Ngo, S. T. Copper Active Site in Polysaccharide Monooxygenases. Coord. Chem. Rev. 2018, 368, 134-157.
- 263. Kracher, D.; Andlar, M.; Furtmüller, P. G.; Ludwig, R. Active-Site Copper Reduction Promotes Substrate Binding of Fungal Lytic Polysaccharide Monooxygenase and Reduces Stability. J. Biol. Chem. 2018, 293, 1676–1687.
- 264. Hedegård, E. D.; Ryde, U. Multiscale Modelling of Lytic Polysaccharide Monooxygenases. ACS Omega 2017, 2, 536-545.
- 265. Gudmundsson, M.; Kim, S.; Wu, M.; Ishida, T.; Momeni, M. H.; Vaaje-Kolstad, G.; Lundberg, D.; Royant, A.; Ståhlberg, J.; Eijsink, V. G. H.; et al. Structural and Electronic Snapshots During the Transition From a Cu(II) to Cu(I) Metal Center of a Lytic Polysaccharide Monooxygenase by X-ray Photoreduction. *J. Biol. Chem.* 2014, 289, 18782–18792.
- 266. Bissaro, B.; Røhr, Å.K.; Müller, G.; Chylenski, P.; Skaugen, M.; Forsberg, Z.; Horn, S. J.; Vaaje-Kolstad, G.; Eijsink, V. G. H. Oxidative Cleavage of Polysaccharides by Monocopper Enzymes Depends on H₂O₂. *Nat. Chem. Biol.* **2017**, *13*, 1123–1128.
- 267. Hangasky, J. A.; lavarone, A. T.; Marletta, M. A. Reactivity of O₂ Versus H₂O₂ With Polysaccharide Monooxygenases. Proc. Natl. Acad. Sci. 2018, 115, 4915–4920.
- 268. Kuusk, S.; Bissaro, B.; Kuusk, P.; Forsberg, Z.; Eijsink, V. G. H.; Sørlie, M.; Valjamae, P. Kinetics of H₂O₂-Driven Degradation of Chitin by a Bacterial Lytic Polysaccharide Monooxygenase. *J. Biol. Chem.* 2018, *293*, 523–531.
- 269. Walton, P. H.; Davies, G. J. On the Catalytic Mechanisms of Lytic Polysaccharide Monooxygenases. Curr. Opin. Chem. Biol. 2016, 31, 195–207.
- 270. Kim, S.; Ginsbach, J. W.; Lee, J. Y.; Peterson, R. L.; Liu, J. J.; Siegler, M. A.; Sarjeant, A. A.; Solomon, E. I.; Karlin, K. D. Amine Oxidative N-Dealkylation via Cupric Hydroperoxide Cu-OOH Homolytic Cleavage Followed by Site-Specific Fenton Chemistry. J. Am. Chem. Soc. 2015, 137, 2867–2874.
- 271. Frandsen, K. E. H.; Poulsen, J.-C. N.; Tandrup, T.; Lo Leggio, L. Unliganded and Substrate Bound Structures of the Cellooligosaccharide Active Lytic Polysaccharide Monooxygenase LsAA9A at Low pH. Carbohydr. Res. 2017, 448, 187–190.
- 272. Hu, J.; Arantes, V.; Pribowo, A.; Gourlay, K.; Saddler, J. N. Substrate Factors That Influence the Synergistic Interaction of AA9 and Cellulases During the Enzymatic Hydrolysis of Biomass. Energ. Environ. Sci. 2014, 7, 2308–2315.
- 273. Steenken, S.; Neta, P. One-Electron Redox Potentials of Phenols. Hydroxy- and Aminophenols and Related Compounds of Biological Interest. *J. Phys. Chem.* 1982, 86, 3661–3667.
- 274. Ruscic, B. Active Thermochemical Tables: Sequential Bond Dissociation Enthalpies of Methane, Ethane, and Methanol and the Related Thermochemistry. *J. Phys. Chem. A* 2015, 119, 7810–7837.
- 275. Balasubramanian, R.; Rosenzweig, A. C. Structural and Mechanistic Insights Into Methane Oxidation by Particulate Methane Monooxygenase. Acc. Chem. Res. 2007, 40, 573–580
- 276. Cao, L.; Caldararu, O.; Rosenzweig, A. C.; Ryde, U. Quantum Refinement Does Not Support Dinuclear Copper Sites in Crystal Structures of Particulate Methane Monooxygenase. Angew. Chem. Int. Ed. 2018, 57, 162–166.
- 277. Ross, M. O.; MacMillan, F.; Wang, J.; Nisthal, A.; Lawton, T. J.; Olafson, B. D.; Mayo, S. L.; Rosenzweig, A. C.; Hoffman, B. M. Particulate Methane Monooxygenase Contains Only Mononuclear Copper Centers. *Science* 2019, *364*, 566–570.
- 278. Patel, I.; Kracher, D.; Ma, S.; Garajova, S.; Haon, M.; Faulds, C. B.; Berrin, J.-G.; Ludwig, R.; Record, E. Salt-responsive lytic polysaccharide monooxygenases from the mangrove fungus *Pestalotiopsis* sp. NCi6. *Biotechnol. Biofuels* 2016, *9*, 108.
- 279. Yu, M.-J.; Yoon, S.-H.; Kim, Y.-W. Overproduction and Characterization of a Lytic Polysaccharide Monooxygenase in *Bacillus subtilis* Using an Assay Based on Ascorbate Consumption. *Enzyme Microb. Technol.* **2016**, *93*–*94*, 150–156.
- 280. Li, F.; Ma, F.; Zhao, H.; Zhao, S.; Wang, L.; Zhang, X.; Yu, H. A White-Rot Fungal Lytic Polysaccharide Monooxygenase Drives the Degradation of Lignin by a Versatile Peroxidase. *Appl. Environ. Microbiol.* 2019, *85*, e02803–e02818.
- 281. Niu, L.; Liao, W. Hydrogen Peroxide Signaling in Plant Development and Abiotic Responses: Crosstalk With Nitric Oxide and Calcium. Front. Plant Sci. 2016, 7, 230.
- 282. Gauron, C.; Meda, F.; Dupont, E.; Albadri, S.; Quenech'Du, N.; Ipendey, E.; Volovitch, M.; Del Bene, F.; Joliot, A.; Rampon, C.; et al. Hydrogen Peroxide (H₂O₂) Controls Axon Pathfinding During Zebrafish Development. *Dev. Biol.* 2016, 414, 133–141.
- 283. Petrov, V. D.; Van Breusegem, F. Hydrogen peroxide—A central hub for information flow in plant cells. AoB Plants 2012, 2012, pls014.
- 284. Wang, B.; Johnston, E. M.; Li, P.; Shaik, S.; Davies, G. J.; Walton, P. H.; Rovira, C. QM/MM Studies Into the H₂O₂-Dependent Activity of Lytic Polysaccharide Monooxygenases: Evidence for the Formation of a Caged Hydroxyl Radical Intermediate. *ACS Catal.* 2018, *8*, 1346–1351.
- 285. Hedegård, E. D.; Ryde, U. Molecular Mechanism of Lytic Polysaccharide Monooxygenases. *Chem. Sci.* **2018**, *9*, 3866–3880.
- 286. Bertini, L.; Breglia, R.; Lambrughi, M.; Fantucci, P.; De Gioia, L.; Borsari, M.; Sola, M.; Bortolotti, C. A.; Bruschi, M. Catalytic Mechanism of Fungal Lytic Polysaccharide Monooxygenases Investigated by First-Principles Calculations. *Inorg. Chem.* 2017, *57*, 86–97.
- 287. Kuusk, S.; Kont, R.; Kuusk, P.; Heering, A.; Sørlie, M.; Bissaro, B.; Eijsink, V. G. H.; Väljamäe, P. Kinetic Insights Into the Role of the Reductant in H₂O₂-Driven Degradation of Chitin by a Bacterial Lytic Polysaccharide Monooxygenase. *J. Biol. Chem.* 2019, *294*, 1516–1528.
- 288. Gao, J.; Thomas, D. A.; Sohn, C. H.; Beauchamp, J. L. Biomimetic Reagents for the Selective Free Radical and Acid-Base Chemistry of Glycans: Application to Glycan Structure Determination by Mass Spectrometry. J. Am. Chem. Soc. 2013, 135, 10684–10692.
- 289. Luo, Y. R. Handbook of Bond Dissociation Energies in Organic Compounds; CRC Press: Boca Raton, FL, 2003.
- 290. Li, X.; Beeson, W. T.; Phillips, C. M.; Marletta, M. A.; Cate, J. H. D. Structural Basis for Substrate Targeting and Catalysis by Fungal Polysaccharide Monooxygenases. *Structure* 2012, *20*, 1051–1061.
- 291. Kim, S.; Lee, J. Y.; Cowley, R. E.; Ginsbach, J. W.; Siegler, M. A.; Solomon, E. I.; Karlin, K. D. A N₃S_(thioether)-Ligated Cu^{II}-Superoxo With Enhanced Reactivity. *J. Am. Chem. Soc.* 2015, *137*, 2796–2799.
- 292. McMillen, D. F.; Golden, D. M. Hydrocarbon Bond Dissociation Energies. Annu. Rev. Phys. Chem. 1982, 33, 493.
- 293. Wang, B.; Walton, P. H.; Rovira, C. The Molecular Mechanisms of Oxygen Activation and Hydrogen Peroxide Formation in Lytic Polysaccharide Monooxygenases. *ACS Catal.* **2019**, *9*, 4958–4969.

- 294. Yamaguchi, S.; Nagatomo, S.; Kitagawa, T.; Funahashi, Y.; Ozawa, T.; Jitsukawa, K.; Masuda, H. Copper Hydroperoxo Species Activated by Hydrogen-Bonding Interaction With Its Distal Oxygen. *Inorg. Chem.* 2003, *42*, 6968–6970.
- 295. Mann, S. I.; Heinisch, T.; Ward, T. R.; Borovik, A. S. Peroxide Activation Regulated by Hydrogen Bonds Within Artificial Cu Proteins. J. Am. Chem. Soc. 2017, 139, 17289–17292.
- 296. Poulos, T. L. Heme Enzyme Structure and Function. Chem. Rev. 2014, 114, 3919-3962.
- 297. Rezabal, E.; Gauss, J.; Matxain, J. M.; Berger, R.; Diefenbach, M.; Holthausen, M. C. Quantum Chemical Assessment of the Binding Energy of CuO+. J. Chem. Phys. 2011, 134, 064304.
- 298. Dietl, N.; Van Der Linde, C.; Schlangen, M.; Beyer, M. K.; Schwarz, H. Diatomic [CuO]⁺ and Its Role in the Spin-Selective Hydrogen- and Oxygen-Atom Transfers in the Thermal Activation of Methane. *Angew. Chem. Int. Ed.* 2011, *50*, 4966–4969.
- 299. Srnec, M.; Navrátil, R.; Andris, E.; Jašík, J.; Roithová, J. Experimentally Calibrated Analysis of the Electronic Structure of CuO +: Implications for Reactivity. *Angew. Chem. Int. Ed.* 2018, *57*, 17053–17057.
- 300. Yassaghi, G.; Andris, E.; Roithova, J. Reactivity of Copper(III)-Oxo Complexes in the Gas Phase. ChemPhysChem 2017, 18, 2217-2224.
- 301. Schröder, D.; Holthausen, M. C.; Schwarz, H. Radical-Like Activation of Alkanes by the Ligated Copper Oxide Cation (Phenanthroline)CuO⁺. J. Phys. Chem. B 2004, 108, 14407–14416.
- 302. Dhar, D.; Tolman, W. B. Hydrogen Atom Abstraction From Hydrocarbons by a Copper(III)-Hydroxide Complex. J. Am. Chem. Soc. 2015, 137, 1322-1329.
- 303. Dhar, D.; Yee, G. M.; Spaeth, A. D.; Boyce, D. W.; Zhang, H.; Dereli, B.; Cramer, C. J.; Tolman, W. B. Perturbing the Copper(III)-Hydroxide Unit Through Ligand Structural Variation. J. Am. Chem. Soc. 2016, 138, 356–368.
- 304. Donoghue, P. J.; Tehranchi, J.; Cramer, C. J.; Sarangi, R.; Solomon, E. I.; Tolman, W. B. Rapid C-H Bond Activation by a Monocopper(III)-Hydroxide Complex. J. Am. Chem. Soc. 2011, 133, 17602–17605.
- 305. Hedegård, E. D.; Ryde, U. Targeting the Reactive Intermediate in Polysaccharide Monooxygenases. J. Biol. Inorg. Chem. 2017, 22, 1029-1037.
- 305a. Singh, R. K.; Blossom, B. M.; Russo, D. A.; Singh, R.; Weihe, H.; Andersen, N. H.; Tiwari, M. K.; Jensen, P. E.; Felby, C.; Bjerrum, M. J. Detection and Characterization of a Novel Copper-Dependent Intermediate in a Lytic Polysaccharide Monooxygenase. *Chem. A Eur. J.* 2020, *26*, 454–463.
- 306. Hori, C.; Ishida, T.; Igarashi, K.; Samejima, M.; Suzuki, H.; Master, E.; Ferreira, P.; Ruiz-Dueñas, F. J.; Held, B.; Canessa, P.; et al. Analysis of the *Phlebiopsis gigantea* Genome, Transcriptome and Secretome Provides Insight Into Its Pioneer Colonization Strategies of Wood. *PLoS Genet.* 2014, 10, e1004759.
- 307. Vanden Wymelenberg, A.; Gaskell, J.; Mozuch, M.; Sabat, G.; Ralph, J.; Skyba, O.; Mansfield, S. D.; Blanchette, R. A.; Martinez, D.; Grigoriev, I.; et al. Comparative Transcriptome and Secretome Analysis of Wood Decay Fungi *Postia placenta* and *Phanerochaete chrysosporium*. Appl. Environ. Microbiol. 2010, 76, 3599–3610.
- 308. Henriksson, G.; Johansson, G.; Pettersson, G. A Critical Review of Cellobiose Dehydrogenases. J. Biotechnol. 2000, 78, 93-113.
- 309. Langston, J. A.; Shaghasi, T.; Abbate, E.; Xu, F.; Vlasenko, E.; Sweeney, M. D. Oxidoreductive Cellulose Depolymerization by the Enzymes Cellobiose Dehydrogenase and Glycoside Hydrolase 61. Appl. Environ. Microbiol. 2011, 77, 7007–7015.
- 310. Tan, T. C.; Kracher, D.; Gandini, R.; Sygmund, C.; Kittl, R.; Haltrich, D.; Hällberg, B. M.; Ludwig, R.; Divne, C. Structural Basis for Cellobiose Dehydrogenase Action During Oxidative Cellulose Degradation. *Nat. Commun.* **2015**, *6*, 7542.
- 311. Laurent, C. V. F. P.; Breslmayr, E.; Tunega, D.; Ludwig, R.; Oostenbrink, C. Interaction Between Cellobiose Dehydrogenase and Lytic Polysaccharide Monooxygenase. Biochemistry 2019, 58, 1226–1235.
- 312. Bodenheimer, A. M.; O'Dell, W. B.; Oliver, R. C.; Qian, S.; Stanley, C. B.; Meilleur, F. Structural Investigation of Cellobiose Dehydrogenase IIA: Insights From Small Angle Scattering Into Intra- and Intermolecular Electron Transfer Mechanisms. *Biochim. Biophys. Acta, Gen. Subj.* 2018, 1862, 1031–1039.
- 313. Takeda, K.; Matsumura, H.; Ishida, T.; Samejima, M.; Ohno, H.; Yoshida, M.; Igarashi, K.; Nakamura, N. Characterization of a Novel PQQ-Dependent Quinohemoprotein Pyranose Dehydrogenase From *Coprinopsis cinerea* Classified Into Auxiliary Activities Family 12 in Carbohydrate-Active Enzymes. *PLoS One* **2015**, *10*, e0115722–e0115738.
- 314. Matsumura, H.; Umezawa, K.; Takeda, K.; Sugimoto, N.; Ishida, T.; Samejima, M.; Ohno, H.; Yoshida, M.; Igarashi, K.; Nakamura, N. Discovery of a Eukaryotic Pyrroloquinoline Quinone-Dependent Oxidoreductase Belonging to a New Auxiliary Activity Family in the Database of Carbohydrate-Active Enzymes. *PLoS One* **2014**, *9*, e104851–e104859.
- 315. Várnai, A.; Umezawa, K.; Yoshida, M.; Eijsink, V. G. H. The Pyrroloquinoline-Quinone-Dependent Pyranose Dehydrogenase From *Coprinopsis cinerea* Drives Lytic Polysaccharide Monooxygenase Action. *Appl. Environ. Microbiol.* **2018**, *84. e00156-18*.
- 316. Winkler, J. R.; Gray, H. B. Long-Range Electron Tunneling. J. Am. Chem. Soc. 2014, 136, 2930–2939.
- 317. Westereng, B.; Cannella, D.; Wittrup Agger, J.; Jørgensen, H.; Larsen Andersen, M.; Eijsink, V. G. H.; Felby, C. Enzymatic Cellulose Oxidation is Linked to Lignin by Long-Range Flectron Transfer Sci. Rep. 2015. 5, 18561.
- 318. Brenelli, L.; Squina, F. M.; Felby, C.; Cannella, D. Laccase-Derived Lignin Compounds Boost Cellulose Oxidative Enzymes AA9. Biotechnol. Biofuels 2018, 11, 10.
- 319. Frommhagen, M.; Koetsier, M. J.; Westphal, A. H.; Visser, J.; Hinz, S. W. A.; Vincken, J. P.; Van Berkel, W. J. H.; Kabel, M. A.; Gruppen, H. Lytic Polysaccharide Monooxygenases From *Myceliophthora thermophila* C1 Differ in Substrate Preference and Reducing Agent Specificity. *Biotechnol. Biofuels* 2016, *9*, 1–17.
- 320. Kracher, D.; Scheiblbrandner, S.; Felice, A. K. G.; Breslmayr, E.; Preims, M.; Ludwicka, K.; Haltrich, D.; Eijsink, V. G. H.; Ludwig, R. Extracellular Electron Transfer Systems Fuel Cellulose Oxidative Degradation. *Science* 2016, *352*, 1098–1101.
- 321. Gardner, J. G.; Crouch, L.; Labourel, A.; Forsberg, Z.; Bukhman, Y. V.; Vaaje-Kolstad, G.; Gilbert, H. J.; Keating, D. H. Systems Biology Defines the Biological Significance of Redox-Active Proteins During Cellulose Degradation in an Aerobic Bacterium. *Mol. Microbiol.* 2014, 94, 1121–1133.
- 322. Tuveng, T. R.; Armtzen, M.Ø.; Bengtsson, O.; Gardner, J. G.; Vaaje-Kolstad, G.; Eijsink, V. G. H. Proteomic Investigation of the Secretome of *Cellvibrio japonicus* During Growth on Chitin. *Proteomics* **2016**. *16*, 1904–1914.
- 323. Arantes, V.; Jellison, J.; Goodell, B. Peculiarities of Brown-Rot Fungi and Biochemical Fenton Reaction With Regard to Their Potential as a Model for Bioprocessing Biomass. *Appl. Microbiol. Biotechnol.* **2012**, *94*, 323–338.
- 324. Zhang, J.; Presley, G. N.; Hammel, K. E.; Ryu, J.-S.; Menke, J. R.; Figueroa, M.; Hu, D.; Orr, G.; Schilling, J. S. Localizing Gene Regulation Reveals a Staggered Wood Decay Mechanism for the Brown Rot Fungus *Postia placenta*. *Proc. Natl. Acad. Sci.* 2016, 113, 10968–10973.
- 325. Presley, G. N.; Schilling, J. S. Distinct Growth and Secretome Strategies for Two Taxonomically Divergent Brown Rot Fungi. Appl. Environ. Microbiol. 2017, 83. e02987-16.
- 326. Borin, G. P.; Sanchez, C. C.; de Santana, E. S.; Zanini, G. K.; dos Santos, R. A. C.; de Oliveira Pontes, A.; de Souza, A. T.; Dal'Mas, R. M. M. T. S.; Riaño-Pachón, D. M.; Goldman, G. H.; et al. Comparative Transcriptome Analysis Reveals Different Strategies for Degradation of Steam-Exploded Sugarcane Bagasse by *Aspergillus niger* and *Trichoderma reesei. BMC Genomics* 2017, *18*, 501.
- 327. Bourdais, A.; Bidard, F.; Zickler, D.; Berteaux-Lecellier, V.; Silar, P.; Espagne, E. Wood Utilization is Dependent on Catalase Activities in the Filamentous Fungus *Podospora* anserina. *PLoS One* 2012, *7*, e29820.
- 328. Castaño, J. D.; Zhang, J.; Schilling, J. S. Evaluation of Colorimetric Assays for Determination of H₂O₂ in planta During Fungal Wood Decomposition. J. Microbiol. Methods 2018, 145. 10–13.
- 329. Scott, B. R.; Huang, H. Z.; Frickman, J.; Halvorsen, R.; Johansen, K. S. Catalase Improves Saccharification of Lignocellulose by Reducing Lytic Polysaccharide Monooxygenase-Associated Enzyme Inactivation. *Biotechnol. Lett.* **2016**, *38*, 425–434.
- 330. Möllers, K. B.; Mikkelsen, H.; Simonsen, T. I.; Cannella, D.; Johansen, K. S.; Bjerrum, M. J.; Felby, C. On the Formation and Role of Reactive Oxygen Species in Light-Driven LPMO Oxidation of Phosphoric Acid Swollen Cellulose. *Carbohydr. Res.* **2017**, *448*, 182–186.